

DYNAMIC MODELING OF JOINTS IN 3D STRUCTURAL MODELS

A THESIS SUBMITTED TO
THE GRADUATE SCHOOL OF NATURAL AND APPLIED SCIENCES
OF
MIDDLE EAST TECHNICAL UNIVERSITY

BY

MERVE TEKİN

IN PARTIAL FULFILLMENT OF THE REQUIREMENTS
FOR
THE DEGREE OF MASTER OF SCIENCE
IN
MECHANICAL ENGINEERING

NOVEMBER 2019

Approval of the thesis:

DYNAMIC MODELING OF JOINTS IN 3D STRUCTURAL MODELS

submitted by **MERVE TEKİN** in partial fulfillment of the requirements for the degree of **Master of Science in Mechanical Engineering Department, Middle East Technical University** by,

Prof. Dr. Halil Kalıpçılar
Dean, Graduate School of **Natural and Applied Sciences**

Prof. Dr. M. A. Sahir Arıkan
Head of Department, **Mechanical Engineering**

Prof. Dr. H. Nevzat Özgüven
Supervisor, **Mechanical Engineering, METU**

Examining Committee Members:

Prof. Dr. Ender Cığeroğlu
Mechanical Engineering Dept., METU

Prof. Dr. H. Nevzat Özgüven
Mechanical Engineering, METU

Assoc. Prof. Dr. M. Bülent Özer
Mechanical Engineering Dept., METU

Assist. Prof. Dr. Orkun Özşahin
Mechanical Engineering Dept., METU

Assoc. Prof. Dr. Can U. Doğruer
Mechanical Engineering Dept., Hacettepe University

Date: 25.11.2019

I hereby declare that all information in this document has been obtained and presented in accordance with academic rules and ethical conduct. I also declare that, as required by these rules and conduct, I have fully cited and referenced all material and results that are not original to this work.

Name, Surname: Merve Tekin

Signature:

ABSTRACT

DYNAMIC MODELING OF JOINTS IN 3D STRUCTURAL MODELS

Tekin, Merve
Master of Science, Mechanical Engineering
Supervisor: Prof. Dr. H. Nevzat Özgüven

November 2019, 132 pages

In the design and development stages of mechanical structures, one of the most challenging part is modelling joints. Due to complex dynamic behavior of joints, it is difficult to build a reliable model for joints using only theoretical approaches, and therefore usually methods based on experimental measurements are employed. In this study, a structural modification method is used to find dynamic characteristics of a bolted joint connecting two beams. A simple formulation based on a structural modification method is suggested to represent a bolted joint with a complex stiffness matrix. The method requires the measurement of only the assembled structure, not individual substructures connected with a bolted joint. The method proposed is validated by using simulated experiments. The ultimate purpose of this work is to find a complex stiffness matrix representing a bolted joint in more complicated structures. Therefore, in the finite element formulation of beams, 3D solid elements are used, and the complex stiffness matrix corresponding to 3 translations and 3 rotations is identified from measured FRFs. The performance of the method is compared with a similar identification using FRF decoupling. The results showed that this new approach is less sensitive to measurement errors and gives better results compared to those of the FRF decoupling method.

Keywords: Joint Modeling, Dynamics of Bolted Connections, Structural Modification Method, Joint Parameter Identification, Finite Element Modeling

ÖZ

3 BOYUTLU YAPISAL MODELLERDEKİ BAĞLANTILARIN DİNAMİK MODELLENMESİ

Tekin, Merve
Yüksek Lisans, Makina Mühendisliği
Tez Danışmanı: Prof. Dr. H. Nevzat Özgüven

Kasım 2019, 132 sayfa

Mekanik yapıların tasarım ve geliştirme aşamalarında, en zorlu kısımlardan biri de bağlantıları modellemektir. Bağlantıların karmaşık dinamik davranışları sebebi ile sadece teorik yaklaşımlar kullanılarak güvenilir bir bağlantı modeli oluşturmak zordur, bu sebeple deneysel ölçümlere dayanan yöntemler kullanılır. Bu çalışmada, iki kirişi birbirine bağlayan bağlantı elemanının dinamik karakteristiğini bulmak için yapısal değişiklik yöntemi kullanılmıştır. Civatalı bağlantıyı karmaşık direngenlik matrisi ile temsil etmek amacıyla yapısal değişiklik yönteminden yola çıkılarak basit bir formulasyon önerilmiştir. Bu yöntem sadece montajlanmış yapıdan ölçüm almayı gerektirir, civata ile bağlanmış alt yapılardan ölçüm almaya gerek yoktur. Önerilen yöntem, simüle edilmiş deneyler ile doğrulanmıştır. Bu çalışmanın nihai amacı daha karmaşık yapılarda kullanılan civatalı bağlantıları karmaşık direngenlik matrisi ile temsil edebilmektir. Bu nedenle kirişlerin sonlu elemanlar ile modellenmesinde 3 boyutlu katı elemanlar kullanılmış, 3 yöndeki ötelenme ve 3 yöndeki dönmeye karşı gelen karmaşık direngenlik matrisi, ölçülmüş Frekans Tepki Fonksiyonları (FTF) kullanılarak bulunmuştur. Bu metodun performansı FTF ayrıştırma kullanılarak yapılan benzer tanılama yöntemleri ile karşılaştırılmıştır. Sonuçlar göstermiştir ki bu yeni yaklaşım, kullanılan diğer FTF ayrıştırma yöntemleri ile karşılaştırıldığında, ölçüm hatalarına daha az duyarlıdır ve daha iyi sonuçlar vermektedir.

Anahtar Kelimeler: Baęlantı Modellemesi, Cıvatalı Baęlantıların Dinamięi, Yapısal Deęişiklik Yöntemi, Baęlantı Parametresi Saptama, Sonlu Elemanlar Modellemesi

to my family and Uğur

ACKNOWLEDGEMENTS

I would like to present my deepest appreciations to my supervisor Prof. Dr. H. Nevzat Özgüven for his guidance and contributions. His wisdom and encouragements motivated me and I am very happy to graduate as his master student.

I am very grateful to my company ROKETSAN for their support through my graduate studies.

I would like to thank to my father, Murat Tekin and to my mother, Şule Tekin for their love, support and encouragement in every stage of my life. I also would like to thank to my sister, Buse Tekin for her friendship and precious advices.

Last but not the least, I want to give my deepest gratitude to Uğur, my fiancé; he encourages me and support me. I am so glad to have him in my life.

TABLE OF CONTENTS

ABSTRACT	v
ÖZ	vii
ACKNOWLEDGEMENTS	x
TABLE OF CONTENTS	xi
LIST OF TABLES	xiv
LIST OF FIGURES	xv
CHAPTERS	
1. INTRODUCTION	1
1.1 Overview	1
1.2 Literature Survey	3
1.3 Objective.....	6
1.4 Scope of the Thesis.....	7
2. JOINTS DYNAMIC MODELING AND IDENTIFICATION OF MODEL PARAMETERS	9
2.1. Theory of Substructure Coupling with Elastic Connection Dynamics	9
2.2. Identifying Joint Parameters by Using Inverse Structural Modification Approach	15
2.2.1. Matrix Inversion Method	15
2.2.2. Using Inverse Structural Modification Method in Identifying Joint Parameters.....	16
2.2.3. Identifying Joint Parameters	18
2.3. Identifying Joints Parameters by Using FRF Decoupling Approach	20

2.4. Estimation of FRFs	21
2.4.1. Estimation of FRFs Corresponding to RDOF	22
3. JOINT DYNAMICS IDENTIFICATION IN A LUMPED MODEL AND IN BEAMS - TWO DIMENSIONAL SPACE	25
3.1. Identification in Discrete Model	25
3.2. Identification in Beams Using Finite Element Method	32
3.3. Identification in Beams Using Finite Element Software	39
3.3.1. Comparison of Two Methods when Applied to 2D Structural Systems ..	52
4. IDENTIFICATION OF JOINT DYNAMICS IN BEAMS – THREE DIMENSIONAL SPACE	57
4.1. Finite Element Simulation of Coupled Beams by Using Spring/Dashpot Elements for Bolted Joint.....	58
4.2. Finite Element Simulation of Two Beams Coupled with a Bolted Joint by Using 3D Brick Elements	61
4.2.1. Selecting Solver.....	61
4.2.2. Description of the Finite Element Model	62
4.2.3. Interaction Properties	65
4.2.4. Bolt Preload.....	67
4.2.5. Direct Steady-State Dynamic Analysis	71
4.3. Identification of Joint Properties in Beams in 3D Space	71
4.3.1. Case Study 1	71
4.3.2. Comparison of Two Methods when Applied to 3D Structural Systems ..	90
4.3.3. Case Study 2.....	103
4.3.3.1. Error Analysis.....	117
5. CONCLUSION AND FUTURE WORK.....	123

5.1. Summary and Conclusions	123
5.2. Future Work	126
REFERENCES.....	129

LIST OF TABLES

TABLES

Table 3-1 Dynamic Properties of the Discrete Model Elements	26
Table 3-2 Identified Joint Properties	38
Table 3-3 Material and Geometric Properties of Beams	40
Table 3-4 Identified Joint Parameters and Percentage Errors for Different Noise Level Representing Measurement Errors	51
Table 4-1 Joint Parameters for Coupled Structures	74
Table 4-2 Sensitive Regions	84
Table 4-3 Identified Translational Joint Parameters and Percentage Errors	89
Table 4-4 Identified Rotational Joint Parameters and Percentage Errors	90
Table 4-5 Comparison of Identified Translational Joint Parameters and Percentage Errors	95
Table 4-6 Comparison of Identified Rotational Joint Parameters and Percentage Errors	95
Table 4-7 Amplitude and Frequency Errors for the Receptance HssC in x – Direction	99
Table 4-8 Amplitude and Frequency Errors for the Receptance HssC in y – Direction	101

LIST OF FIGURES

FIGURES

Figure 2-1 Connection of Two Substructures with Joints.....	10
Figure 2-2 Substructures Free Body Diagrams	10
Figure 2-3 Coupled System with Initially Estimated Bolt Parameters	18
Figure 2-4 Simulated Experiment Model.....	19
Figure 2-5 Finite Difference Method	23
Figure 3-1 a) Two Substructures with a Flexible Joint Element b) Coupled System [15].....	26
Figure 3-2 Comparison of Receptance $H_{rr}C$ Calculated Using Initial and Actual (Predefined) Complex Stiffness Values	28
Figure 3-3 $H_{jj}C$ for the Coupled Structure	29
Figure 3-4 Sensitivity Analysis for Coupled System.....	30
Figure 3-5 Identified Stiffness of the Joint	30
Figure 3-6 Identified Damping of the Joint.....	31
Figure 3-7 Regenerated FRF of the Coupled Structure at Point r.....	32
Figure 3-8 Two Beams Connection with Elastic Joint.....	32
Figure 3-9 Receptances at Points r and s	34
Figure 3-10 $H_{jj}C$ for the Coupled Structure	35
Figure 3-11 Coupled Structure Receptance Sensitivity to k_{Fy}	36
Figure 3-12 Coupled Structure Receptance Sensitivity to $k_{M\theta}$	36
Figure 3-13 Identified Translational and Rotational Stiffnesses Representing the Joint	37
Figure 3-14 Identified Translational and Rotational Damping Representing the Joint	38
Figure 3-15 Substructures Coupled with a Joint	39
Figure 3-16 Mode Shapes of the Coupled Structure	41

Figure 3-17 Translational Receptance Values for Point s	43
Figure 3-18 Translational Receptance Values for Point r	43
Figure 3-19 Sensitivity of System Response at Point s to kF_y	44
Figure 3-20 Sensitivity of System Response at Point s to $kM\theta$	44
Figure 3-21 Sensitivity of System Response at Point r to kF_y	45
Figure 3-22 Sensitivity of System Response at r to $kM\theta$	45
Figure 3-23 Identified value of Translational Stiffness by Using Different Frequency Regions	47
Figure 3-24 Identified value of Translational Damping by Using Different Frequency Regions	48
Figure 3-25 Identified value of Rotational Stiffness by Using Different Frequency Regions	49
Figure 3-26 Identified value of Rotational Damping by Using Different Frequency Regions	50
Figure 3-27 Effects of Measurement Errors on Identified Joint Parameters	51
Figure 3-28 Coupled Structure [15].....	53
Figure 3-29 Coupled Structure [15].....	53
Figure 3-30 Identified Translational Stiffness Obtained by Using ISMM and FRF DM	54
Figure 3-31 Identified Translational Damping Obtained by Using ISMM and FRF DM	54
Figure 3-32 Identified Rotational Stiffness Obtained by Using ISMM and FRF DM	55
Figure 3-33 Identified Rotational Damping Obtained by Using ISMM and FRF DM	55
Figure 3-34 Comparison of the FRFs of the tip Point Calculated Using Joint Parameters Identified by Using ISMM and FRF DM	56
Figure 4-1 Coupled Structure Finite Element Model	58
Figure 4-2 Contact Surfaces	59
Figure 4-3 Representation of RPs and Coupling Elements	60

Figure 4-4 Section View of the Model.....	60
Figure 4-5 The Finite Element Modeling of Coupled Structure	62
Figure 4-6 Section View of the 3D Bolted Connection	62
Figure 4-7 3D Modelling of Bolt Head, Bolt Shank and Nut as One Part.....	63
Figure 4-8 Contact Regions Between 1) Bolt Head and Beam A 2) Nut and Beam B	64
Figure 4-9 Contact Region Between Beams	64
Figure 4-10 Frictional Behavior [31]	66
Figure 4-11 Default pressure-overclosure relationship [33]	67
Figure 4-12 Preloaded Bolt	68
Figure 4-13 Contact Pressure at Surface Nodes for Substructure A.....	69
Figure 4-14 Contact Pressure at Surface Nodes for Substructure B	70
Figure 4-15 Contact Pressure at Surface Nodes for Bolt	70
Figure 4-16 Using Predefined Complex Stiffness Matrix for Both Systems.....	72
Figure 4-17 Receptances at Points r and s in y-direction.....	76
Figure 4-18 Sensitivity of the System Response at Point s to kFx	78
Figure 4-19 Sensitivity of the System Response at Point s to kFy	79
Figure 4-20 Sensitivity of the System Response at Point s to kFz	80
Figure 4-21 Sensitivity of the System Response at Point s to $kM\theta_x$	81
Figure 4-22 Sensitivity of the System Response at Point s to $kM\theta_y$	82
Figure 4-23 Sensitivity of the System Response at Point s to $kM\theta_z$	83
Figure 4-24 Identified Translational Stiffnesses	85
Figure 4-25 Identified Translational Damping	86
Figure 4-26 Identified Rotational Stiffnesses	87
Figure 4-27 Identified Rotational Damping	88
Figure 4-28 Identified Translational Stiffnesses Obtained by Using ISMM and FRF DM	91
Figure 4-29 Identified Translational Damping Obtained by Using ISMM and FRF DM	92

Figure 4-30 Identified Rotational Stiffnesses Obtained by Using ISMM and FRF DM	93
Figure 4-31 Identified Rotational Damping Obtained by Using ISMM and FRF DM	94
Figure 4-32 Natural Frequencies and Mode Shapes of the Coupled System	96
Figure 4-33 Natural Frequencies and Mode Shapes of the Coupled System	97
Figure 4-34 Comparison of the FRFs of the Tip Point Calculated Using Joint Parameters Identified by Using ISMM and FRF DM in x Direction	98
Figure 4-35 Comparison of the FRFs of the Tip Point in Frequency Ranges	99
Figure 4-36 Comparison of the FRFs of the Tip Point Calculated Using Joint Parameters Identified by Using ISMM and FRF DM in y Direction	100
Figure 4-37 Comparison of the FRFs of the Tip Point Calculated Using Joint Parameters Identified by Using ISMM and FRF DM	101
Figure 4-38 Comparison of the FRFs of the Tip Point Calculated Using Joint Parameters Identified by Using ISMM and FRF DM in z Direction	102
Figure 4-39 Finite Difference Method.....	104
Figure 4-40 Measurement Points for j coordinate	105
Figure 4-41 Force Points for j coordinate.....	105
Figure 4-42 Measurement Points for k coordinate	105
Figure 4-43 Force Points for k coordinate.....	106
Figure 4-44 Measurement 1 Points.....	106
Figure 4-45 Measurement 1 Points for the Calculation of $E H_{jj}C$	107
Figure 4-46 Measurement 1 Points for the Calculation of $E H_{kj}C$	108
Figure 4-47 Measurement 2 Points.....	108
Figure 4-48 Measurement 2 Points for the Calculation of $E H_{jj}C$	109
Figure 4-49 Measurement 2 Points for the Calculation of $E H_{kj}C$	110
Figure 4-50 Measurement 3 Points.....	110
Figure 4-51 Measurement 3 Points for the Calculation of $E H_{jj}C$	111
Figure 4-52 Measurement 3 Points for the Calculation of $E H_{kj}C$	112
Figure 4-53 Measurement 4 Points.....	112

Figure 4-54 Measurement 4 Points for the Calculation of E_{HjjC}	113
Figure 4-55 Measurement 4 Points for the Calculation of E_{HkjC}	114
Figure 4-56 Regenerated FRF of the Coupled Structure Using Identified Joint Properties in y Direction	115
Figure 4-57 Regenerated FRF of the Coupled Structure Using Identified Joint Properties in x Direction	115
Figure 4-58 Regenerated FRF of the Coupled Structure (using shorter beam for substructure B) Using Identified Joint Properties in y Direction.....	116
Figure 4-59 Regenerated FRF of the Coupled Structure (using shorter beam for substructure B) Using Identified Joint Properties in x Direction.....	117
Figure 4-60 Unmeasurable Points.....	118
Figure 4-61 Measurement Scheme	118
Figure 4-62 The Effect of Unmeasured FRFs on Stiffness Parameters	120
Figure 4-63 The Effect of Unmeasured FRFs on Damping Parameters	120
Figure 4-64 The Effect of Unmeasured FRFs on Stiffness Parameters	121
Figure 4-65 The Effect of Unmeasured FRFs on Damping Parameters	121

CHAPTER 1

INTRODUCTION

1.1 Overview

In many engineering applications, it is very common to have systems assembled by means of bolts. They often play a critical role; failure of them can cause the structure or machine fail catastrophically. Thanks to recent advances in Finite Element (FE) techniques and availability of FE packages, which are frequently used for the solution of structural problems, when a solid structure is modeled, a reasonable accuracy is obtained. However, most of the engineering structures are composed of assembled substructures, and for the assembled structures, the results of actual tests are generally different from those of the FE analysis. The most important reason behind this discrepancy is difficulties in modeling bolted-joints.

Although a joint is known as a source of flexibility in an assembled structure, its behavior is still not implicitly understood when subjected to dynamic loading. The ability to model and predict bolted joint behavior is of great concern, especially for high-impact applications such as defense, aerospace, and automotive engineering industries. For instance, missiles which are one of the defense industry products that are being developed in these days, are subjected to vibration due to several reasons such as stage separation, air turbulence, wind, etc. If these vibrations are at a frequency close to one of the missile's natural frequencies, system comes to resonance, which is the most undesired situation. Extensive studies have revealed over the past years that the stiffness of joints influences the dynamics of a missile considerably. Bending stiffness of most rockets and missiles may be reduced by 20-30% due to joints which may cause decreases in natural frequencies, especially the first modal frequency, as much as 10-20%. Moreover, the mode shapes and nodal lines would change [1].

Therefore, it is essential to carry out the modal analysis of a missile accurately. Especially, finding the first modal frequency correctly has great significance. Other than considering natural frequencies, bolted flange connections are essential parts of the missile as they connect stages, and flange connections weaken the whole structure's load-bearing capacity. Because of the structure's strong nonlinear characteristics, the geometric continuity of the missile body is destroyed, and some difficulties such as excessive local deformation and stress concentration can happen during loading [2].

Current analytical techniques for modeling bolted joint regions are based on the assumptions of either a rigid joint connection or simplified linear models. Nevertheless, they are highly nonlinear. The stiffnesses of joint members in compression are proportional to the joint members' interface contact area which depends on the joint preload and the external loads carried by the joint [3]. The tightening of bolts creates static loads in the joint. These static loads will add on to dynamic loads during dynamic excitation of the system. If dynamic load changes are small compared to static loads, then the dynamic response will have affected slightly in terms of natural frequency and dissipation [4]. In other words, overall joint region stiffness is a function of the external loads carried by the joint and this is the reason for the nonlinearity of a jointed connection.

In light of the above discussion, it can be concluded that accurate modelling of connection dynamics is a difficult task, and when there are higher loads, it usually requires a nonlinear model. However, even a nonlinear model is required, the starting point is to identify the joint parameters corresponding to the linear part of the model, such as the stiffnesses and damping coefficients. Furthermore, in some applications using a linear model may be sufficient to obtain reliable results. So it can be seen that the identification of linear model parameters of joints is important, which also serves to understand the effect of the joint on the dynamic response of the mechanical system.

1.2 Literature Survey

For many years, numerous studies have been conducted on modeling structural joints and identifying joint properties. The first category of these studies is the model updating approaches which require the combined use of experimental data and FEM model results. However, in order to use updating schemes, the mass and stiffness matrices of the whole structure including joints are necessary, and in complex systems obtaining these properties and using them in an updating algorithms is expensive. Besides, most model updating studies require measured natural frequencies and modal vectors simultaneously and the application of curve fitting operations in the extraction of these experimental data, which causes inevitable approximation errors [5-7].

Li [7] proposed a model updating method that uses the so-called reduced-order characteristic polynomial (ROCP) and it is focused on joint stiffness identification. In this method, since measured natural frequencies are the only experimental data required, some of the issues associated with the spatial incompleteness of the measured displacement/FRF information can be avoided.

The second category of joint identification studies include the methods based on experimental data which can be either modal or frequency response function (FRF). In the past, many studies have used modal parameters for the estimation of joint properties. Some researchers combined mode shapes of structures from experimental modal analysis with FE model to investigate the joint stiffness and damping properties [8, 9]. These methods require extraction of accurate mode shapes and natural frequencies that are prone to measurement errors. Due to complexity of measurements, they are impractical in real applications. In order to overcome such difficulties, FRFs of the assembled system and its substructures were directly used for the identification. The response coupling methods, receptance and impedance coupling, are the subsets of FRF based methods, in which the assembled structures' FRFs can be generated using experimentally or analytically obtained FRFs of the substructures [10, 11]. Conversely, to identify joint parameters, inverse coupling methods can be used.

In the past decades, many researchers have identified joint parameters using FRF based substructuring methods. These methods are based on identifying the dynamic behavior of the connection by using known (measured) dynamic behavior of the coupled system and those of the subsystems. If we consider bolted connections, structure with joints is referred to as the coupled system and structures obtained when joint is removed are referred to as the substructures. The joints are modeled with stiffness and damping elements, and these properties are identified from the information about the dynamic responses of the coupled system and substructures.

Hong and Lee [12] presented a hybrid method that makes use of the measured, incomplete FRFs and FRFs computed from an auxiliary finite element model of the system. The proposed method is straightforward and requires neither modal parameters nor any condensation techniques for the model.

Yang and Park [13] proposed an iterative method that combines measured FRFs with the analytical model for the identification of linearized joint parameters. They estimated unmeasured FRFs from the measured ones by solving an overdetermined set of linear equations. After the needed FRFs obtained, joint parameters are identified iteratively with the minimization of loss function. Three different joint models are evaluated. In the first one, only translational properties are considered. In the second one, both translational and rotational parameters are included and in the final model, they additionally considered cross-coupled terms. They have shown that cross-coupled terms of joints have no significant effect on the response of the assembled system.

Lee and Hwang [14] proposed an FRF based substructuring method with an iterative optimization technique, realizing that an inherent error comes from using directly obtained FRFs. To enhance the efficiency of the iterations during optimization, an analytic sensitivity formula is proposed and used in the identification procedure.

Tol and Özgüven [15] have used a method based on FRF decoupling in order to successfully identify linear joint parameters of a bolted connection in beams. In that

method, they used FRFs of the substructures obtained theoretically or experimentally and measured FRFs of the assembled structure. Using these data, translational, rotational and cross-coupling joint properties, in terms of stiffness and damping values, are calculated by first applying FRF decoupling formulation and then an optimization algorithm.

Klaassen et al. [16] extended the work of Tol and Özgüven [15] by using the System Equivalent Model Mixing (SEMM) technique in order to expand the measurement DOF set. The aim in that study was to identify the joint properties in six DOFs.

Although inevitable measurement errors, ill-conditioning problems and difficulties in obtaining FRFs corresponding to rotational DOFs cause poor results in real structures when FRF based substructuring approaches are used, not requiring modal information is considered as an advantage. Several studies are still being carried out to apply different approaches to solve the problems of these FRF based methods.

FRF Decoupling method gives accurate results when exact values are used for all FRFs. However, for the coupled structure it is a must to use measured FRFs, and the problem mainly comes from the inability to measure FRFs corresponding to rotational DOFs, especially at the subsystem interface. Different approaches have been used to solve this problem. Some researchers used modal expansion techniques, such as SEREP and Guyan expansions and others applied the so-called Equivalent Multi-Point Connection (EMPC) method [17,18] in literature.

De Klerk et al. [17] presented the application of EMPC method in their work. They proposed measuring the subsystems' interface at multiple nodes in multiple translational directions as in the case of finite element analysis. As the number of FRFs used in this kind of coupling corresponds to the number of DOF describing the interface, rotational information can be implicitly accounted for. They claimed that to describe all motions of a rigid interface, a minimum of 6 coupling DOF at three nodes is enough.

1.3 Objective

The objective of this thesis is the modeling and identification of bolted joints in structures. As can be seen from the review of the previous works in section 1.2, due to complex dynamic behavior of joints, it is challenging to build a reliable model for joints using only theoretical approaches, and therefore usually methods based on experimental measurements are employed. In this study, a structural modification method which is an FRF based method, is used to identify the parameters of a linear bolted model. As mentioned above, in several applications a linear model may be adequate, and for the applications where a nonlinear model is required, the first stage of constructing a nonlinear model is obtaining linear part of the model. Therefore, an accurate method to identify the parameters of a linear joint model is very important. The method proposed in this study requires the measurement of only the FRFs of the assembled structure, not individual substructures connected with a bolted joint. As it further explained in Section 1.2, there are several methods developed for the identification of joint parameters, but almost all of them are focused on two-dimensional structures, so that even more complicated structures are simplified to 2D structures. However, most real structures do not have dynamic characteristic which makes it possible to represent them accurately with simple 2D elements. Therefore, an identification method for 3D structures is needed. The proposed methodology is applicable to 2D structures where only two degrees of freedom (DOFs) in translation and rotation are involved, as well as to 3D structures where all DOFs in translation and rotation are involved. The bolted joint is modeled with translational and rotational stiffness and damping elements, for all six DOFs. Therefore, the proposed technique accounts for the effects of RDOFs. Since such an approach requires the measurement of FRFs related with rotational DOFs, finite difference method is used and FRFs corresponding to rotational DOFs are approximated with translational FRFs of the assembled structure. The applicability of the method suggested is demonstrated and validated with simulated experiments.

In this study, the FRF Decoupling method developed in an earlier work is also expanded so that it can be used for 3D structural models, and finally the performance of the method proposed in this study is compared with that of the FRF Decoupling method.

1.4 Scope of the Thesis

The outline of the thesis is as follows:

Chapter 2 provides the basic theory of the joint model used and the identification methods employed. First, the theory of connection dynamics is explained. Then, the Inverse Structural Modification Method (ISMM) proposed in this study is introduced. Finally, the FRF decoupling method and its extension to systems with 6 DOF per node are given. The importance of the RDOF in joint modeling is also explained in this chapter, and the estimation methods for FRFs corresponding rotational DOF are presented.

In Chapter 3, several case studies are given to verify and illustrate the application of the suggested method to 2D structures. In these case studies, where lumped mass systems and beam structures are used, the joint parameters are extracted in terms of stiffness and damping matrices by using both the proposed method and the FRF Decoupling method. The effects of measurement errors on the identified parameters in both methods are studied and compared with each other extensively.

In Chapter 4, the details of the 3D finite element model used for a bolt connection, and the simulated experiments using 3D elements are given. Case studies using 3D elements are presented in this chapter in order to demonstrate the application of proposed method. The comparison of the performance of the method proposed with that of the FRF Decoupling method is also presented in this chapter.

Finally, general conclusions and recommendations for future research are presented in Chapter 5.

CHAPTER 2

JOINTS DYNAMIC MODELING AND IDENTIFICATION OF MODEL PARAMETERS

Complex structures compose of various substructures that are joined together with the help of different types of joints. Among them, the most commonly used one is bolted joint. If the dynamics of the joint is known, the dynamics of the whole assembled structure can be found by using the dynamics of the substructures. However, predicting the dynamics of the joint accurately is not an easy task since it depends on various factors such as pretension on the bolt, coefficient of friction, conditions of the contact surfaces, etc. Once the joint dynamics is determined, the assembled structure's dynamics can be found by using mathematical relationships.

In this chapter, firstly, the dynamics of two substructures connected with a joint represented by a complex stiffness matrix between connecting degrees of freedom is studied. Then, two different approaches proposed in identifying the parameters of the joint model employed are given. The first approach is a new method, whereas the second one is the extended version of a method proposed in a previous study [15]. In section 2.1, the theory of substructure coupling with connection dynamics is explained. In sections 2.2 and 2.3, it is shown how structural modification method and FRF decoupling method are used to identify joint parameters, respectively.

2.1. Theory of Substructure Coupling with Elastic Connection Dynamics

Let us consider that a joint element connects substructures A and B elastically, as shown in Figure 2-1. The points j and k represent joint degrees of freedom (DOFs), while r and s represent internal DOFs, and they are not involved in the joint interface. In this figure, K^* is a complex stiffness matrix of the joint and it represents the joint

dynamics. It consists of the stiffness and damping elements. The free body diagrams of the substructures and the connecting element are given in Figure 2-2.

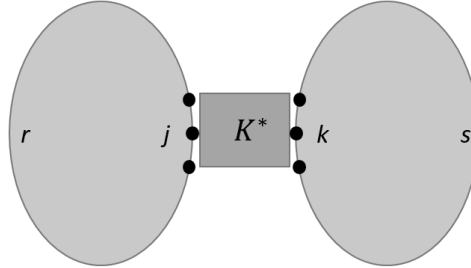


Figure 2-1 Connection of Two Substructures with Joints

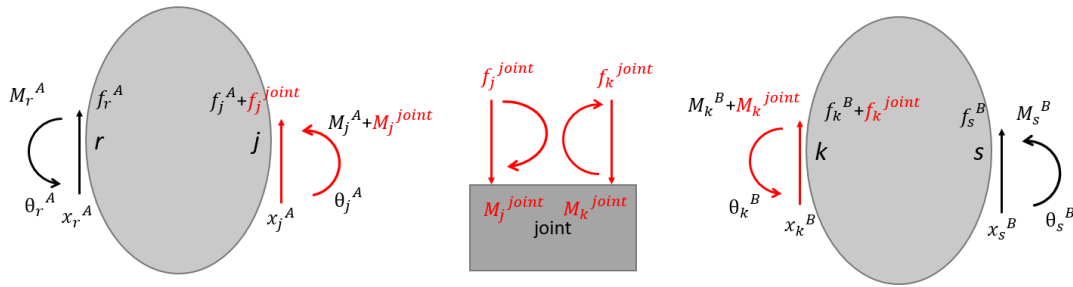


Figure 2-2 Substructures Free Body Diagrams

The relationship between the displacement vectors and the force vectors (composed of applied forces and moments) in each substructure can be defined as follows:

For substructure A:

$$\{x_A\} = [\alpha_A]\{F_A\}$$

$$\begin{Bmatrix} x_r^A \\ \theta_r^A \\ x_j^A \\ \theta_j^A \end{Bmatrix} = \begin{bmatrix} h_{rr} & l_{rr} & h_{rj} & l_{rj} \\ n_{rr} & p_{rr} & n_{rj} & p_{rj} \\ h_{jr} & l_{jr} & h_{jj} & l_{jj} \\ n_{jr} & p_{jr} & n_{jj} & p_{jj} \end{bmatrix} \begin{Bmatrix} f_r^A \\ M_r^A \\ f_j^A + f_j^{joint} \\ M_j^A + M_j^{joint} \end{Bmatrix} \quad (2.1)$$

For substructure B:

$$\{x_B\} = [\alpha_B]\{F_B\}$$

$$\begin{Bmatrix} x_k^B \\ \theta_k^B \\ x_s^B \\ \theta_s^B \end{Bmatrix} = \begin{bmatrix} h_{kk} & l_{kk} & h_{ks} & l_{ks} \\ n_{kk} & p_{kk} & n_{ks} & p_{ks} \\ h_{sk} & l_{sk} & h_{ss} & l_{ss} \\ n_{jk} & p_{sk} & n_{ss} & p_{ss} \end{bmatrix} \begin{Bmatrix} f_k^B + f_k^{joint} \\ M_k^B + M_k^{joint} \\ f_s^B \\ M_s^B \end{Bmatrix} \quad (2.2)$$

where x_p and θ_p represent the translational and rotational displacement vectors at location p while f_p and M_p represent the force and moment at location p . $[\alpha_A]$ and $[\alpha_B]$ represent receptance matrices for substructures A and B, respectively.

The receptance matrix components are defined as;

$$h_{pq} = \frac{x_p}{f_q} \quad (2.3)$$

$$l_{pq} = \frac{x_p}{M_q} \quad (2.4)$$

$$n_{pq} = \frac{\theta_p}{f_q} \quad (2.5)$$

$$p_{pq} = \frac{\theta_p}{M_q} \quad (2.6)$$

The substructure FRFs can be combined by using the joint interface's equilibrium and compatibility conditions to form the FRFs of the assembled structure [19]. It is assumed that the joint segment is an element that mainly imposes stiffness and damping to the structure. In other words, the connection dynamics is modelled by a complex stiffness matrix between the connection degrees of freedom.

Assume that there is no forces and moments acting on joints externally and that flexible connection is massless, the equilibrium condition at the joint can be written as:

$$\begin{Bmatrix} f_j^{joint} \\ M_j^{joint} \end{Bmatrix} + \begin{Bmatrix} f_k^{joint} \\ M_k^{joint} \end{Bmatrix} = 0 \quad (2.7)$$

$$\begin{Bmatrix} f_j^{joint} \\ M_j^{joint} \end{Bmatrix} = - \begin{Bmatrix} f_k^{joint} \\ M_k^{joint} \end{Bmatrix} \quad (2.8)$$

Then the compatibility of translational and rotational displacements at connection DOFs can be written by using Eqn. (2.7) as follows:

$$c_x(\dot{x}_k^B - \dot{x}_j^A) + k_x(x_k^B - x_j^A) = f_j^{joint} \quad (2.9)$$

$$c_\theta(\dot{\theta}_k^B - \dot{\theta}_j^A) + k_\theta(\theta_k^B - \theta_j^A) = M_j^{joint} \quad (2.10)$$

Let us define joint complex stiffness matrix in frequency domain as:

$$[K^*(\omega)] = \begin{bmatrix} k_x + ic_x\omega & 0 \\ 0 & k_\theta + ic_\theta\omega \end{bmatrix} \quad (2.11)$$

Now, Eqns. (2.9) and (2.10) can be written as

$$\begin{Bmatrix} x_k^B - x_j^A \\ \theta_k^B - \theta_j^A \end{Bmatrix} = [K^*(\omega)]^{-1} \begin{Bmatrix} f_j^{joint} \\ M_j^{joint} \end{Bmatrix} \quad (2.12)$$

H_{joint} denotes the inverse of complex stiffness matrix $[K^*(\omega)]$

$$[H_{joint}] = \begin{bmatrix} h_{tt}^{joint} & 0 \\ 0 & h_{rr}^{joint} \end{bmatrix} = [K^*(\omega)]^{-1} \quad (2.13)$$

where subscript t refers to translational information and subscript r refers to rotational information of the joint model.

By using Eqn. (2.1), x_j^A and θ_j^A can be written as

$$x_j^A = h_{jr}f_r^A + l_{jr}M_r^A + h_{jj}(f_j^A + f_j^{joint}) + l_{jj}(M_j^A + M_j^{joint}) \quad (2.14)$$

$$\theta_j^A = n_{jr}f_r^A + p_{jr}M_r^A + n_{jj}(f_j^A + f_j^{joint}) + p_{jj}(M_j^A + M_j^{joint}) \quad (2.15)$$

and by using Eqn. (2.2), x_k^B and θ_k^B can be written as

$$x_k^B = h_{kk}(f_k^B + f_k^{joint}) + l_{kk}(M_k^B + M_k^{joint}) + h_{ks}f_s^B + l_{ks}M_s^B \quad (2.16)$$

$$\theta_k^B = n_{kk}(f_k^B + f_k^{joint}) + p_{kk}(M_k^B + M_k^{joint}) + n_{ks}f_s^B + p_{ks}M_s^B \quad (2.17)$$

Then, by using Eqn. (2.12) and replacing f_k^{joint} with $-f_j^{joint}$ and M_k^{joint} with $-M_j^{joint}$ the following equations can be written

$$\begin{cases} h_{tt}^{joint} f_j^{joint} \\ h_{rr}^{joint} M_j^{joint} \end{cases} = \begin{cases} x_k^B - x_j^A \\ \theta_k^B - \theta_j^A \end{cases} \quad (2.18)$$

By using Eqns. (2.16) and (2.14), the first element of the vector can be written as

$$\begin{aligned} h_{tt}^{joint} f_j^{joint} &= h_{kk}f_k^B - h_{kk}f_j^{joint} + l_{kk}M_k^B - l_{kk}M_j^{joint} + h_{ks}f_s^B + l_{ks}M_s^B - \\ &h_{jr}f_r^A - l_{jr}M_r^A - h_{jj}f_j^{joint} - h_{jj}f_j^A - l_{jj}M_j^A - l_{jj}M_j^{joint} \end{aligned} \quad (2.19)$$

and by using Eqns. (2.17) and (2.15) the second element of the vector can be written as

$$\begin{aligned} h_{rr}^{joint} M_j^{joint} &= n_{kk}f_k^B - n_{kk}f_j^{joint} + p_{kk}M_k^B - p_{kk}M_j^{joint} + n_{ks}f_s^B + \\ &p_{ks}M_s^B - n_{jr}f_r^A - p_{jr}M_r^A - n_{jj}f_j^A - n_{jj}f_j^{joint} - p_{jj}M_j^A - p_{jj}M_j^{joint} \end{aligned} \quad (2.20)$$

By rearranging Eqn. (2.19), the following equation can be written

$$\begin{aligned} [h_{tt}^{joint} + h_{kk} + h_{jj} \quad l_{kk} + l_{jj}] \begin{Bmatrix} f_j^{joint} \\ M_j^{joint} \end{Bmatrix} &= [h_{kk} \quad l_{kk}] \begin{Bmatrix} f_k^B \\ M_k^B \end{Bmatrix} + \\ [h_{ks} \quad l_{ks}] \begin{Bmatrix} f_s^B \\ M_s^B \end{Bmatrix} &- [h_{jr} \quad l_{jr}] \begin{Bmatrix} f_r^A \\ M_r^A \end{Bmatrix} - [h_{jj} \quad l_{jj}] \begin{Bmatrix} f_j^A \\ M_j^A \end{Bmatrix} \end{aligned} \quad (2.21)$$

and by rearranging Eqn. (2.20), the following equation can be written

$$\begin{aligned}
& [n_{kk} + n_{jj} \quad h_{rr}^{joint} + p_{kk} + p_{jj}] \begin{Bmatrix} f_j^{joint} \\ M_j^{joint} \end{Bmatrix} = [n_{kk} \quad p_{kk}] \begin{Bmatrix} f_k^B \\ M_k^B \end{Bmatrix} + \\
& [n_{ks} \quad p_{ks}] \begin{Bmatrix} f_s^B \\ M_s^B \end{Bmatrix} - [n_{jr} \quad p_{jr}] \begin{Bmatrix} f_r^A \\ M_r^A \end{Bmatrix} - [n_{jj} \quad p_{jj}] \begin{Bmatrix} f_j^A \\ M_j^A \end{Bmatrix}
\end{aligned} \tag{2.22}$$

Combining Eqns. (2.21) and (2.22) results in

$$\begin{aligned}
& \begin{bmatrix} h_{tt}^{joint} + h_{kk} + h_{jj} & l_{kk} + l_{jj} \\ n_{kk} + n_{jj} & h_{rr}^{joint} + p_{kk} + p_{jj} \end{bmatrix} \begin{Bmatrix} f_j^{joint} \\ M_j^{joint} \end{Bmatrix} = \begin{bmatrix} h_{kk} & l_{kk} \\ n_{kk} & p_{kk} \end{bmatrix} \begin{Bmatrix} f_k^B \\ M_k^B \end{Bmatrix} + \\
& \begin{bmatrix} h_{ks} & l_{ks} \\ n_{ks} & p_{ks} \end{bmatrix} \begin{Bmatrix} f_s^B \\ M_s^B \end{Bmatrix} - \begin{bmatrix} h_{jr} & l_{jr} \\ n_{jr} & p_{jr} \end{bmatrix} \begin{Bmatrix} f_r^A \\ M_r^A \end{Bmatrix} - \begin{bmatrix} h_{jj} & l_{jj} \\ n_{jj} & p_{jj} \end{bmatrix} \begin{Bmatrix} f_j^A \\ M_j^A \end{Bmatrix}
\end{aligned} \tag{2.23}$$

Rearranging Eqn. (2.23) yields

$$\begin{aligned}
& \begin{Bmatrix} f_j^{joint} \\ M_j^{joint} \end{Bmatrix} = - \begin{Bmatrix} f_k^{joint} \\ M_k^{joint} \end{Bmatrix} = [Z]^{-1} [H_{kk}] \begin{Bmatrix} f_k^B \\ M_k^B \end{Bmatrix} + [Z]^{-1} [H_{ks}] \begin{Bmatrix} f_s^B \\ M_s^B \end{Bmatrix} - \\
& [Z]^{-1} [H_{jr}] \begin{Bmatrix} f_r^A \\ M_r^A \end{Bmatrix} - [Z]^{-1} [H_{jj}] \begin{Bmatrix} f_j^A \\ M_j^A \end{Bmatrix}
\end{aligned} \tag{2.24}$$

where $[Z] = [H_{joint} + H_{kk} + H_{jj}] = [K^*(\omega)]^{-1} + [H_{kk}] + [H_{jj}]$

Substitution of Eqn. (2.24) into Eqns. (2.1) and (2.2) leads to the assembled structure's FRFs in terms of the substructures' FRFs as [20]:

$$\begin{Bmatrix} X_r \\ X_j \\ X_k \\ X_s \end{Bmatrix} = \begin{bmatrix} H_{rr}^C & H_{rj}^C & H_{rk}^C & H_{rs}^C \\ H_{jr}^C & H_{jj}^C & H_{jk}^C & H_{js}^C \\ H_{kr}^C & H_{kj}^C & H_{kk}^C & H_{ks}^C \\ H_{sr}^C & H_{sj}^C & H_{sk}^C & H_{ss}^C \end{bmatrix} \begin{Bmatrix} F_r^A \\ F_j^A \\ F_k^B \\ F_s^B \end{Bmatrix} \tag{2.25}$$

$$\begin{Bmatrix} X_r \\ X_j \\ X_k \\ X_s \end{Bmatrix} = \begin{bmatrix} H_{rr} - H_{rj}Z^{-1}H_{jr} & H_{rj} - H_{rj}Z^{-1}H_{jj} & H_{rj}Z^{-1}H_{kk} & H_{rj}Z^{-1}H_{ks} \\ H_{jr} - H_{jj}Z^{-1}H_{jr} & H_{jj} - H_{jj}Z^{-1}H_{jj} & H_{jj}Z^{-1}H_{kk} & H_{jj}Z^{-1}H_{ks} \\ H_{kr}Z^{-1}H_{jr} & H_{kr}Z^{-1}H_{jj} & H_{kk} - H_{kk}Z^{-1}H_{kk} & H_{ks} - H_{kk}Z^{-1}H_{ks} \\ H_{sr}Z^{-1}H_{jr} & H_{sr}Z^{-1}H_{jj} & H_{sk} - H_{sk}Z^{-1}H_{kk} & H_{ss} - H_{sk}Z^{-1}H_{ks} \end{bmatrix} \begin{Bmatrix} F_r^A \\ F_j^A \\ F_k^B \\ F_s^B \end{Bmatrix} \tag{2.26}$$

Note that, in the above equations Z and H represent submatrices, and for simplicity matrix sign is not used.

2.2. Identifying Joint Parameters by Using Inverse Structural Modification Approach

2.2.1. Matrix Inversion Method

The matrix inversion method was first proposed to calculate the receptances of damped structures by using those of the undamped structures for a non-proportionally damped structure by Özgüven [21]. Later, it is presented as a general structural modification method, in which basically, the FRFs of a modified structure are obtained from those of the original system and the modification matrix [22].

Consider a system represented by a stiffness matrix $[K]$, a mass matrix $[M]$ and a structural damping matrix $[H]$. The equation of a motion of the structure can be written as

$$[M]\{\ddot{x}\} + i[H]\{\dot{x}\} + [K]\{x\} = \{F\} \quad (2.27)$$

For a harmonic excitation $\{F\}$, the steady response of the structure is given by

$$\{x\} = ([K] - \omega^2[M] + i[H])^{-1}\{F\} \quad (2.28)$$

from which, the receptance matrix of the structure $[\alpha]$ can be obtained as

$$[\alpha] = ([K] - \omega^2[M] + i[H])^{-1} \quad (2.29)$$

If the structure is modified, then the receptance matrix of the modified system can be written, in a similarly way, as

$$[\gamma] = ([K] + [\Delta K] - \omega^2[M] + [\Delta M] + i[H] + [\Delta H])^{-1} \quad (2.30)$$

where $[\Delta K]$, $[\Delta M]$ and $[\Delta H]$ are the matrices representing stiffness, mass and damping modifications, respectively. Inverting both sides of the Eqns. (2.29) and (2.30), and then combining them yields

$$[\gamma]^{-1} = [\alpha]^{-1} + [D] \quad (2.31)$$

where $[D]$ is the dynamic structural modification matrix and is expressed as

$$[D] = [\Delta K] - \omega^2[\Delta M] + i[\Delta H] \quad (2.32)$$

If Eqn. (2.31) is pre-multiplied by $[\alpha]$ and post-multiplied by $[\gamma]$, it gives

$$[\alpha] = [\gamma] + [\alpha][D][\gamma] \quad (2.33)$$

from which $[\gamma]$ can be obtained as

$$[\gamma] = [[I] + [\alpha][D]]^{-1}[\alpha] \quad (2.34)$$

As discussed in [21] and [22], the above formulation is most advantageous when the structural modification is local, that is, when

$$[D] = \begin{bmatrix} [D_{mm}] & [0] \\ [0] & [0] \end{bmatrix} \quad (2.35)$$

Then, the receptance matrix of the modified system can be obtained as [22]:

$$[\gamma_{mm}] = [[I] + [\alpha_{mm}][D_{mm}]]^{-1}[\alpha_{mm}]$$

$$[\gamma_{mu}]^T = [\gamma_{um}] = [\alpha_{mu}][[I] - [D_{mm}][\gamma_{mm}]]$$

$$[\gamma_{uu}] = [\alpha_{uu}] - [\alpha_{um}][D_{mm}][\gamma_{mu}]$$

Here, subscripts m and u correspond to the structure's modified and unmodified regions respectively. Briefly, here the aim is to find the receptances of the modified system by using the dynamic structural modification matrix $[D]$ (it is $[D_{mm}]$ when the modification is local) and the receptance matrix of the original structure.

2.2.2. Using Inverse Structural Modification Method in Identifying Joint Parameters

The structural modification formulation used in the Matrix Inversion Method (MIM) is employed in this approach in reverse direction in order to identify the dynamic properties of a joint. The calculated FRFs of two subsystems coupled with a bolted joint by using an initially estimated complex stiffness matrix representing the joint dynamics are taken as the FRFs of the original system, $[\alpha]$. The measured FRFs of the

same assembly are taken as the FRFs of the modified system, $[\gamma]$ and the modification matrix (in the form of complex stiffness matrix) is calculated by using the formulation obtained from the Structural Modification Method (SMM) MIM. Thus, the calculated modification matrix will give the required modification in the initially estimated complex stiffness matrix in order to have the calculated and measured FRFs be the same. The complex stiffness matrix representing the bolted joint then can be obtained by adding the calculated modification matrix to the initially estimated complex stiffness matrix.

By rewriting Eqn. (2.33) as

$$\begin{bmatrix} [\alpha_{mm}] & [\alpha_{mu}] \\ [\alpha_{um}] & [\alpha_{uu}] \end{bmatrix} = \begin{bmatrix} [\gamma_{mm}] & [\gamma_{mu}] \\ [\gamma_{um}] & [\gamma_{uu}] \end{bmatrix} + \begin{bmatrix} [\alpha_{mm}] & [\alpha_{mu}] \\ [\alpha_{um}] & [\alpha_{uu}] \end{bmatrix} \begin{bmatrix} [D_{mm}] & [0] \\ [0] & [0] \end{bmatrix} \begin{bmatrix} [\gamma_{mm}] & [\gamma_{mu}] \\ [\gamma_{um}] & [\gamma_{uu}] \end{bmatrix} \quad (2.36)$$

$$\begin{bmatrix} [\alpha_{mm}] & [\alpha_{mu}] \\ [\alpha_{um}] & [\alpha_{uu}] \end{bmatrix} = \begin{bmatrix} [\gamma_{mm}] & [\gamma_{mu}] \\ [\gamma_{um}] & [\gamma_{uu}] \end{bmatrix} + \begin{bmatrix} [[\alpha_{mm}][D_{mm}][\gamma_{mm}]] & [[\alpha_{mm}][D_{mm}][\gamma_{mu}]] \\ [[\alpha_{um}][D_{mm}][\gamma_{mm}]] & [[\alpha_{um}][D_{mm}][\gamma_{mu}]] \end{bmatrix} \quad (2.37)$$

and using Eqn. (2.37) yields

$$[\alpha_{mm}] = [\gamma_{mm}] + [\alpha_{mm}][D_{mm}][\gamma_{mm}] \quad (2.38)$$

$$[\alpha_{mm}] - [\gamma_{mm}] = [\alpha_{mm}][D_{mm}][\gamma_{mm}] \quad (2.39)$$

If Eqn. (2.39) is pre-multiplied by $[\alpha_{mm}]^{-1}$ and post-multiplied by $[\gamma_{mm}]^{-1}$, dynamic structural modification matrix can be obtained as

$$[D_{mm}] = [\alpha_{mm}]^{-1}([\alpha_{mm}] - [\gamma_{mm}])[\gamma_{mm}]^{-1} \quad (2.40)$$

In the method proposed, the above equation is used to calculate $[D_{mm}]$ from the measured FRFs represented by $[\gamma_{mm}]$ and the FRFs calculated $[\alpha_{mm}]$ by using the

initially estimated complex stiffness matrix representing the bolted joint. It should be noted that in order to calculate $[D_{mm}]$ we need only the receptances corresponding to the joint coordinates. Therefore, $[D_{mm}]$ is the modification matrix in the size of the joint DOFs.

2.2.3. Identifying Joint Parameters

The procedure for modeling a bolted joint is as follows: Firstly, $[\alpha_{mm}]$ is calculated by using finite element model of the structure and an initially estimated complex stiffness matrix representing the bolted joint. The only measurement required is the FRFs of the bolted structure at the connection points of the bolt, which defines $[\gamma_{mm}]$. Then the modification matrix $[D_{mm}]$ is calculated by using Eqn. (2.40), and finally, the complex stiffness matrix representing the bolted joint is calculated by adding $[D_{mm}]$ to the initially estimated complex stiffness matrix. It can be seen that the computational effort will be considerably reduced since only the receptances corresponding to the degrees of freedom of the “modified” region is used.

The receptance matrix corresponding to the connection coordinates of the system with initially estimated bolt parameters can be expressed as follows

$$[\alpha_{mm}] = \begin{bmatrix} {}_l H_{jj}^c & {}_l H_{jk}^c \\ {}_l H_{kj}^c & {}_l H_{kk}^c \end{bmatrix} \quad (2.41)$$

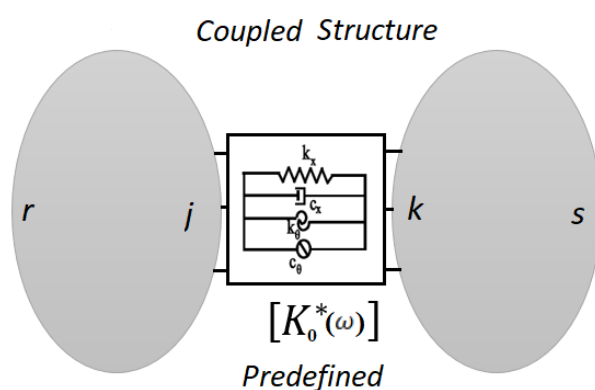


Figure 2-3 Coupled System with Initially Estimated Bolt Parameters

By using the FRFs of the substructures and predefined (initially estimated) complex stiffness matrix, coupled system receptance matrix components can be obtained by using Eqn. (2.26) as follows:

$$[{}_I H_{jj}^C] = [H_{jj}] - [H_{jj}] \left[[K_0^*(\omega)]^{-1} + [H_{kk}] + [H_{jj}] \right]^{-1} [H_{jj}] \quad (2.42)$$

$$[{}_I H_{jk}^C] = [H_{jj}] \left[[K_0^*(\omega)]^{-1} + [H_{kk}] + [H_{jj}] \right]^{-1} [H_{kk}] \quad (2.43)$$

$$[{}_I H_{kk}^C] = [H_{kk}] - [H_{kk}] \left[[K_0^*(\omega)]^{-1} + [H_{kk}] + [H_{jj}] \right]^{-1} [H_{kk}] \quad (2.44)$$

$$[{}_I H_{kj}^C] = [H_{kk}] \left[[K_0^*(\omega)]^{-1} + [H_{kk}] + [H_{jj}] \right]^{-1} [H_{jj}] \quad (2.45)$$

where $[K_0^*(\omega)]$ is the initially estimated complex stiffness matrix.

Experimentally measured FRFs of the assembled substructure, as shown in Figure 2-4 can be expressed as follows,

$$[\gamma_{mm}] = \begin{bmatrix} {}_E H_{jj}^C & {}_E H_{jk}^C \\ {}_E H_{kj}^C & {}_E H_{kk}^C \end{bmatrix} \quad (2.46)$$

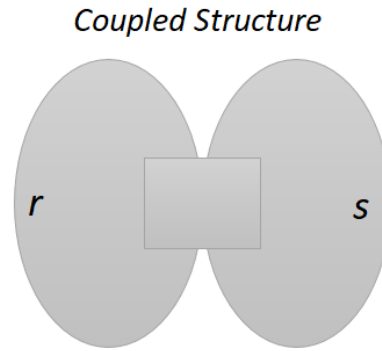


Figure 2-4 Simulated Experiment Model

$$[D_{mm}] = \underbrace{[\alpha_{mm}]^{-1}}_{2n \times 2n} \left(\underbrace{[\alpha_{mm}] - [\gamma_{mm}]}_{2n \times 2n} \right) \underbrace{[\gamma_{mm}]^{-1}}_{2n \times 2n} \quad (2.47)$$

\downarrow
 $2n \times 2n$

$$[D_{mm}] = \begin{bmatrix} j \text{ coord.} & -\Delta \\ -\Delta & k \text{ coord.} \end{bmatrix} \quad (2.48)$$

In this work the simulated experimental results calculated using ABAQUS software were employed, and Eqn. (2.47) is used to calculate $[D_{mm}]$ from these simulated experimental FRFs represented by $[\gamma_{mm}]$, and $[\alpha_{mm}]$, the FRFs calculated by using initially estimated complex stiffness matrix $[K_0^*(\omega)]$ representing the bolted joint, which is an $n \times n$ matrix, whereas the receptance matrices are $2n \times 2n$ matrices. Here "n" represents the size of the joint degree of freedoms. After the calculation of dynamic structural modification matrix $[D_{mm}]$, adding off-diagonal terms of that into $[K_0^*(\omega)]$ will give the identified complex stiffness matrix $[K^*(\omega)]$. Real parts of this matrix are used to find stiffnesses and respectively, imaginary parts are used for damping values which represent the bolted joint characteristics.

2.3. Identifying Joints Parameters by Using FRF Decoupling Approach

This method is proposed in an earlier study [23] to identify contact dynamics in machine tools, and later applied to bolted joints [15]. It is based on substructure coupling method which is commonly used and well-understood for predicting coupled structures' dynamics from those of substructures and coupling dynamics.

Let us consider the system shown in Figure 2-4. The assembled system receptance matrices can be obtained by using Eqn. (2.26) as follows

$$[H_{rr}^c] = [H_{rr}] - [H_{rj}] \left[[K^*(\omega)]^{-1} + [H_{kk}] + [H_{jj}] \right]^{-1} [H_{jr}] \quad (2.49)$$

$$[H_{rs}^c] = [H_{rj}] \left[[K^*(\omega)]^{-1} + [H_{kk}] + [H_{jj}] \right]^{-1} [H_{ks}] \quad (2.50)$$

$$[H_{sr}^c] = [H_{sk}] \left[[K^*(\omega)]^{-1} + [H_{kk}] + [H_{jj}] \right]^{-1} [H_{jr}] \quad (2.51)$$

$$[H_{ss}^c] = [H_{ss}] - [H_{sk}] \left[[K^*(\omega)]^{-1} + [H_{kk}] + [H_{jj}] \right]^{-1} [H_{ks}] \quad (2.52)$$

Complex stiffness matrix, coupling two substructures can be obtain from any of the equations given above (Eqns. (2.49) to (2.52)):

$$[K^*] = \left[[H_{jr}] \left[[H_{rr}] - [H_{rr}^c] \right]^{-1} [H_{rj}] - [H_{jj}] - [H_{kk}] \right]^{-1} \quad (2.53)$$

$$[K^*] = \left[[H_{ks}] [H_{rs}^c]^{-1} [H_{rj}] - [H_{jj}] - [H_{kk}] \right]^{-1} \quad (2.54)$$

$$[K^*] = \left[[H_{jr}] [H_{sr}^c]^{-1} [H_{sk}] - [H_{jj}] - [H_{kk}] \right]^{-1} \quad (2.55)$$

$$[K^*] = \left[[H_{ks}] \left[[H_{ss}] - [H_{ss}^c] \right]^{-1} [H_{sk}] - [H_{jj}] - [H_{kk}] \right]^{-1} \quad (2.56)$$

If the assembled structure's and substructures' FRF matrices are available at any frequency, by using any of the above equations, joint identification can be accomplished and theoretically speaking, it does not make any difference which equation is used in the identification of the joint parameters. Similarly, theoretically speaking it also does not make any difference at which frequency these equations are used. However, the earlier study [15] shows that the equations are very sensitive to FRF values, some of which are unavoidably measured ones. Therefore, the application of this method is not very straightforward.

2.4. Estimation of FRFs

Frequency response functions (FRFs) are frequently used in vibration analysis to find the dynamic characteristics of a structure. Measuring FRFs accurately for all relevant degrees of freedom is very important. However, measurement of certain FRFs is impossible due to difficulty in reaching to these points. Besides, measuring all the elements of an FRF matrix experimentally is very time consuming and expensive. In this work, in some case studies, three translational and three rotational components have to be used and measurements of the rotational components are the most

challenging part due to the need for special and dedicated equipment. Under these conditions, it is useful to have some solutions that help to obtain accurate estimation for unmeasured FRFs.

2.4.1. Estimation of FRFs Corresponding to RDOF

In order to obtain the complete description of the system dynamics, it is extremely important to have information about the rotational FRFs. Silva et al. [24] claim that FRFs involving rotational information represent 75% of the whole FRF matrix and cannot be ignored.

The main problem in obtaining FRFs related with rotational degrees of freedom is the difficulty in applying a pure moment to a test structure, especially to a specified measurement points and measuring angular displacements. There are several options for moment excitation, such as twin shaker arrangements, blocks, magnetostrictive exciters, and synchronized hammers. Among these approaches, twin shaker type and magnetostrictive type moment exciters have been shown to be particularly successful but they have an important drawback; exciters inevitably affect the behavior of the test structure due to the shaker arrangement and they occupy large space. Therefore, they are impractical for use in many real applications. The approach of using synchronized hammers is shown to be feasible, but it requires accessibility from both sides of the test structures which often will not be the case [25]. On the other hand, a particular finite difference approach referred to as the “central difference” method [26] provides a simple way of obtaining FRFs involving rotational DOFs with a practical application. Therefore, in this study, the finite difference technique is used to acquire rotational data from the translational measurements.

Depending on the position of the accelerometer and the position of the excitation point, three different formulas can be used. In this work, the central difference approach by using three points formula is used because of the needed accuracy requirement.

In Figure 2-5, an illustration of an arbitrary test structure is shown. Three points on the structure can be defined: point 2 is the reference point at which RDOF FRFs are required, and points 1 and 3 are measurement points. The close-accelerometers method has been performed with three accelerometers placed in constant distance close to one another, as shown in figure.

Predicted FRFs, $[H_{pred}]$, which include rotational and coupled information for the reference point (point 2) from measured translational FRFs can be obtained as

$$[H_{pred}] = \begin{bmatrix} H_{yy} & H_{y\theta_z} \\ H_{\theta_z y} & H_{\theta_z \theta_z} \end{bmatrix} = [T_{2c}] \cdot [H_{meas}] \cdot [T_{2c}]^T \quad (2.57)$$

where $[H_{meas}]$ represents the measured translational FRF matrix

$$[H_{meas}] = \begin{bmatrix} H_{11} & H_{12} & H_{13} \\ H_{21} & H_{22} & H_{23} \\ H_{31} & H_{32} & H_{33} \end{bmatrix} \quad (2.58)$$

and $[T_{2c}]$ denotes the central difference transformation matrix

$$[T_{2c}] = \frac{1}{2\Delta x} \begin{bmatrix} 0 & 2\Delta x & 0 \\ -1 & 0 & 1 \end{bmatrix} \quad (2.59)$$

where Δx is the constant spacing between points.

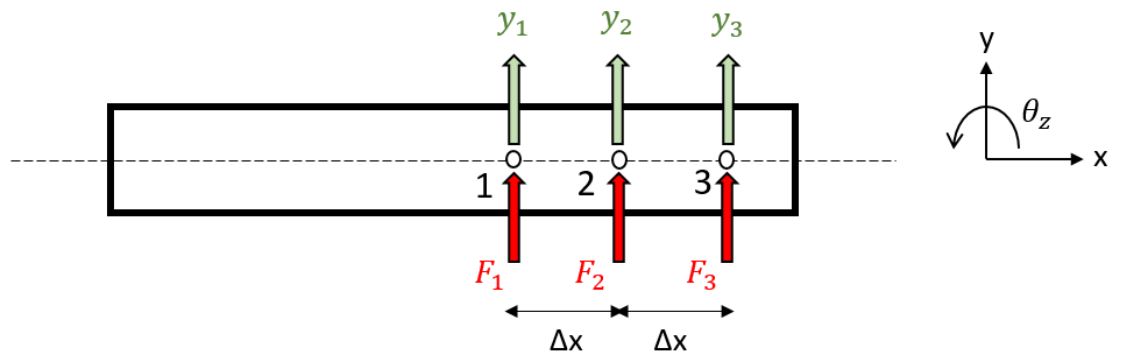


Figure 2-5 Finite Difference Method

Duarte and Ewins [27] claim that spacing between accelerometers affects the quality of the predictions too much and sensitivity to measurement noise is regarded as being a drawback of the approach.

It is accepted that it is possible to improve the accuracy of a finite difference equation by reducing the spacing, but as spacing decreases, small errors or perturbations in the input data, such as noise or misalignment, result in large errors in the output. Therefore, it is necessary to find a solution that balances the numerical error of the finite difference equation with the perturbation propagation error from the data. Gibbons et al. [28] presented an analytical error analysis to prove the instability of the finite difference method, and then they proposed a new optimum spacing. This method requires that the structure exhibits beam-like dynamic behavior.

CHAPTER 3

JOINT DYNAMICS IDENTIFICATION IN A LUMPED MODEL AND IN BEAMS - TWO DIMENSIONAL SPACE

In this chapter, the suggested method is verified and demonstrated in three case studies. In section 3.1, the connection is identified in a discrete system. Then, in sections 3.2 and 3.3, the applications of the proposed method to two beams connected with a lap-type bolted joint is presented and the bolted joint properties are extracted in terms of stiffness and damping matrices. In section 3.2, substructures are modeled by using finite element method (FEM). Euler-Bernoulli beam elements are used in obtaining elemental stiffness and mass matrices, from which FRFs are calculated. In section 3.3, FRFs of the substructures are obtained directly by using the finite element software ABAQUS, in order to have more accurate results to verify the proposed method (ISMM). The identified joint parameters are compared with the actual values, as well as with the values identified by using FRF Decoupling method [15] without using optimization.

3.1. Identification in Discrete Model

In the first case study, in order to demonstrate and validate the proposed joint identification method, a system composed of two substructures, each has two DOFs, and connected with an elastic element is considered. Here, translational stiffness and a viscous damping element are used in modeling the joint, as illustrated in Figure 3-1.

These two elements can be combined as a joint complex stiffness which can be written as follows:

$$K^*(\omega) = (k + j\omega c) \quad (3.1)$$

Dynamic properties of the substructures and the joint are tabulated in Table 3-1. These are the values used in the work of Tol [15].

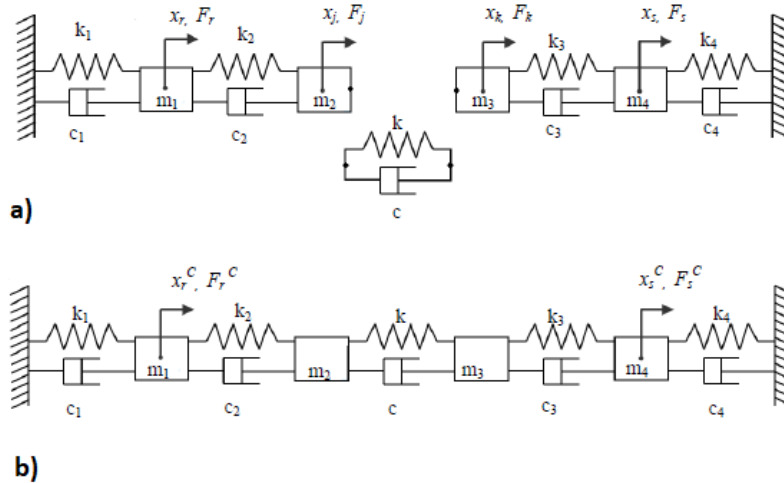


Figure 3-1 a) Two Substructures with a Flexible Joint Element b) Coupled System [15]

Table 3-1 Dynamic Properties of the Discrete Model Elements

Index	Mass, m [kg]	Stiffness, k [N/m]	Damping, c [N.s/m]
1	5	2500	3
2	3	3500	4
3	4	2000	2
4	2	2500	1
joint	-	2000	3

$K_1^*(\omega)$ which is the initially estimated complex stiffness value, is taken as

$$K_1^*(\omega) = (1000 + j\omega 1.5) \text{ N/m} \quad (3.2)$$

The receptance matrix corresponding to the connection coordinates of the system, which is represented by $[\alpha_{mm}]$ in Eqn. (2.40), with initially estimated bolt parameters can be expressed as follows

$$[\alpha_{mm}] = \begin{bmatrix} {}_I H_{jj}^C & {}_I H_{jk}^C \\ {}_I H_{kj}^C & {}_I H_{kk}^C \end{bmatrix} = \begin{bmatrix} \alpha_{22} & \alpha_{23} \\ \alpha_{32} & \alpha_{33} \end{bmatrix} \quad (3.3)$$

For the experimentally measured FRFs of the assembled structure, simulated experimental results were used. In this chapter, all calculations are done numerically. Therefore, in order to obtain simulated experimental results, predefined complex stiffness value $K_2^*(\omega)$ is used.

$$K_2^*(\omega) = (2000 + j\omega 3) N/m \quad (3.4)$$

Experimentally measured FRFs of the assembled substructure corresponding to the connection coordinates of the system can be written as follows

$$[\gamma_{mm}] = \begin{bmatrix} {}_E H_{jj}^C & {}_E H_{jk}^C \\ {}_E H_{kj}^C & {}_E H_{kk}^C \end{bmatrix} = \begin{bmatrix} \gamma_{22} & \gamma_{23} \\ \gamma_{32} & \gamma_{33} \end{bmatrix} \quad (3.5)$$

Since the only measurement required is the FRFs of the bolted system, corresponding to the connection coordinates, the size of the receptance matrices $[\alpha_{mm}]$ and $[\gamma_{mm}]$ will be 2x2.

$$[D_{mm}] = [\alpha_{mm}]^{-1}([\alpha_{mm}] - [\gamma_{mm}])[\gamma_{mm}]^{-1} \quad (3.6)$$

Eqn. (3.6) is used to calculate $[D_{mm}]$ from simulated experimental FRFs represented by $[\gamma_{mm}]$, and $[\alpha_{mm}]$, the FRFs calculated by using initially estimated complex stiffness $K_1^*(\omega)$ representing the bolted joint:

$$[D_{mm}] = \begin{bmatrix} j \text{ coord.} & -\Delta \\ -\Delta & k \text{ coord.} \end{bmatrix} \quad (3.7)$$

As explained in Chapter 2, after the calculation of dynamic structural modification matrix $[D_{mm}]$, adding the off-diagonal terms of it to $K_1^*(\omega)$ will give the identified complex stiffness $K^*(\omega)$ representing the joint dynamics. The real part of this value

will give the joint stiffnesses, and the imaginary part will give the damping value, combination of which represents the bolted joint.

In Figure 3-2 the comparison of the predicted FRF using initially estimated complex stiffness $K_1^*(\omega)$, and the measured FRF using $K_2^*(\omega)$ for the assembled substructure at point r are given.

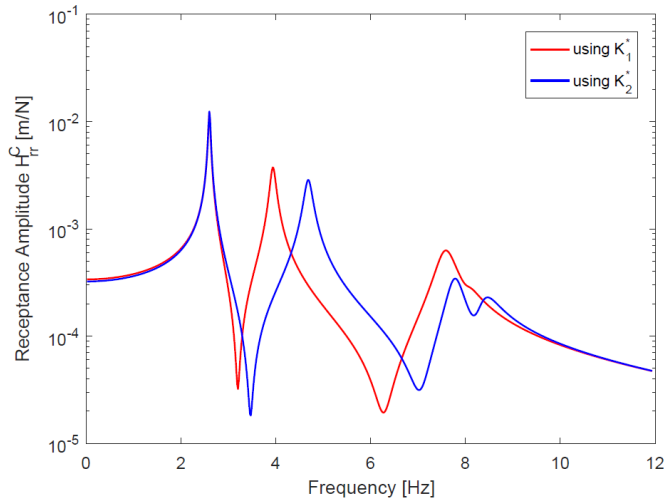


Figure 3-2 Comparison of Receptance H_{rr}^C Calculated Using Initial and Actual (Predefined) Complex Stiffness Values

Since the simulated experimental FRFs are taken exactly the same as calculated values, FRFs predicted by using identified joint parameters come out to be identical to the simulated experimental FRFs. However, in real applications, the experimental values will include some experimental errors, therefore the same identification is made by using polluted FRF values. After calculating all required FRFs of the coupled system, $\{ {}_E H_{jj}^C \}$, $\{ {}_E H_{kk}^C \}$, $\{ {}_E H_{jk}^C \}$ and $\{ {}_E H_{kj}^C \}$, they are polluted by adding $\pm 5\%$ noise to simulate real experimental measurements. The noise is generated with the "normrnd" function of MATLAB with zero mean, normal distribution and standard deviation of 5% of the maximum amplitude of the system response calculated at that frequency, as shown in Figure 3-3.

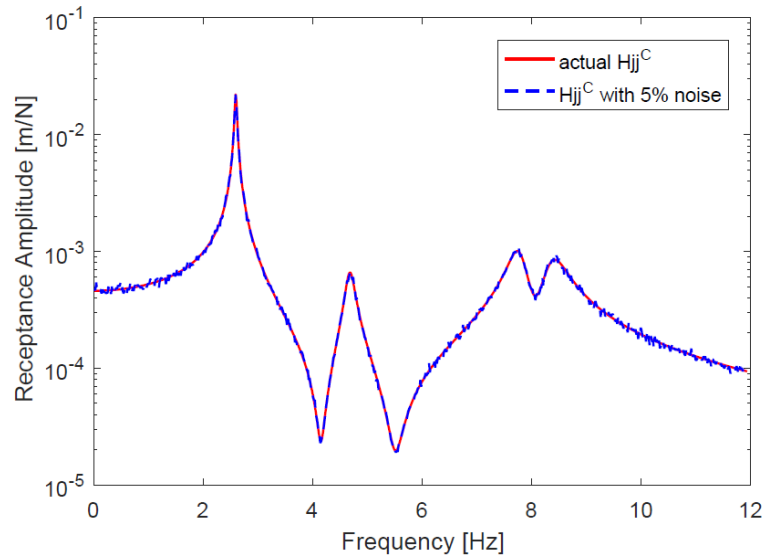


Figure 3-3 H_{jj}^C for the Coupled Structure

The joint identification can be made at any frequency in the spectrum using the associated equations. Theoretically, the same values of stiffness and damping should be found in each case. However, at certain frequencies, the calculated values vary considerably from the actual values due to the noise in measurements and sensitivity of the equations to such errors. Therefore, the frequency interval at which joint dynamics has the maximum effect on the coupled system FRF should be found first. After that, the average values in that sensitive frequency range is taken as the identified value. It can be seen from Figure 3-4 that, changing the joint stiffness has no effect on the FRF of the coupled system between 0-3 Hz (at the first mode). Hence, there is no point to make identification in that region. However, the situation is totally different at the second and third modes, therefore the joint parameters are identified at this sensitive frequency range, which is between 3-9 Hz.

The identified joint stiffness and damping values are given in Figure 3-5 and Figure 3-6, respectively, at all frequency range and also at the sensitive region.

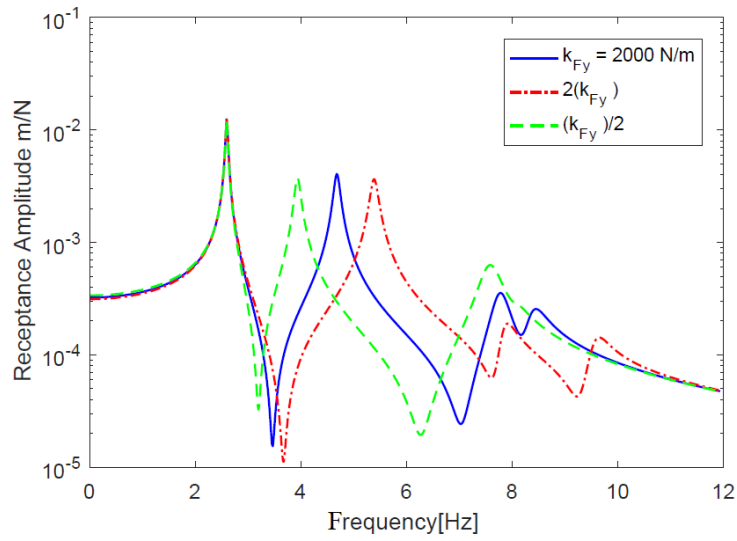


Figure 3-4 Sensitivity Analysis for Coupled System

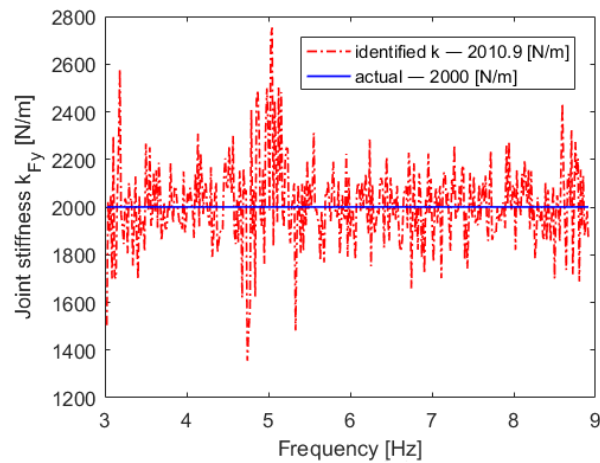
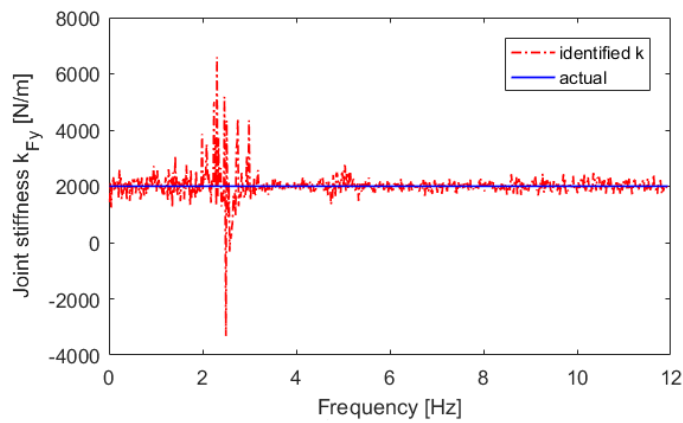


Figure 3-5 Identified Stiffness of the Joint

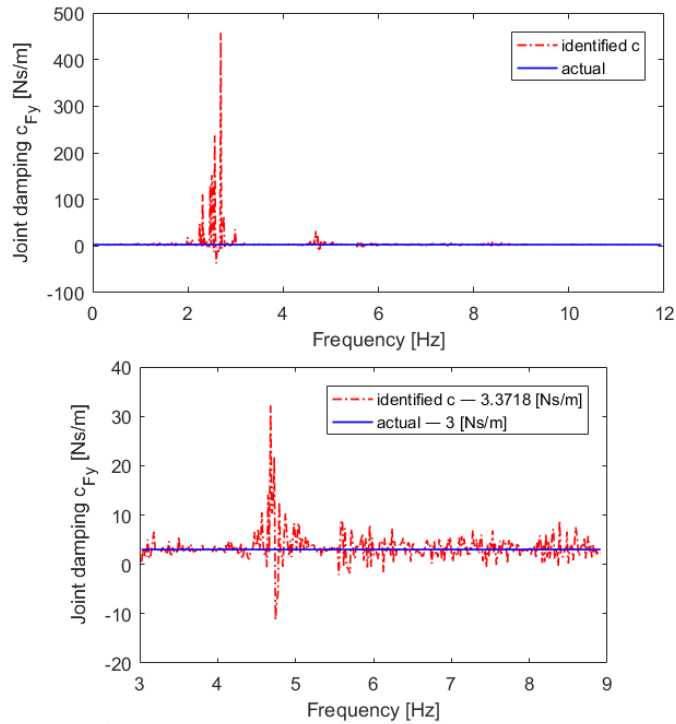


Figure 3-6 Identified Damping of the Joint

The results show that in the sensitive frequency range, which is 3-9 Hz for this case, the proposed method (ISMM) works well. When average values are calculated, results are found to be 2010.9 N/m for the stiffness and 3.37 N.s/m for damping, whereas the actual values are 2000 N/m and 3 N.s/m- respectively. The actual values deviate from 0.54 % and 12.4 %, respectively.

In Figure 3-7, the receptance of the coupled system at point r, H_{rr}^C is regenerated using identified stiffness and damping values for the joint. As can be seen from the figure, the regenerated and actual FRFs match perfectly.

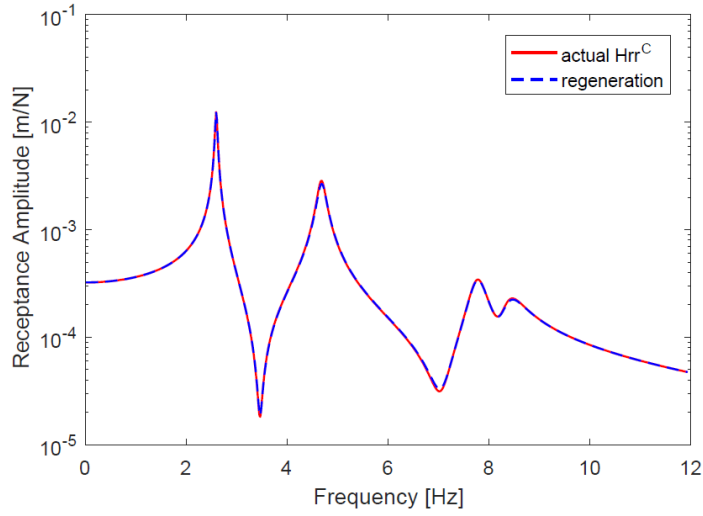


Figure 3-7 Regenerated FRF of the Coupled Structure at Point r

From now on, identified joint parameters are shown only in the sensitive regions, not in the entire frequency range.

3.2. Identification in Beams Using Finite Element Method

In the second case study, two beams connected with an elastic joint, as shown in Figure 3-8 is used. The boundary condition of substructure A is fixed-free and that of substructure B is free-free. In order to model the beams, the finite element method (FEM) is used. The mass and stiffness matrices are found by using finite element equations [15]. To model the substructures, three nodes are used for beam A and two nodes are used for beam B. For each node, two degrees of freedom displacement data are used, one translational and one rotational.

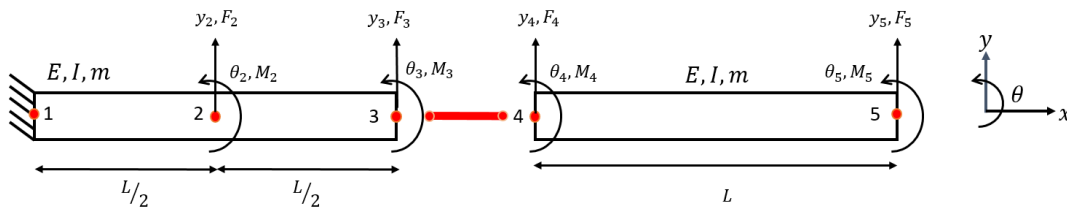


Figure 3-8 Two Beams Connection with Elastic Joint

For the beams, the same material and dimensional properties are used with Tol [15]. The complex stiffness matrix representing the elastic joint can be defined as follows

$$[K^*] = \begin{bmatrix} k_{Fy} + j\omega c_{Fy} & 0 \\ 0 & k_{M\theta} + j\omega c_{M\theta} \end{bmatrix} \quad (3.8)$$

where k_{Fy} represents the translational stiffness, c_{Fy} represents the translational damping, $k_{M\theta}$ represents the rotational stiffness and $c_{M\theta}$ represents the rotational damping properties of the joint.

As explained before, two different complex stiffness matrices are defined. One represents the initially estimated matrix which is used to calculate FRFs of the initial system, and the other represents the actual complex stiffness of the system (which needs to be identified). The second complex stiffness matrix is used to calculate the FRFs which represent the measured FRFs.

Complex stiffness matrix used for the initial system is as follows

$$[K_1^*(\omega)] = \begin{bmatrix} 10^6 + j\omega 25 & 0 \\ 0 & 10^3 + j\omega 5 \end{bmatrix} \quad \begin{bmatrix} N/m & \\ & Nm/rad \end{bmatrix} \quad (3.9)$$

The receptance matrix corresponding to the connection coordinates of the system with initially estimated bolt parameters can be expressed as

$$[\alpha_{mm}] = \begin{bmatrix} {}_I H_{jj}^c & {}_I H_{jk}^c \\ {}_I H_{kj}^c & {}_I H_{kk}^c \end{bmatrix} = \begin{bmatrix} [\alpha_{33}] & [\alpha_{34}] \\ [\alpha_{43}] & [\alpha_{44}] \end{bmatrix} \quad (3.10)$$

and complex stiffness matrix used in the computation of the simulated experimental values is as follows

$$[K_2^*(\omega)] = \begin{bmatrix} 6 * 10^6 + j\omega 50 & 0 \\ 0 & 5 * 10^3 + j\omega 15 \end{bmatrix} \quad (3.11)$$

Simulated experimental FRFs of the assembled substructure obtained by using $[K_2^*(\omega)]$, for the connection coordinates of the system can be written as

$$[\gamma_{mm}] = \begin{bmatrix} {}_E H_{jj}^C & {}_E H_{jk}^C \\ {}_E H_{kj}^C & {}_E H_{kk}^C \end{bmatrix} = \begin{bmatrix} [\gamma_{33}] & [\gamma_{34}] \\ [\gamma_{43}] & [\gamma_{44}] \end{bmatrix} \quad (3.12)$$

Again, the only measurement required is the FRFs of the coupled structure corresponding to the connection coordinates, and therefore the size of the receptance matrices $[\alpha_{mm}]$ and $[\gamma_{mm}]$ will be 4 x 4, since the joint model is composed of both translational and rotational parameters.

The comparison of the receptance values obtained for the coupled systems at points r and s, by using initially estimated and actual complex stiffness matrices are shown in Figure 3-9.

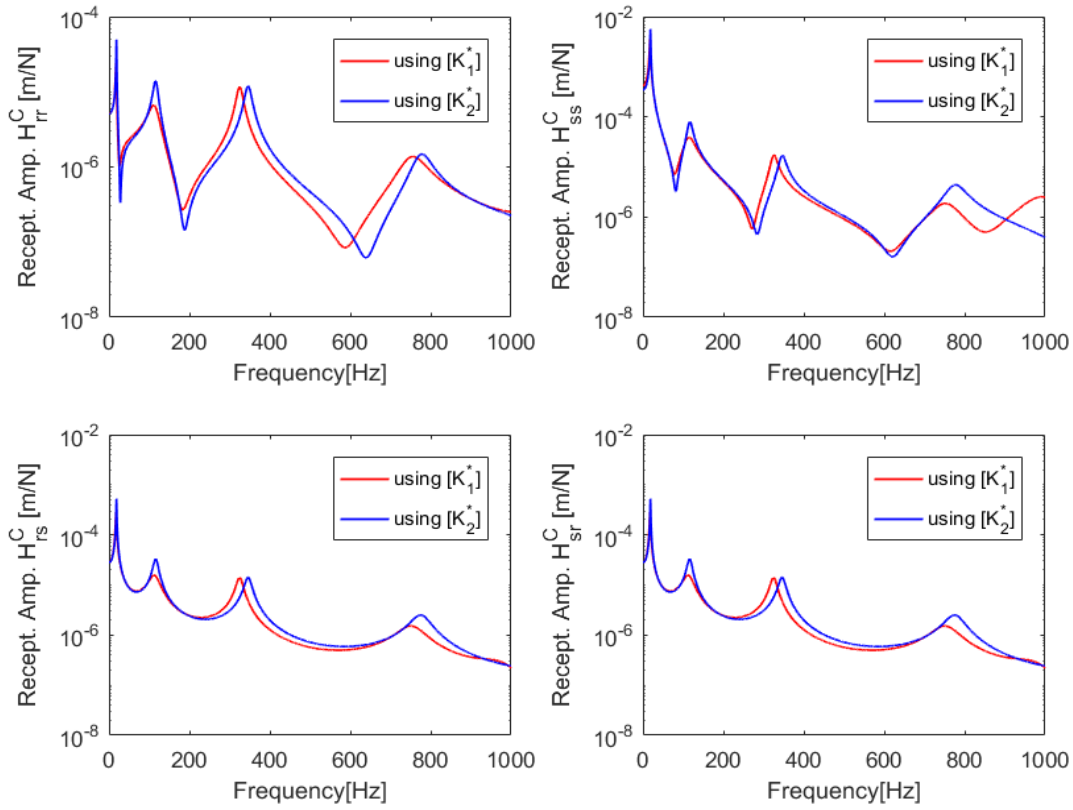


Figure 3-9 Receptances at Points r and s

After calculating all required FRFs of the coupled system, $[_E H_{jj}^C]$, $[_E H_{kk}^C]$, $[_E H_{jk}^C]$ and $[_E H_{kj}^C]$, they are polluted with $\pm 5\%$ noise in order to simulate experimental

measurements. FRFs of the coupled system are directly multiplied with uniformly distributed data with a mean of 1 with a 5% standard deviation. The noise is generated with “rand” function of MATLAB. Noise contamination is uniform in all regions of the FRF curve, as in Figure 3-10.

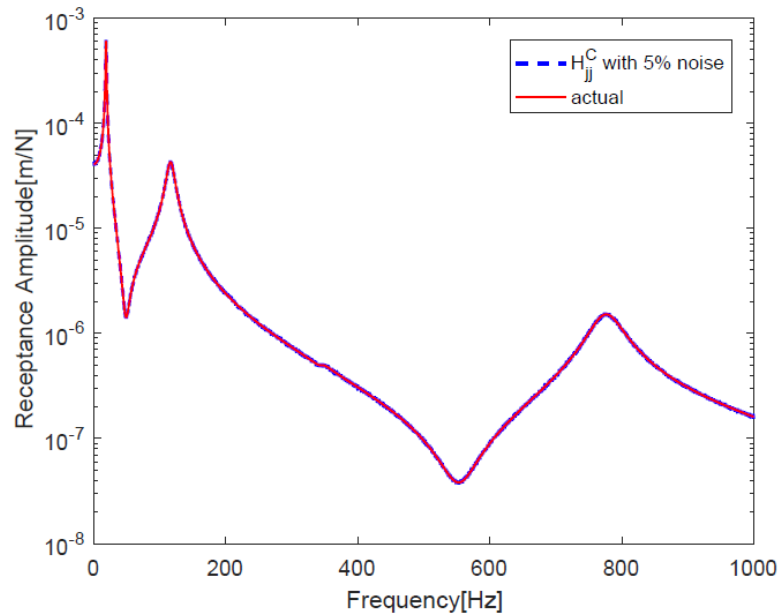


Figure 3-10 H_{jj}^C for the Coupled Structure

As discussed in the first case study, to identify joint properties, we should examine the frequency regions where changing joint properties affect the response of the coupled system most. Then, the joint properties are identified by taking an average of the results in that range of frequency.

In this case study, the following ranges are used in the identification of the joint properties: 200-900 Hz for the translational joint properties and 15-200 Hz for the rotational joint properties, after studying the effects of joint stiffnesses on FRFs in Figure 3-11 and Figure 3-12.

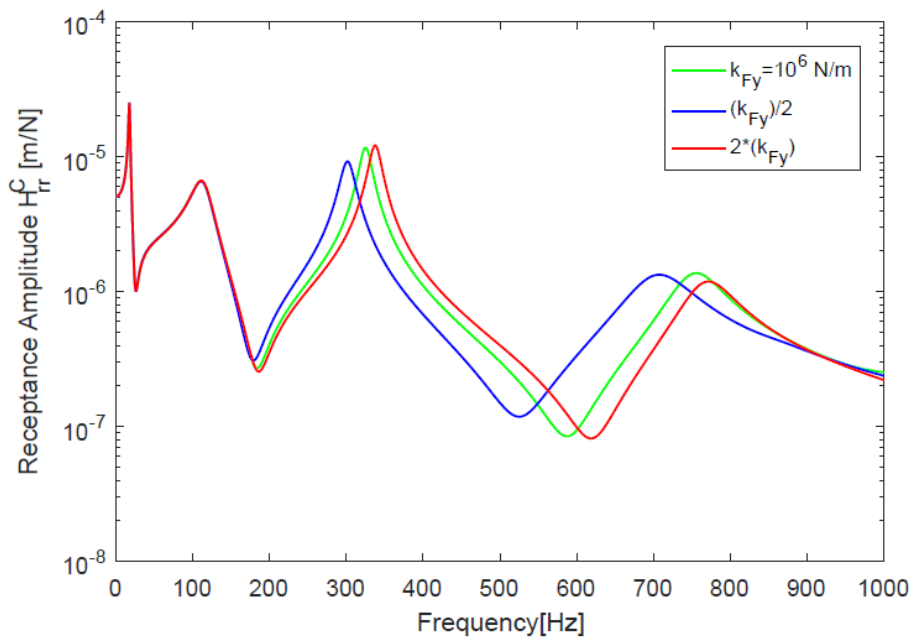


Figure 3-11 Coupled Structure Receptance Sensitivity to k_{Fy}

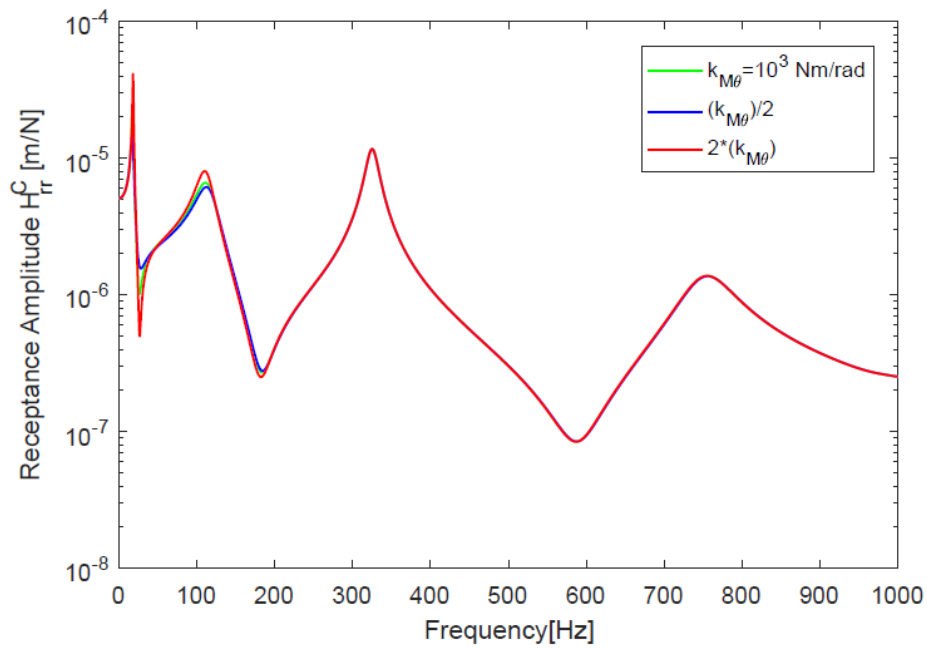


Figure 3-12 Coupled Structure Receptance Sensitivity to $k_{M\theta}$

Identified joint stiffnesses and damping values for translational and rotational DOFs are given in Figure 3-13 and Figure 3-14, respectively.

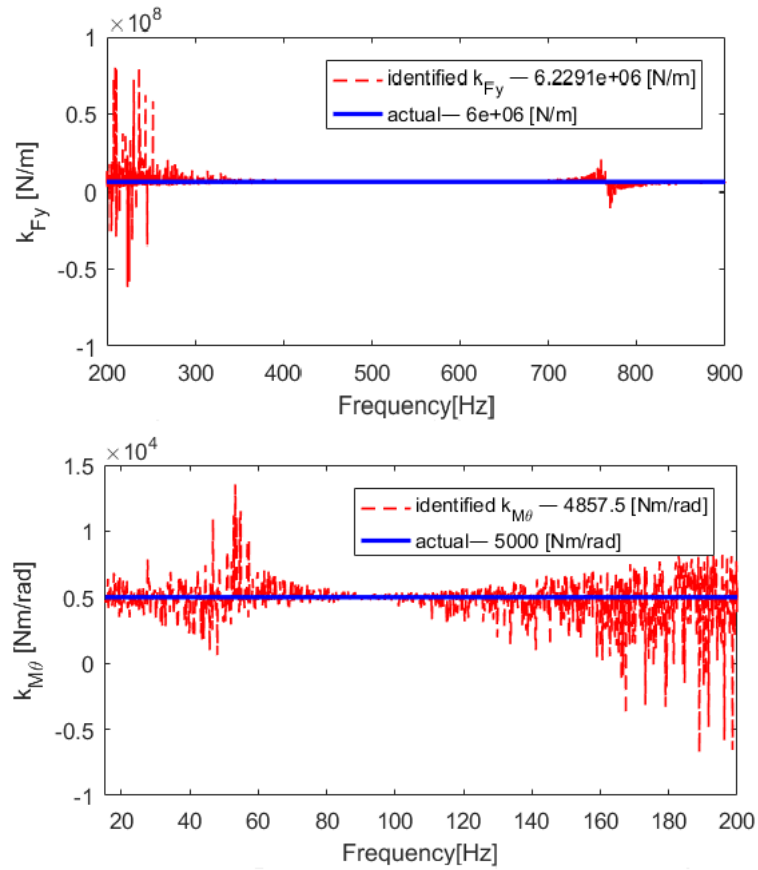


Figure 3-13 Identified Translational and Rotational Stiffnesses Representing the Joint

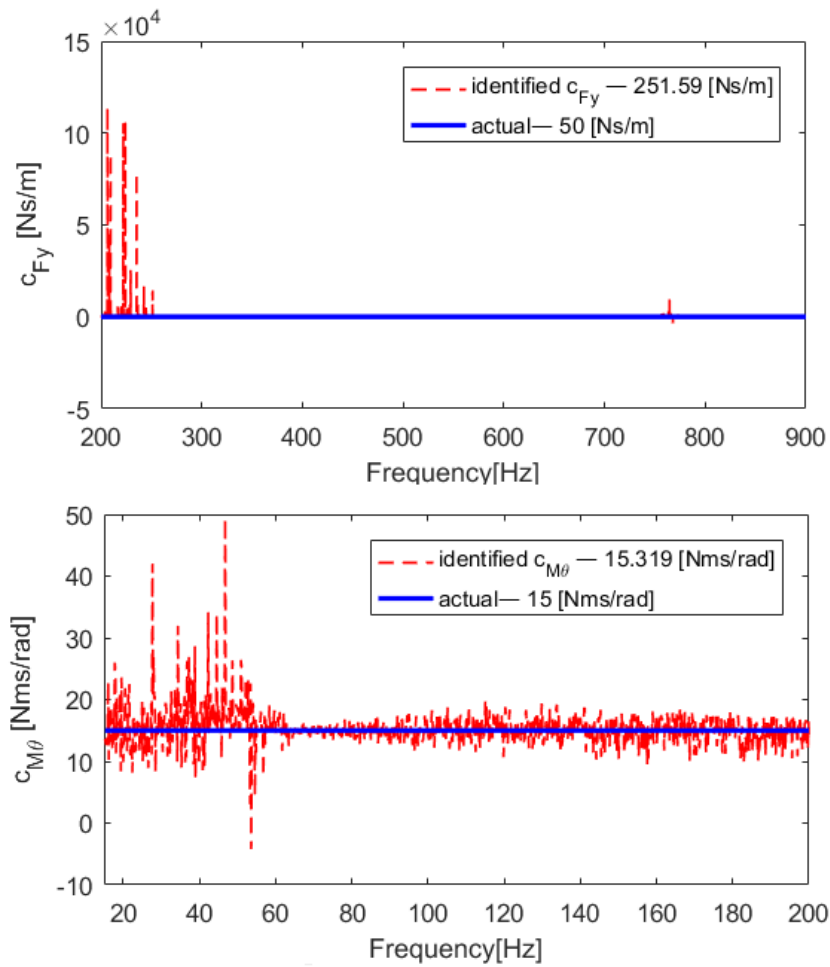


Figure 3-14 Identified Translational and Rotational Damping Representing the Joint
 The joint parameters identified by using proposed method and the percentage differences from the actual values are given in Table 3-2.

Table 3-2 Identified Joint Properties

	k_{Fy} [N/m]	c_{Fy} [Ns/m]	$k_{M\theta}$ [Nm/rad]	$c_{M\theta}$ [Nms/rad]
Actual values	$6 * 10^6$	50	5000	15
Identified values	$6.23 * 10^6$	251.59	4857.5	15.32
Error (%)	3.83	-403.2	-2.85	-2.13

3.3. Identification in Beams Using Finite Element Software

In this section, the application of the proposed method to two beams connected with a lap-type bolted joint is presented. As illustrated in Figure 3-15, substructure A has fixed-free boundary conditions and substructure B has free-free boundary conditions. Points j and k represent joint coordinates at substructures A and B, respectively. Point s is tip point of the coupled structure and point r is the middle point of the substructure A.

Each substructure is modeled with 5 mm length beam elements using finite element software. In order to model beams, two-dimensional beam elements are used which is called B21 in ABAQUS. B21 is a linear, Euler-Bernoulli type beam element. Rectangular cross-section is assigned to these elements. Global mesh size is 1 mm, therefore for the meshing, 300 elements are used for beam A and 225 elements are used for beam B. Each node has 3 DOFs. For the boundary condition of clamped beam, “encastre” type is selected. Since the FEM model is two dimensional, we are able to obtain both translational and rotational displacement data of the nodes.

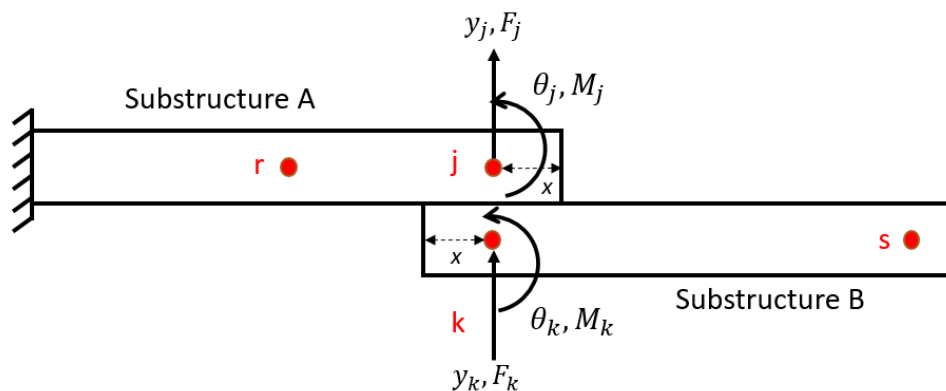


Figure 3-15 Substructures Coupled with a Joint

Data used to model the beams are given in Table 3-3.

Table 3-3 Material and Geometric Properties of Beams

Material properties		Beam properties	
Density (kg/m^3)	$\rho = 2700$	Beam width (m)	$w = 0.025$
Modulus of elasticity (N/m^2)	$E = 67.10^9$	Beam height (m)	$h = 0.006$
Structural Damping	0.01	Length (m)	$L_A = 0.3, L_B = 0.225$

This system is modeled in ABAQUS to see the dynamic response of the coupled structure. In order to simulate the bolted joint, translational and rotational spring-damping elements connected in parallel are used at the matting section, which are acting in the direction of the degrees of freedom used to define the motion of the structure. The damping in the joints is assumed viscous. Spring stiffness is defined as the force per relative displacement, while the viscous damping coefficients defined as the force per relative velocity.

As can be seen from Figure 3-16, the mode shapes of the coupled structure resemble those of a cantilever beam, as expected. Therefore, it can be said that to model joint properly, both translational and rotational parameters have to be used.

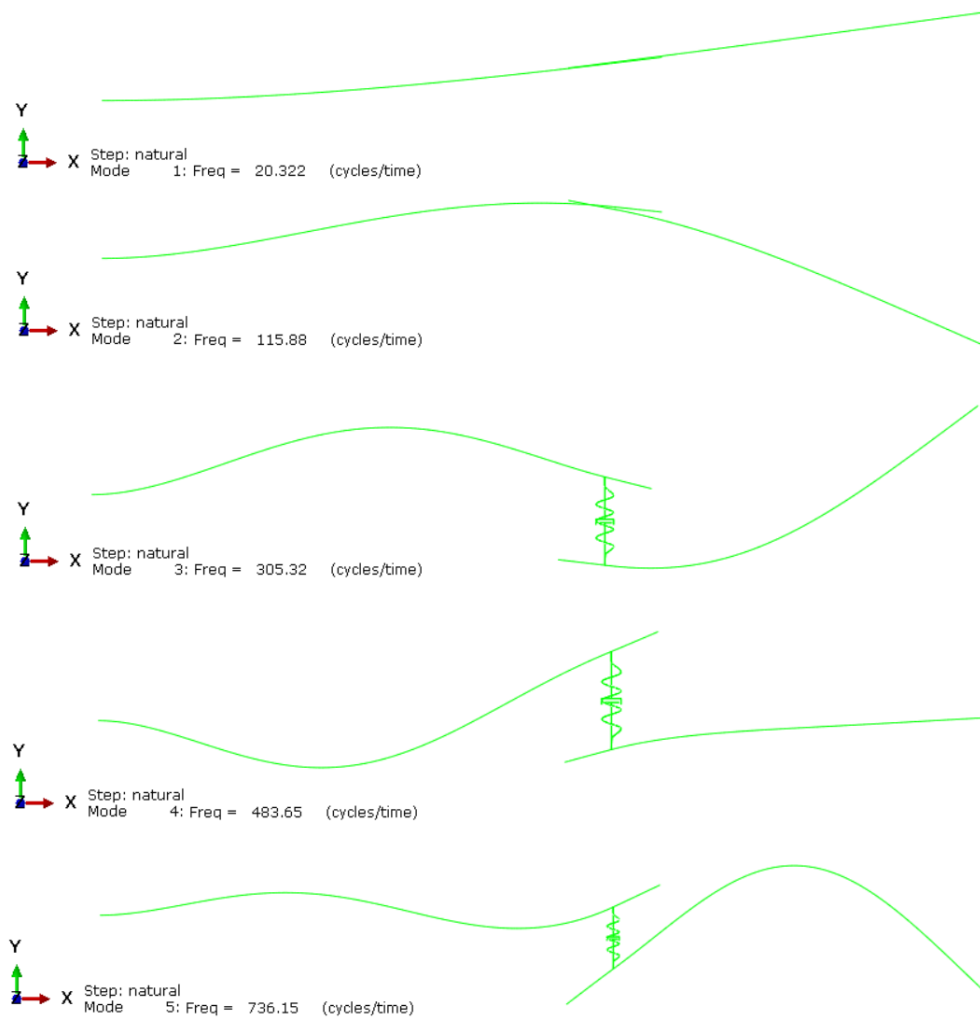


Figure 3-16 Mode Shapes of the Coupled Structure

In this joint model, both rotational and translational joint parameters are used in the complex joint stiffness matrix, as in the previous case study. In order to increase the difference between FRFs at the tip point s in the coupled system where the initially estimated complex joint stiffness $[K_1^*(\omega)]$ is used, and in the actual system which assumed to have the complex joint stiffness $[K_2^*(\omega)]$, considerably different complex stiffness values are used in this case study as shown below.

Complex stiffness matrix used in the initial system:

$$[K_1^*(\omega)] = \begin{bmatrix} 10^5 + j\omega 5 & 0 \\ 0 & 10^3 + j\omega 0.5 \end{bmatrix} \quad (3.13)$$

and complex stiffness matrix used in the actual system (the system of which response is taken as simulated experimental values) is as follows:

$$[K_2^*(\omega)] = \begin{bmatrix} 6 * 10^5 + j\omega 20 & 0 \\ 0 & 5 * 10^3 + j\omega 1.5 \end{bmatrix} \quad (3.14)$$

The elements of the complex stiffness matrix representing the bolted joint are defined in Eqn. (3.8).

The comparison of the receptance amplitudes in both coupled systems (coupled by using initially estimated joint parameters and by using the actual values) at points s and r are shown in Figure 3-17 and Figure 3-18, respectively. Compared to previous case study, the difference is deliberately increased to see the performance of the method when the initially estimated complex stiffness matrix is considerably different from the actual value. As a matter of fact, various different initial estimates are used to investigate the performance of the method, and it is observed that the initial estimate does not affect the performance of the method.

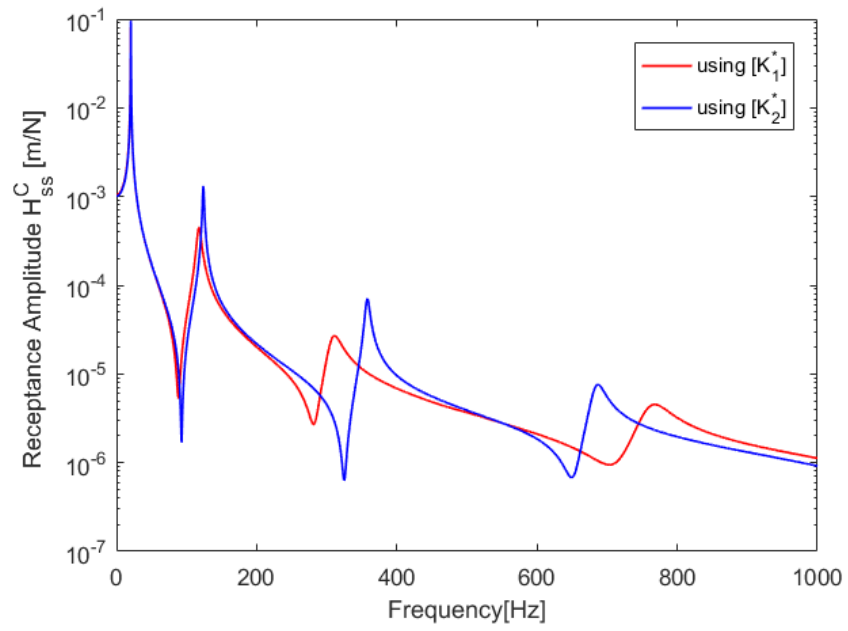


Figure 3-17 Translational Receptance Values for Point s

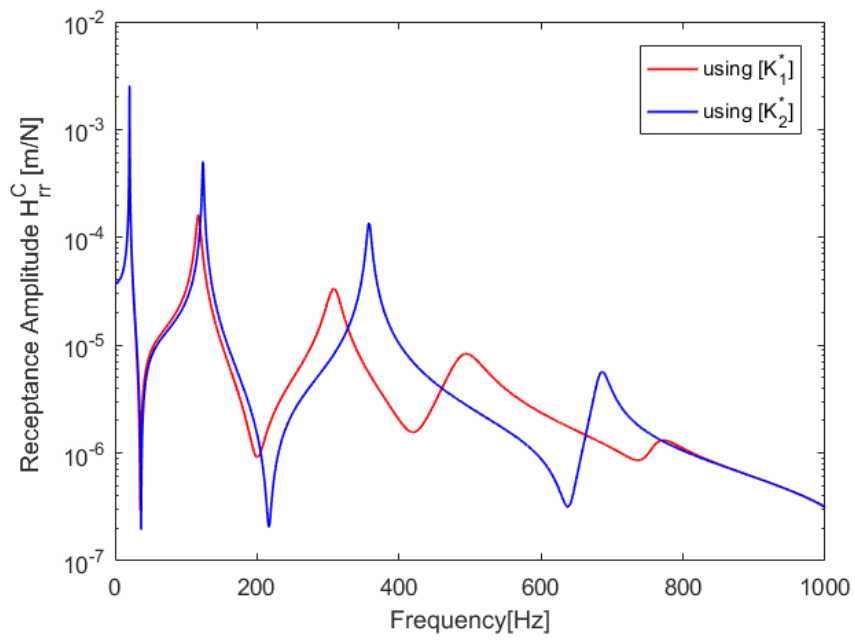


Figure 3-18 Translational Receptance Values for Point r

The sensitivity of FRFs to translational and rotational joint stiffnesses in different frequency regions are determined before the identification of joint parameters. In order to find sensitive frequency regions, FRFs of the coupled system are used.

The sensitivities of FRFs of the tip point s to joint translational and rotational stiffnesses are shown in Figure 3-19 and Figure 3-20, respectively.

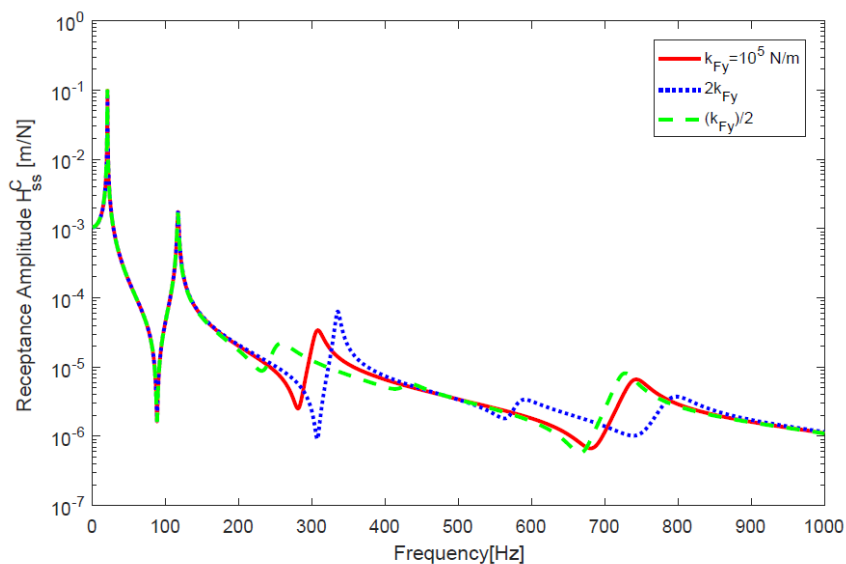


Figure 3-19 Sensitivity of System Response at Point s to k_{FY}

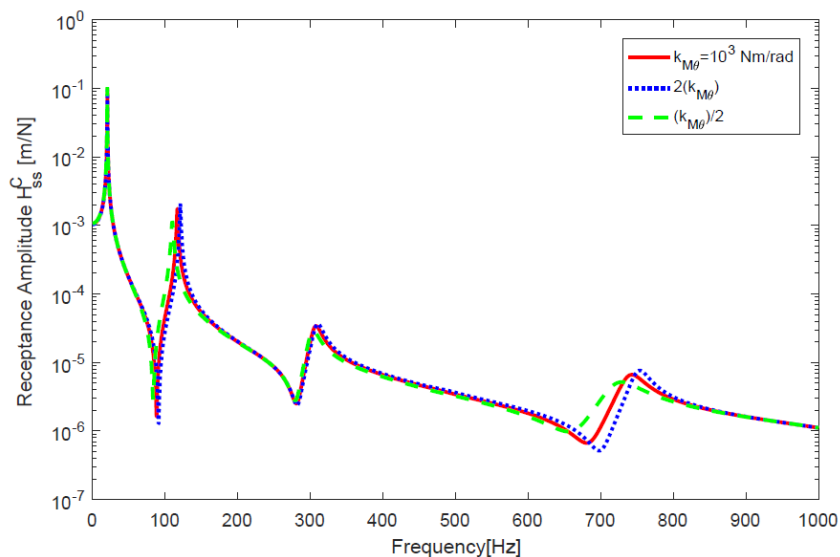


Figure 3-20 Sensitivity of System Response at Point s to $k_{M\theta}$

From the Figure 3-19 and Figure 3-20, it can be seen that, for the translational joint parameters, the sensitive frequency regions are between 200-400 Hz and between 600-800 Hz, and that for the rotational joint parameters is between 650-800 Hz.

On the other hand, if we examine sensitivity of FRFs at point r , we can see that the sensitive frequency regions may show some variation, as can be seen in Figure 3-21 and Figure 3-22.

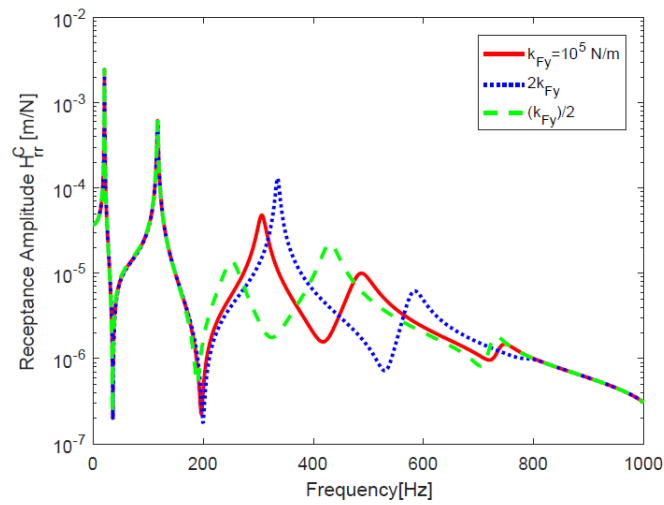


Figure 3-21 Sensitivity of System Response at Point r to k_{Fy}

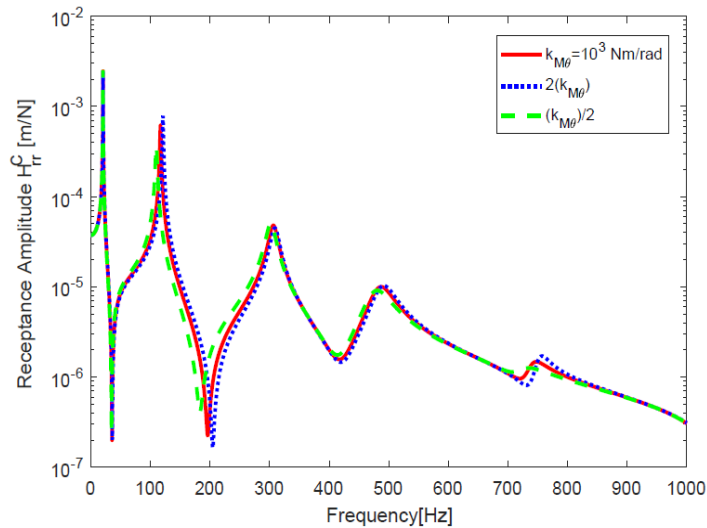


Figure 3-22 Sensitivity of System Response at r to $k_{M\theta}$

From Figure 3-21 and Figure 3-22, it can be seen that, for the translational joint parameters, the sensitive frequency region is between 200-800 Hz, and that for the rotational joint parameters is between 700-800 Hz. As can be seen there are slight changes in sensitive frequency regions, and since identified values are obtained by averaging results in the sensitive frequency range, changing this range will affect the identified values. The reason for selecting different frequency regions will be explained in the next section in more detail; but in brief, FRFs of different points may be sensitive to each joint parameter at different frequency regions.

Since the equations used for identification in both methods are exact, when exact FRFs calculated for the actual system are used as simulated experimental results, it is expected to identify the joint parameters accurately. Any deviation, which may be considerably high depending on the approach used, is due to experimental measurement errors. Therefore, in order to simulate experimental measurements realistically, the calculated FRFs for the actual system are polluted with 5% noise as described in the previous case studies. By using the polluted values of FRFs calculated for the actual system and employing Eqn. (3.6), the structural modification matrix required to modify the initial estimates for the joint parameters is calculated. Then, the off-diagonal terms of the structural modification matrix are used to modify the initially estimated complex joint stiffness matrix. Thus, the identification of joint parameters is performed.

For translational joint parameters, the identified values by using different frequency ranges, which are 200-400 Hz and 200-800 Hz, are shown in Figure 3-23 and Figure 3-24.

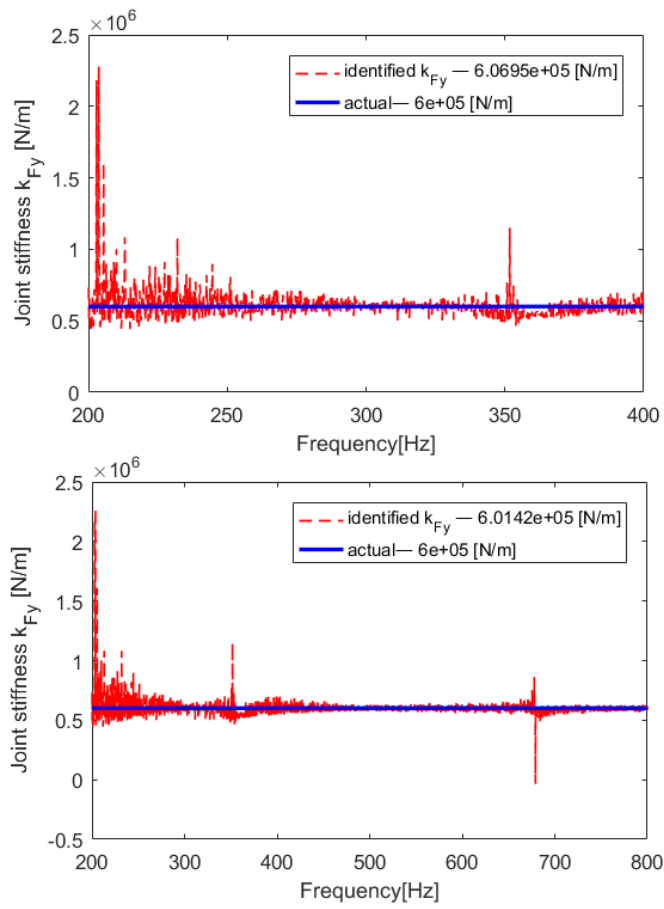


Figure 3-23 Identified value of Translational Stiffness by Using Different Frequency Regions

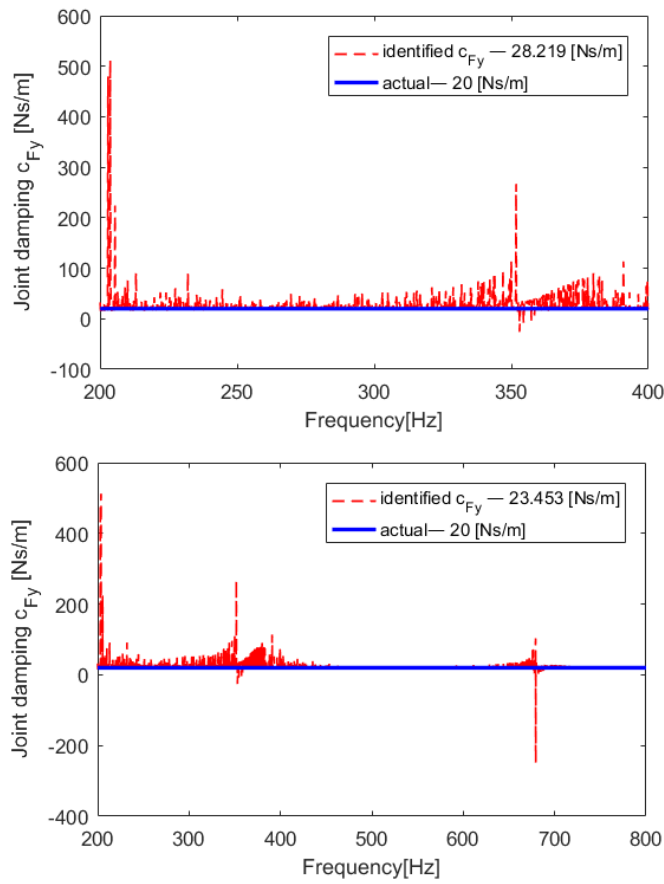


Figure 3-24 Identified value of Translational Damping by Using Different Frequency Regions

For rotational joint parameters, the identified values by using different frequency ranges, which are 650-800 Hz and 700-800 Hz, are shown in Figure 3-25 and Figure 3-26.

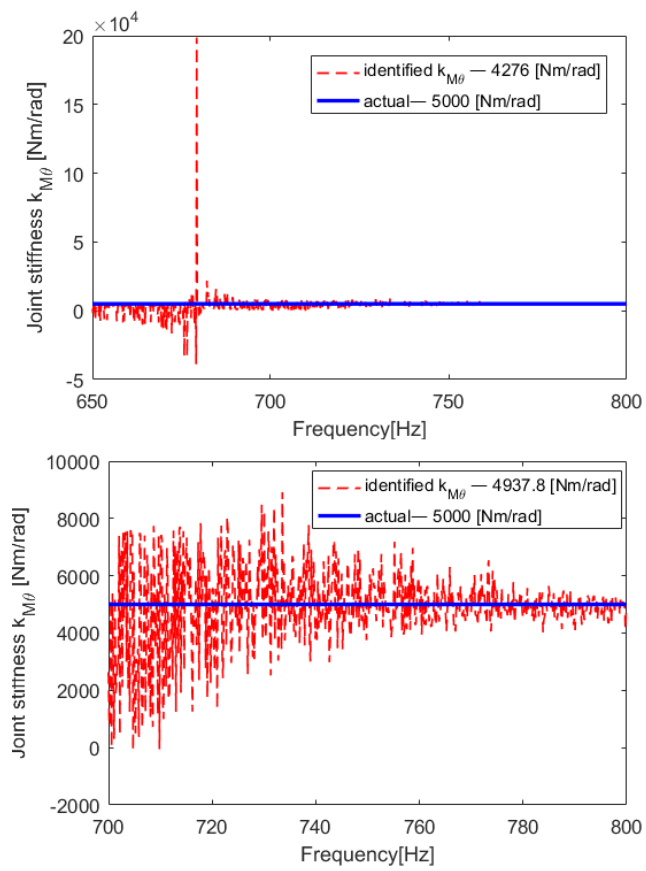


Figure 3-25 Identified value of Rotational Stiffness by Using Different Frequency Regions

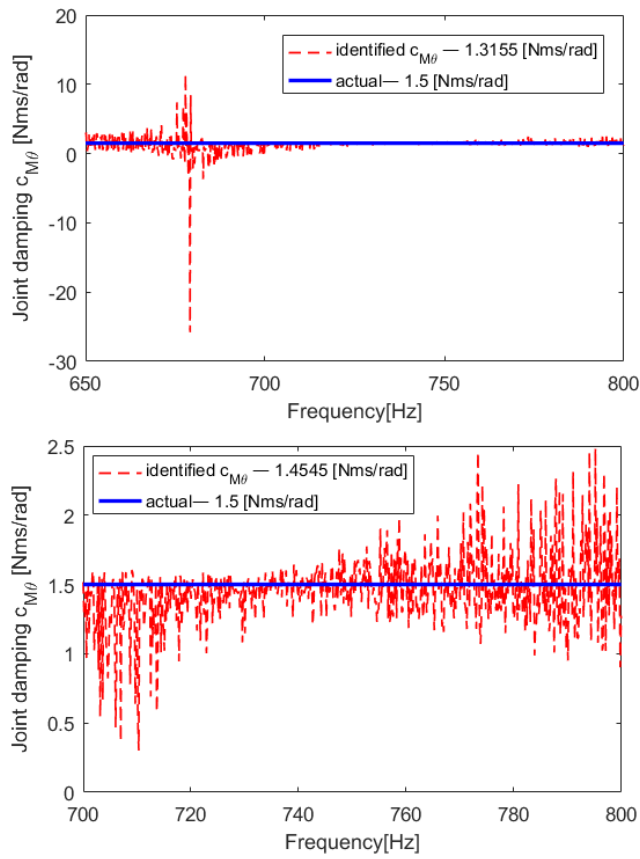


Figure 3-26 Identified value of Rotational Damping by Using Different Frequency Regions

Now, in order to study the effect of the noise on the identification results, FRFs of the coupled structure, $[{}^E H_{jj}^C]$, $[{}^E H_{kk}^C]$, $[{}^E H_{jk}^C]$ and $[{}^E H_{kj}^C]$, are polluted with different levels of random noise (5% and 10%). The identification results are compared in Figure 3-27 and Table 3-4.

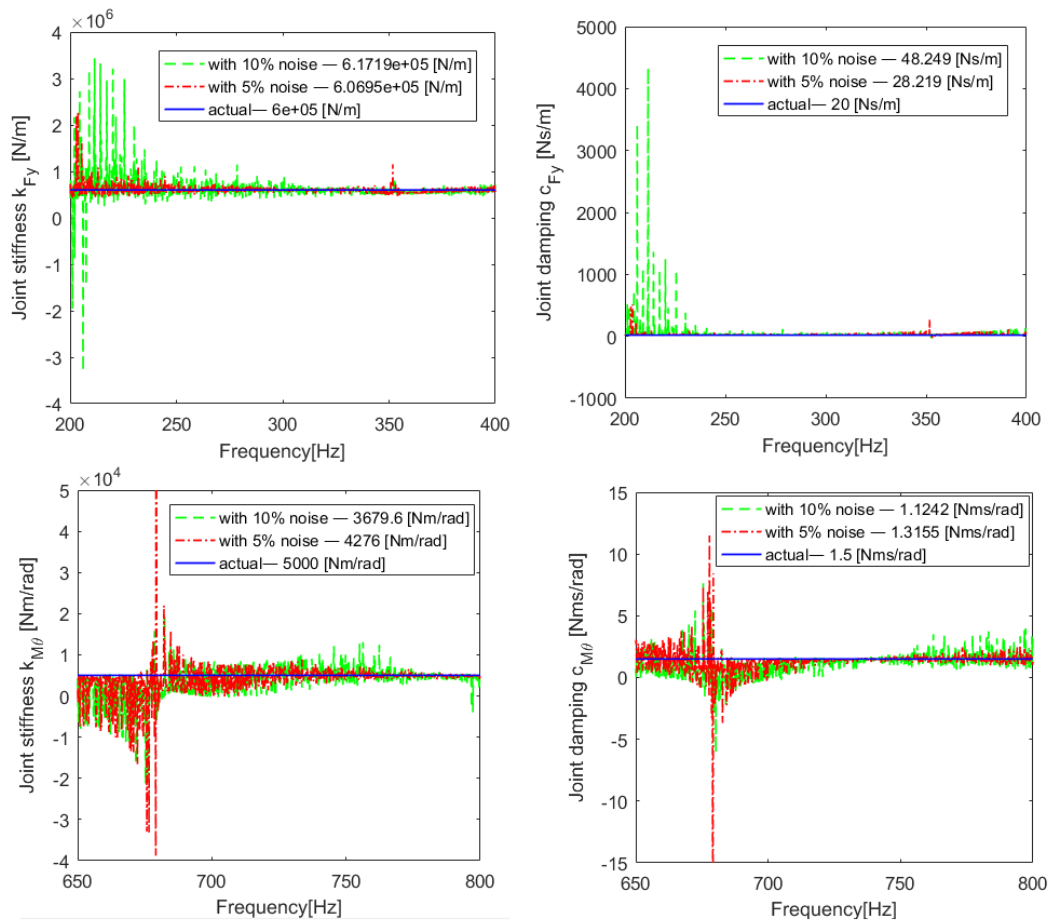


Figure 3-27 Effects of Measurement Errors on Identified Joint Parameters

Table 3-4 Identified Joint Parameters and Percentage Errors for Different Noise Level Representing Measurement Errors

	k_{Fy} [N/m]	c_{Fy} [Ns/m]	$k_{M\theta}$ [Nm/rad]	$c_{M\theta}$ [Nms/rad]
Actual Values	$6 * 10^5$	20	5000	1.5
Identification with 10 % noise	$6.172 * 10^5$	48.249	3679.6	1.124
Error (%10)	2.87	141.24	-26.42	-25.07
Identification with 5 % noise	$6.069 * 10^5$	28.219	4276	1.315
Error (%5)	1.15	41.09	-14.48	-12.33

3.3.1. Comparison of Two Methods when Applied to 2D Structural Systems

As explained in Chapter 2, if FRF matrices of the substructures and that of the coupled structure at any frequency are available, then the FRF Decoupling method can be used and joint identification can be achieved by using any of the four equations, Eqns. (2.53 - 2.56). Each equation uses FRFs of the coupled system for different points. For example, while Eqn. (2.53) uses H_{rr}^C for identification, Eqn. (2.56) uses H_{ss}^C . It was observed that the performance of the equations is different and the most accurate results were obtained when Eqn. (2.53) was used.

However, it was recommended in [15] to use Eqn. (2.56) for identification since it is more practical considering the experiments applicability. Therefore, when sensitivity of the receptance of the coupled system to the joint properties is investigated, FRFs of the related point should be considered in determining the sensitive frequency region. However, in the proposed method (ISMM) there is only one equation to apply, and therefore in finding the sensitive frequency region it may be reasonable to investigate the variation of the response with joint parameters for the points where maximum response is observed.

In FRF Decoupling method, Tol and Özgüven [15] studied the accuracy of using different decoupling equations and concluded that to increase the accuracy of the identification the equation given below is to be used in finding the complex stiffness matrix representing the joint dynamics

$$[K^*] = \left[[H_{ks}] \cdot \left[[H_{ss}] - [H_{ss}^C] \right]^{-1} \cdot [H_{sk}] - [H_{jj}] - [H_{kk}] \right]^{-1} \quad (3.15)$$

In that work Eqn. (3.15) was employed by using the translational and rotational FRFs at the tip point (point s) of the coupled structure. This approach requires the RDOF related FRFs at the tip point, as shown in Figure 3-28. All the FRF matrices in this identification approach are of size 2 by 2.

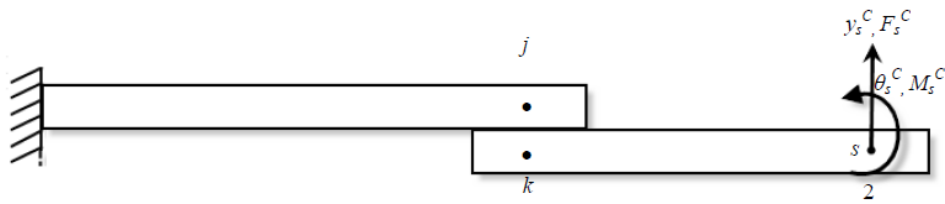


Figure 3-28 Coupled Structure [15]

An alternative way of employing the same equation by avoiding the use of RDOF related FRFs is to use more than one translational FRF at the tip point of the coupled structure, as shown in Figure 3-29. As it was observed in [15] that this approach yields more accurate results than the other approach, it was preferred in their experimental studies. However, extension of this approach to 3 dimensional model is not practical at all, since the extension of this approach to 3D model will require FRFs in more than one point in all directions, including the RDOF related ones. Therefore, the first approach which requires RDOF related FRFs as well, but only in one point, is used for the comparison.

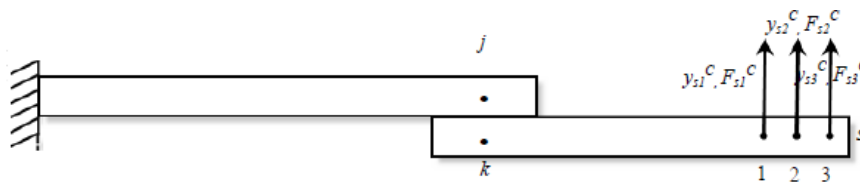


Figure 3-29 Coupled Structure [15]

The joint parameters identified by using the proposed method and the FRF Decoupling method are shown in Figure 3-30 to Figure 3-33.

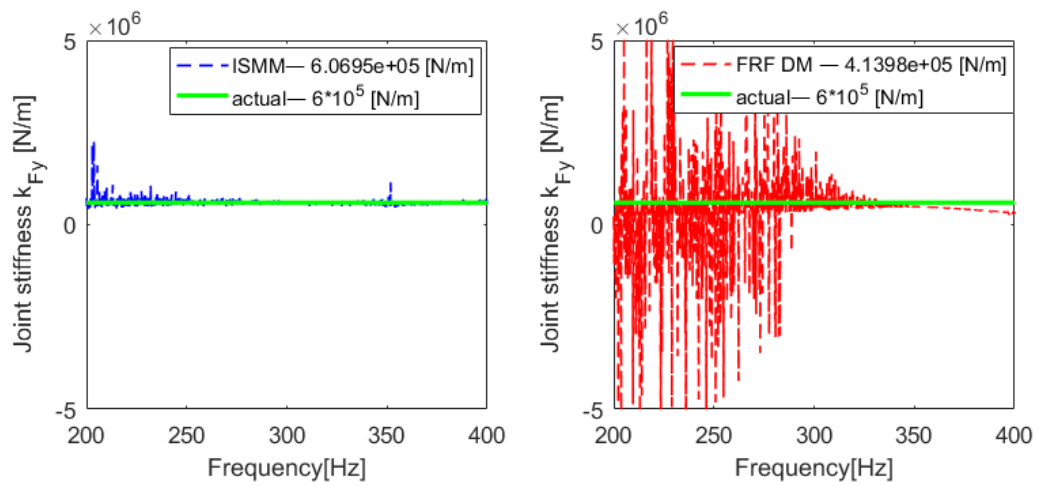


Figure 3-30 Identified Translational Stiffness Obtained by Using ISMM and FRF DM

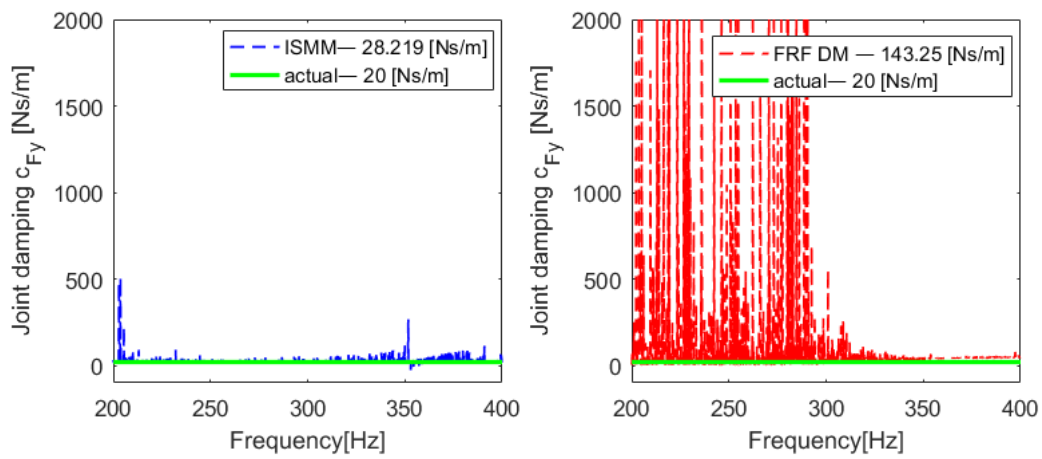


Figure 3-31 Identified Translational Damping Obtained by Using ISMM and FRF DM

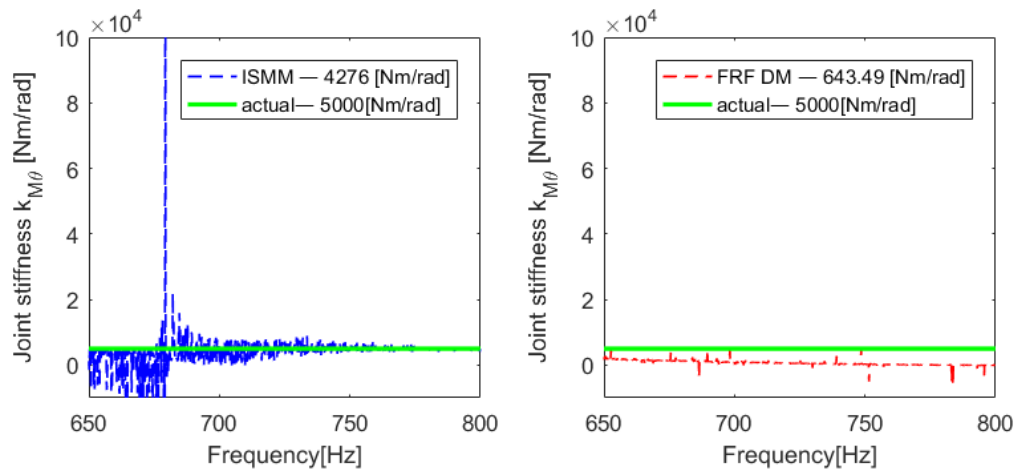


Figure 3-32 Identified Rotational Stiffness Obtained by Using ISMM and FRF DM

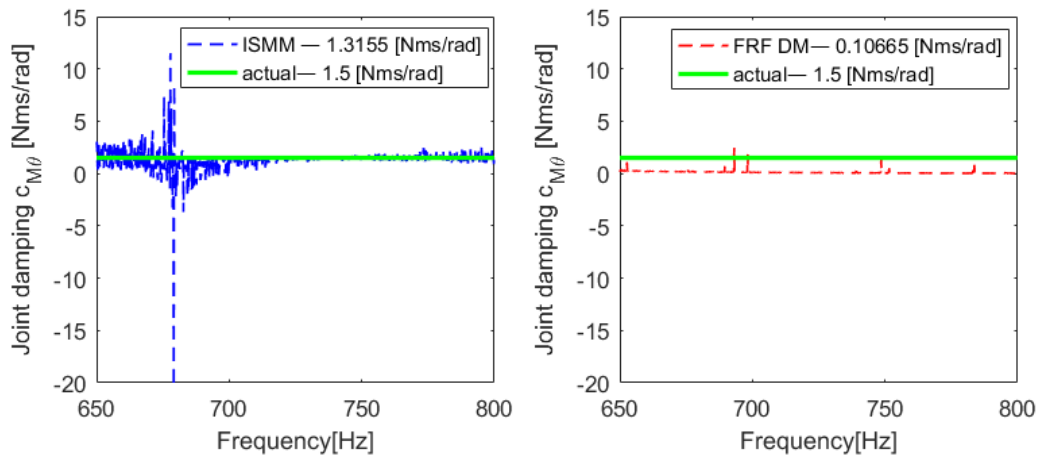


Figure 3-33 Identified Rotational Damping Obtained by Using ISMM and FRF DM

Then, the FRFs of the coupled system at the tip point s are regenerated by using the joint parameters identified, applying ISMM and FRF DM. They are compared with each other, as well as with the actual FRFs in Figure 3-34. It can be observed that ISMM gives much better results.

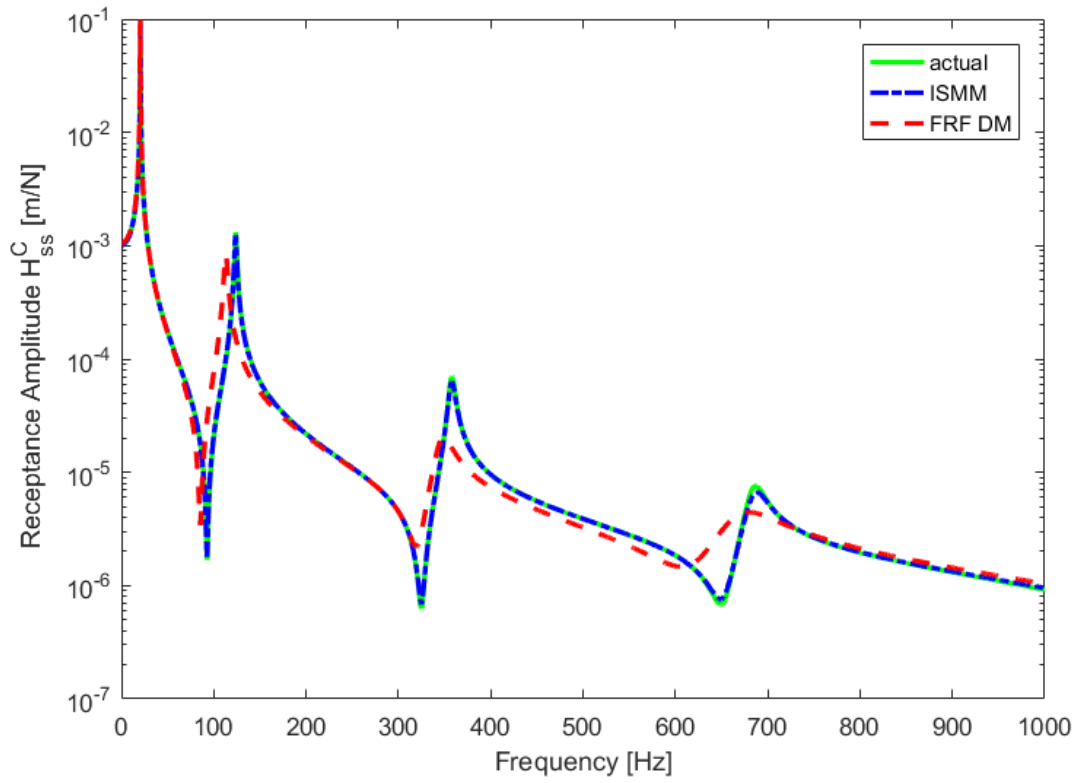


Figure 3-34 Comparison of the FRFs of the tip Point Calculated Using Joint Parameters Identified by Using ISMM and FRF DM

CHAPTER 4

IDENTIFICATION OF JOINT DYNAMICS IN BEAMS – THREE DIMENSIONAL SPACE

In this chapter, a bolted joint connecting two beams modelled in 3D space is identified. The system considered is composed of two beams: The first beam, substructure A, has fixed-free boundary conditions, and the second beam, substructure B, has free-free boundary conditions. Since substructures are modeled using three-dimensional brick elements, each node on substructures has 6 DOFs, including three translational DOFs (TDOFs) and three rotational DOFs (RDOFs). These beams are connected with a bolted joint.

In this chapter, two case studies are given. In the first case study, the bolted joint is modeled by using Spring/Dashpot elements connecting two reference points (RPs), which are located at the center of the mating surfaces. Since RPs are points, rotational displacement information can be obtained directly from the finite element software in order to obtain the FRFs representing the measured values in the simulated experiment. In the second case study, bolted joint is modeled using 3D brick elements. In this model, in order to obtain RDOFs related FRFs, finite difference formulation is used, and therefore some calculations must be done. For both case studies, a complete joint model includes three translational and three rotational DOFs stiffness and damping parameters. Therefore, two different finite element simulations were conducted to investigate the effectiveness of the proposed identification method.

In section 4.1, finite element modeling of the system by using Spring/Dashpot - elements representing the bolted joint is given. Then, in section 4.2, finite element modeling of the system by using three-dimensional model of the bolted joint is presented. In section 4.3, the model used in obtaining simulated experimental data,

validation and demonstration of the proposed method is given. Comparison of the two methods also studied in this section.

4.1. Finite Element Simulation of Coupled Beams by Using Spring/Dashpot Elements for Bolted Joint

In this section, the details of the finite element simulation of coupled beams by using Spring/Dashpot elements for bolted joint is given. In this model, two substructures are connected to each other, as shown in Figure 4-1. Two beams are taken identical. The width of the beams is 0.025 m, the height of the beam cross-sections is 0.006 m, the length of the beams is 0.3 m, and the damping of the beams is taken structural damping with a loss factor of 0.01. The material of the beams is aluminum with a modulus of elasticity (E) of 70 GPa and density of (ρ) 2700 kg/m^3 .

Beams have meshed with C3D8R (eight-node brick element with reduced integration) element which is a general-purpose linear brick element with 3 DOFs at each node. For each beam, the number of elements used is 1030.

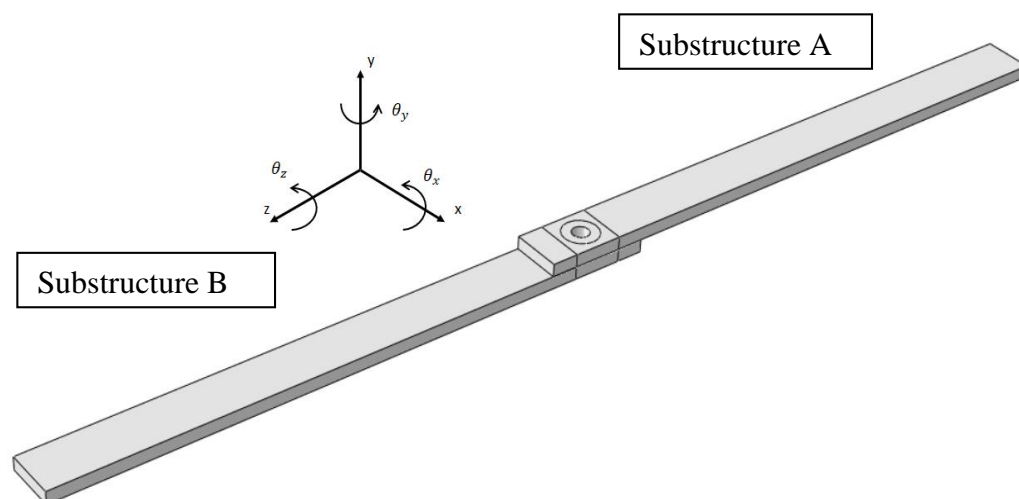


Figure 4-1 Coupled Structure Finite Element Model

The substructure A is clamped, and substructure B is attached to it through the joint. As shown in Figure 4-2, Surface 1 represents the surface of substructure A where the bolt head is in contact, and Surface 2 represents the surface of substructure B where the nut is in contact. Reference points (RPs) are assigned to the centers of the surfaces where the bolt head and the nut are in contact with the beams.

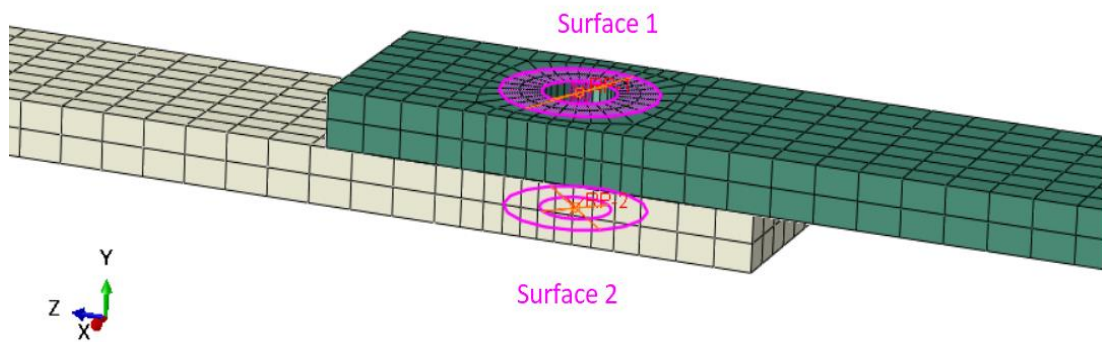


Figure 4-2 Contact Surfaces

In this simplified model, modeling of a bolt is much simpler than solid modeling because there is no need to define contact pairs. The bolt shank is modeled by using Spring/Dashpot elements for the three translational and three rotational directions. As it is shown in Figure 4-3, the nodes (RPs) are connected to the surfaces (Surface 1 and Surface 2) by means of the so-called kinematic coupling constraint. In kinematic coupling constraint, the “coupling” nodes which are the nodes on Surface 1 and Surface 2, are constrained to the rigid body motion of a single node, which are RP1 and RP2. Therefore, the associated nodes (the nodes on the surfaces) are forced to have the same displacement in all six DOF as a result of the coupling condition. After that, Spring/Dashpot elements are placed between these two RPs.

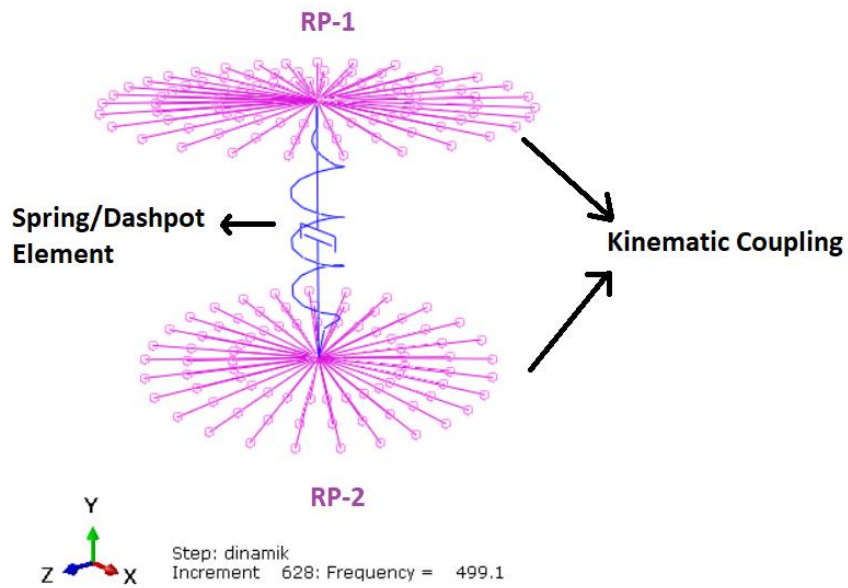


Figure 4-3 Representation of RPs and Coupling Elements

In this approach, the pretension effect is not considered for the bolt. Section cut view of the model can be seen in Figure 4-4.

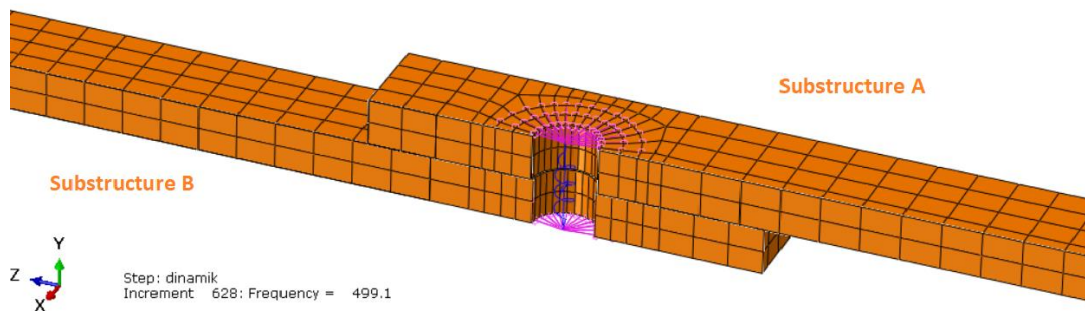


Figure 4-4 Section View of the Model

In order to fully define the joint, three translational and three rotational springs and dashpots elements are used.

4.2. Finite Element Simulation of Two Beams Coupled with a Bolted Joint by Using 3D Brick Elements

Depending on the level of accuracy required, different modeling approaches are available for the bolts in a beam connection when ABAQUS FEA is used. Among several methods, the most accurate method is modeling the bolt's entire geometry, including the components such as bolt head and nut, with solid elements. This modeling method allows contact interactions between all the elements concerned as is the case in reality. This modeling approach will be explained in Section 4.2.3. However, firstly some issues about modeling in ABAQUS, such as solver selection, will be explained.

4.2.1. Selecting Solver

In ABAQUS, two solver options are available, Standard and Explicit. In ABAQUS/Standard, convergence is checked at the end of each load increment. If the results have not converged, the size of the loading increment is reduced before another convergence attempt is made. However, for a very complicated problem, it may not be able to find a converging solution, and in that case, it will fail. Finding convergent solutions at multiple time increments in dynamic loading cases is very expensive. For that reason, ABAQUS/Explicit can be used as an alternative. It uses very small load increments/time steps, and after each load increment/time step is applied, the analysis moves on, regardless whether it converges or not. Thus, by using it, complicated problems can be solved, however it is possible to have a wrong solution. Besides, because of the very small load increments/ time steps used, computing time is much higher than Standard version. Accordingly, if the solution converges, ABAQUS/Standard results in a more accurate solution in less time. Therefore, in this study ABAQUS/Standard version is used for all analyses.

4.2.2. Description of the Finite Element Model

In order to simulate a real experimental case of two beams connected with a bolted joint as accurately as possible, so that the contact interface can be modelled better and the simulated experimental values of the required receptances can be obtained more accurately, the finite element software ABAQUS/Standard is used. It is aimed to model the bolted joint as closely as possible to a real experimental case.

The solid model, as shown in Figure 4-5 and Figure 4-6, is the most realistic finite element model of a bolted connection among other modeling methods, such as using wire elements or beam elements. In this model, in order to mesh both the beams and the bolt, three-dimensional brick elements, called C3D8R in ABAQUS are used. As mentioned before, the element is described by eight-noded, linear elements with 3 DOFs at each node. Therefore, when using a three-dimensional brick element in a model, obtaining rotational displacement information is not possible.

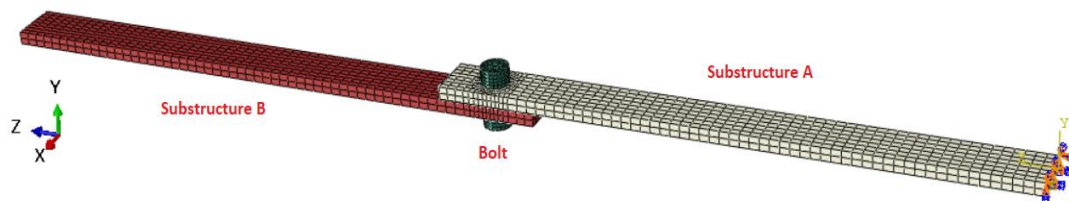


Figure 4-5 The Finite Element Modeling of Coupled Structure

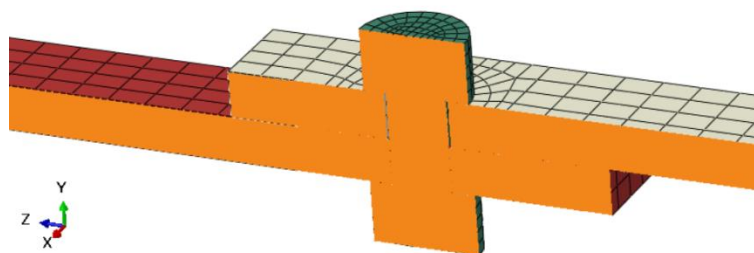


Figure 4-6 Section View of the 3D Bolted Connection

The external diameters of the bolt head and the nut are taken as those of a real M8 bolt and nut. If the bolt shank and all associated elements, such as nut, are modeled as one

part, modeling is faster because of the elimination of tying associated surfaces of the bolt as in Figure 4-7. The reason behind this simplification is that because of the high preload that is likely to exist in the bolt, it can be assumed that there would be no relative motion between the bolt and the nut. Moreover, the bolt thread was not modeled since the performance of thread is not our concern in this study.

According to [29], the small depth of the washer suggests a small variation in contact pressures, high in magnitude, and unlikely to allow any relative movement on either surface of the washer. Therefore, it is concluded not to model the washers underneath the bolt head and the nut, because adding two extra contact interface to the model would have increased the computational time considerably and would not increase the accuracy notably.

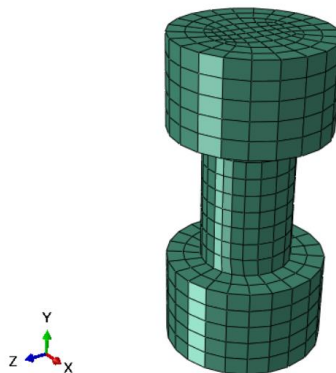


Figure 4-7 3D Modelling of Bolt Head, Bolt Shank and Nut as One Part

As stated above, this approach allows for assigning contact interactions between all relevant components/parts that come into contact in a bolted connection. In Figure 4-8 and Figure 4-9, the contact pairs between bolt and beams, and beam and beam are shown.

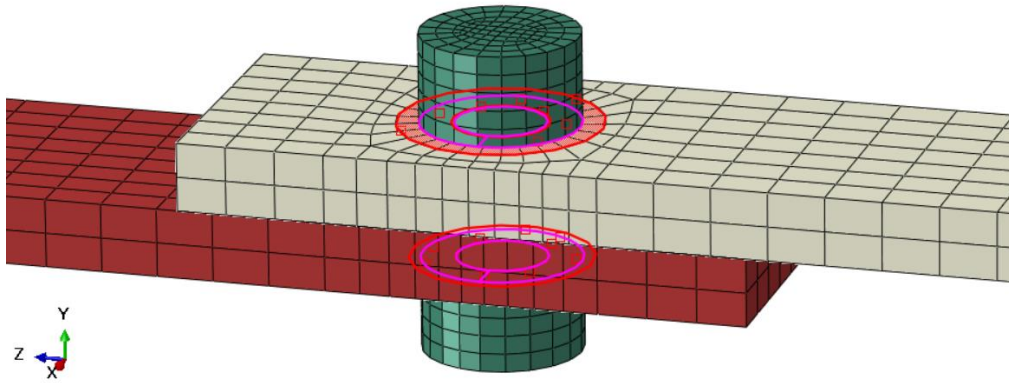


Figure 4-8 Contact Regions Between 1) Bolt Head and Beam A 2) Nut and Beam B

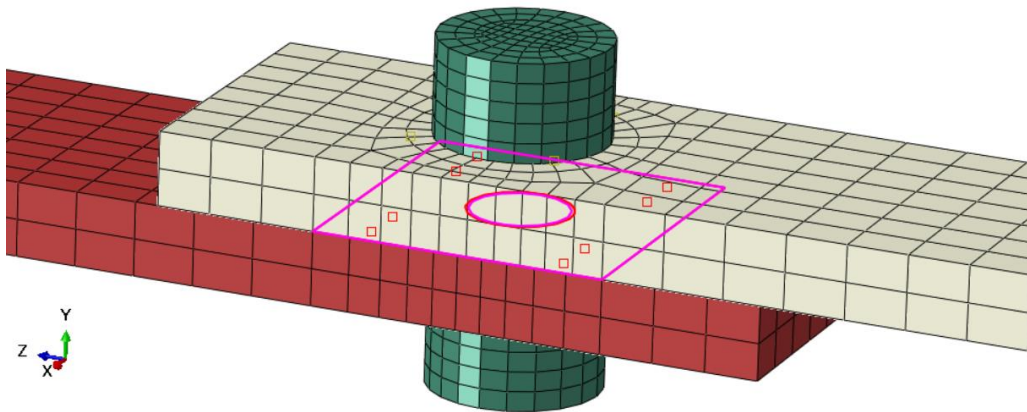


Figure 4-9 Contact Region Between Beams

As visualized in Figure 4-8 and Figure 4-9, the model includes surface-to-surface contact elements, which consists of master and slave nodes. They are used on the interfaces between:

- The bolt head and the upper surface of beam A
- The bolt nut and the lower surface of beam B
- Between the lower surface of beam A and the upper surface of beam B

4.2.3. Interaction Properties

ABAQUS/Standard offers two formulations for the modeling of the interaction of two deformable bodies. The first one is a *small sliding* formulation in which the contact surfaces are only allowed to undergo relatively small sliding relative to each other, but surface rotation is permitted. The second one is a *finite sliding* formulation. This formulation allows the separation of surfaces as well as finite amplitude of sliding and arbitrary rotation of the surfaces [30]. In this study, finite sliding formulation is used.

Contact problems in finite element methods are nonlinear. To determine which nodes are in contact, ABAQUS implements a master/slave contact algorithm. Surfaces generally transmit shear and normal forces across their interface when they are in contact. Therefore, the analysis may need to take into account frictional forces that resist relative sliding of the surfaces. Coulomb friction is a common model of friction used to define the interaction of the contact surfaces. The model uses a friction coefficient μ to characterize the frictional behavior between the surfaces.

The default friction coefficient is zero. Critical shear stress value depends on the normal contact pressure. According to the following equations, the tangential motion, which is sliding, is zero until the surface traction reaches to a critical shear stress value of

$$\tau_{critical} = \mu \cdot p \quad (4.1)$$

$$\text{The equivalent shear stress } \tau_{eq} = \sqrt{\tau_1^2 + \tau_2^2} \quad (4.2)$$

where μ is the coefficient of friction, and p is the contact pressure between the contacting surfaces. So, this equation says that the contacting surfaces will not slide relative to each other until the equivalent shear stress across their interface equals to the limiting frictional shear stress, μp .

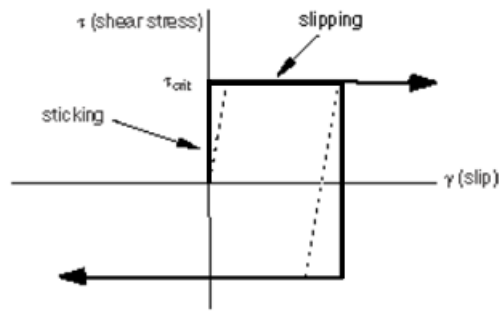


Figure 4-10 Frictional Behavior [31]

In Figure 4-10, the solid line summarizes the Coulomb friction model’s behavior; there is zero slip (zero relative motion) of the surfaces when they are stick condition (shear stress $< \mu p$).

It can be complicated to simulate ideal friction behavior. ABAQUS utilizes a formulation of penalty friction with an allowable “elastic slip” shown by the dotted line in Figure 4-10.

The elastic slip is the small amount of relative motion that occurs between the surfaces when the surfaces should stick. ABAQUS selects the penalty stiffness (the slope of the dotted line) automatically to make this allowable “elastic slip” is a very small fraction of the length of the characteristic element. Since the penalty friction formulation works well for most problems [3], in this study, penalty friction formulation is used together with 0.3 coefficient of friction for aluminum-aluminum contacting surfaces [32]. Contact parameters can be defined from the “Interaction” module in ABAQUS.

A model of the contact characteristics generally needs parameters for the normal behavior in addition to tangential behavior. The “hard” contact pressure- overclosure relationship can be used in ABAQUS to describe the contact model. At constraint locations, it minimizes the penetration of the slave surface into the master surface as shown in Figure 4-11.

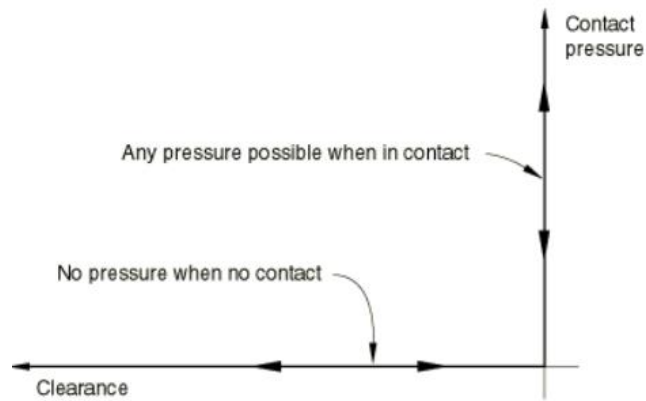


Figure 4-11 Default pressure-overclosure relationship [33]

To sum up, contact properties between contacting surfaces, as stated before, were modeled as a combination of tangential and normal behavior. “Penalty” friction formula with the friction coefficient value of 0.3 is used for tangential behavior, and for normal behavior “hard” contact formula is considered with linear contact stiffness. Since the bolts are more rigid than beam structure, they are denoted as master surfaces in contact pairs.

4.2.4. Bolt Preload

Since the contact stiffness values are determined based on contact preloads, the bolt should be preloaded. The analysis has been performed through the following steps;

Initial step: Defining boundary conditions and describing interaction properties.

Step1: Bolt preloading and activating contact elements.

Step2: Fixing the bolt length.

Step3: Applying dynamic load.

Before the steady-state dynamic analysis step is conducted, a static calculation step is performed to simulate the bolt’s preload. The calculations resulting from this static step bring out additional stiffness to the model as contact pairs are made in the interface, and geometrical non-linearities occur.

The pretension is simulated by dividing the bolt body into two parallel surfaces in the bolt shank and apply preload force, as shown in Figure 4-12.

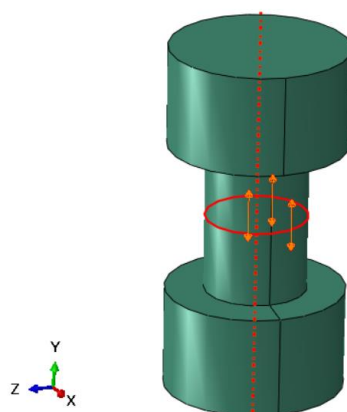


Figure 4-12 Preloaded Bolt

For calculating the preload value, Shigley [34] is taken as a reference. Bowman recommends a preload of 75 percent of proof load [35]. According to Shigley's guidelines, the following is recommended to be used for preload:

$$F_i = 0.75F_p, \text{ for nonpermanent connections, reused fasteners} \quad (4.3)$$

where F_p is the proof load, obtained from the equation

$$F_p = A_t S_p \quad (4.4)$$

Here S_p is the proof strength and A_t is the tensile stress area.

According to the above calculation, the minimum preload must be 22784 N for grade 10 steel bolts.

Bolt length is fixed at its current position after applying bolt load (pretension) to the bolt. This method helps to prevent the problem of elongation of the bolts under the load. Otherwise, ABAQUS will continue to apply pretension force.

All three degrees of freedom in the pretension section is restricted during the first two steps. This degree of freedom served as the artificial boundary condition to avoid the numerical singularity error that can be arisen from rigid body motion. This artificial boundary condition is then removed after preloading and activating the contact properties. Details of the contact pressure (CPRESS output variable) on substructures and bolt surfaces are given in Figure 4-13 to Figure 4-15.

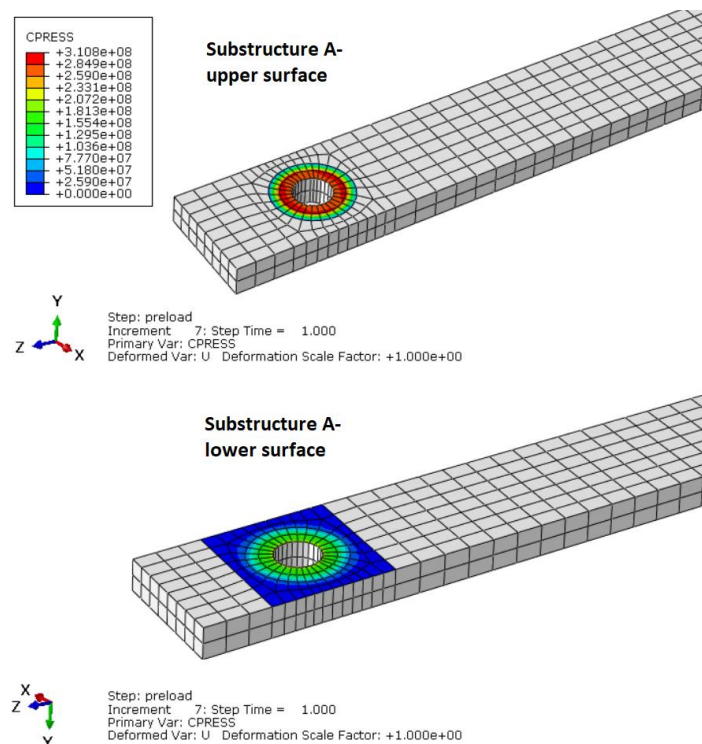


Figure 4-13 Contact Pressure at Surface Nodes for Substructure A

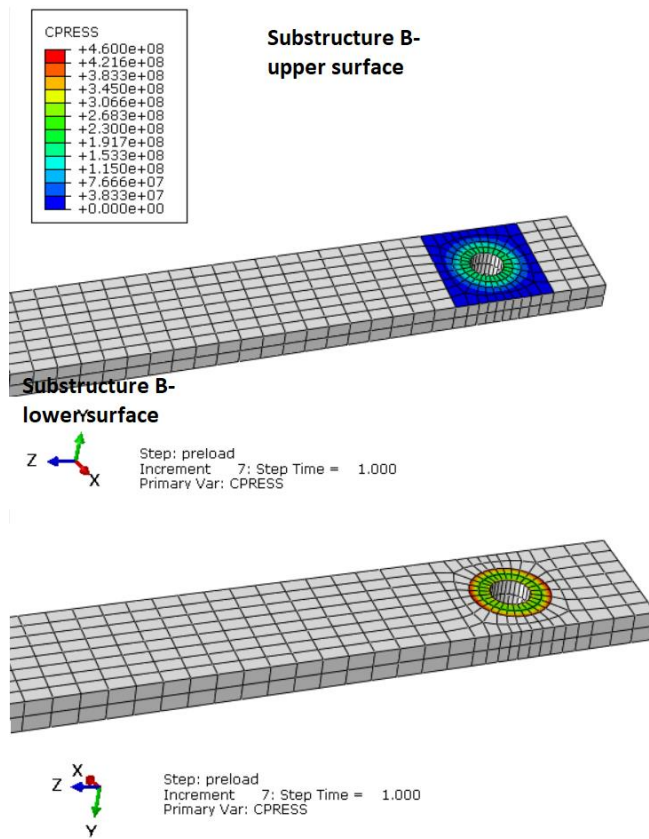


Figure 4-14 Contact Pressure at Surface Nodes for Substructure B

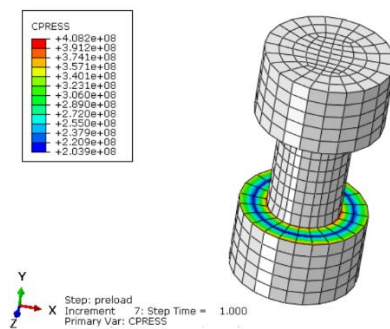


Figure 4-15 Contact Pressure at Surface Nodes for Bolt

4.2.5. Direct Steady-State Dynamic Analysis

ABAQUS /Standard offers a “direct” steady-state dynamic analysis procedure for structures undergoing continuous harmonic excitation.

The structure may exhibit material and geometrical nonlinear behavior as well as contact nonlinearities for the calculation of the base state. Moreover, viscous damping and discrete damping (such as dashpot elements) can be included in this procedure. Considering all of these, it can be seen that direct steady-state dynamic analysis is the most suitable procedure for this study [30]. It should be noted that a “direct solution steady-state dynamic analysis” is used to calculate the steady-state linearized dynamic response of the system to harmonic excitation. In order to obtain FRFs of the assembled structures, 1 N concentrated force is applied and displacement data at the nodes are extracted.

4.3. Identification of Joint Properties in Beams in 3D Space

In this section, in order to verify and demonstrate the implementation of the suggested method, two case studies are given. For both case studies, substructures are modeled using three-dimensional brick elements. The difference between case studies is the modeling method of the bolted joint as explained before.

In the first case study, the receptance values of the initial system and of the measured system are calculated by using RPs values. In the second case study, while receptance values of the initial system are obtained by using RPs values, the receptances in the measured system are obtained by using the simulated experiment model which uses three dimensional elements for bolt.

4.3.1. Case Study 1

In this case study, two identical beams, substructure A having fixed-free boundary conditions and substructure B having free-free boundary conditions, are coupled elastically with a joint. Each substructure is modeled with the three-dimensional brick elements using finite element program ABAQUS. In this model, in order to represent

the bolted joint, spring-/dashpot elements with coupled reference points (RPs) are used.

In order to use the proposed identification method, the FRFs of the assembled structure at the connection coordinates are required. The FRFs of the initially estimated bolted model can be obtained using RPs' translational and rotational displacement information, directly. In this case study, the FRFs of the measured system can also be obtained from the corresponding FE model with the actual values for the connection dynamics in the same manner.

As can be seen from Figure 4-16, three translational and three rotational springs and dashpots are placed between connection points (RPs).

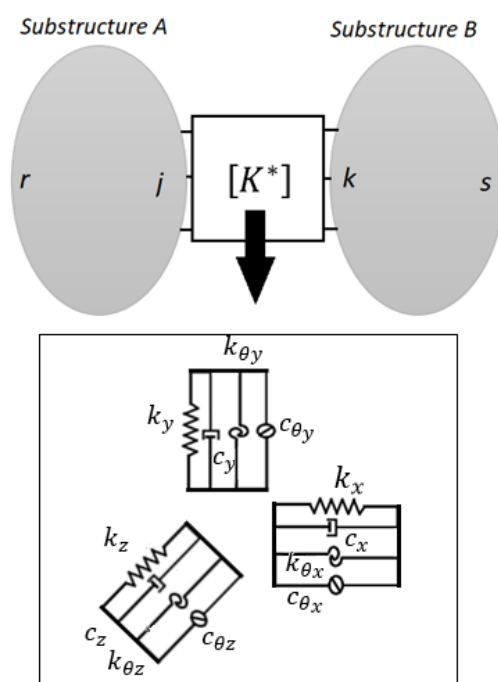


Figure 4-16 Using Predefined Complex Stiffness Matrix for Both Systems

The complex stiffness matrix representing the elastic joint can be defined as follows

$$[K^*] = \begin{bmatrix} k_{Fx} + j\omega c_{Fx} & 0 & 0 & 0 & 0 & 0 \\ 0 & k_{M\theta_y} + j\omega c_{M\theta_y} & 0 & 0 & 0 & 0 \\ 0 & 0 & k_{Fy} + j\omega c_{Fy} & 0 & 0 & 0 \\ 0 & 0 & 0 & k_{M\theta_x} + j\omega c_{M\theta_x} & 0 & 0 \\ 0 & 0 & 0 & 0 & k_{Fz} + j\omega c_{Fz} & 0 \\ 0 & 0 & 0 & 0 & 0 & k_{M\theta_z} + j\omega c_{M\theta_z} \end{bmatrix} \quad (4.5)$$

where k_{Fi} is the force to linear displacement stiffness in the i direction, c_{Fi} is the force to linear displacement damping in i direction and likewise, $k_{M\theta_i}$ is the moment to angular displacement stiffness in i direction and $c_{M\theta_i}$ is the moment to angular displacement damping in i direction of the joint (i can be x, y and z). The dynamic properties of the joint for the initially estimated and measured systems are tabulated in Table 4-1.

The receptance matrix corresponding to the connection coordinates of the system with initially estimated bolt parameters can be expressed as

$$[\alpha_{mm}] = \begin{bmatrix} {}_I H_{jj}^C & {}_I H_{jk}^C \\ {}_I H_{kj}^C & {}_I H_{kk}^C \end{bmatrix} \quad (4.6)$$

Experimentally measured FRFs (simulated experimental values) of the assembled structure at the connection coordinates of the system can be written as

$$[\gamma_{mm}] = \begin{bmatrix} {}_E H_{jj}^C & {}_E H_{jk}^C \\ {}_E H_{kj}^C & {}_E H_{kk}^C \end{bmatrix} \quad (4.7)$$

Table 4-1 Joint Parameters for Coupled Structures

		initially estimated bolt parameters $[K_1^*(\omega)]$	parameters need to be identified $[K_2^*(\omega)]$
k_{Fx}	Translational stiffness in the x -direction $[N/m]$	10^5	10^6
c_{Fx}	Translational damping in the x -direction $[N.s/m]$	1	10
k_{Fy}	Translational stiffness in the y -direction $[N/m]$	10^5	10^6
c_{Fy}	Translational damping in the y -direction $[N.s/m]$	3	30
k_{Fz}	Translational stiffness in the z -direction $[N/m]$	10^5	10^7
c_{Fz}	Translational damping in the z -direction $[N.s/m]$	2	20
$k_{M\theta_x}$	Rotational stiffness in the x -direction $[N.m/rad]$	$5 * 10^3$	10^3
$c_{M\theta_x}$	Rotational damping in the x -direction $[N.m.s/rad]$	1	5
$k_{M\theta_y}$	Rotational stiffness in the y -direction $[N.m/rad]$	$5 * 10^3$	10^4
$c_{M\theta_y}$	Rotational damping in the y -direction $[N.m.s/rad]$	1	10
$k_{M\theta_z}$	Rotational stiffness in the z -direction $[N.m/rad]$	10^2	10^3
$c_{M\theta_z}$	Rotational damping in the z -direction $[N.m.s/rad]$	1	5

As explained before, the only required measurement is the FRFs of the coupled structure at the connection coordinates, and therefore the size of the receptance

matrices $[\alpha_{mm}]$ and $[\gamma_{mm}]$ will be 12x12, since the joint model is composed of translational and rotational parameters for all six DOFs. The components of the receptance matrices are shown in Eqn. (4.8), where p and q represent measurement and excitation points, respectively.

$${}_{l,E}H_{pq}^C = \begin{bmatrix} H_{x_p x_q}^C & H_{x_p \theta_{y_q}}^C & H_{x_p y_q}^C & H_{x_p \theta_{x_q}}^C & H_{x_p z_q}^C & H_{x_p \theta_{z_q}}^C \\ H_{\theta_{y_p} x_q}^C & H_{\theta_{y_p} \theta_{y_q}}^C & H_{\theta_{y_p} y_q}^C & H_{\theta_{y_p} \theta_{x_q}}^C & H_{\theta_{y_p} z_q}^C & H_{\theta_{y_p} \theta_{z_q}}^C \\ H_{y_p x_q}^C & H_{y_p \theta_{y_q}}^C & H_{y_p y_q}^C & H_{y_p \theta_{x_q}}^C & H_{y_p z_q}^C & H_{y_p \theta_{z_q}}^C \\ H_{\theta_{x_p} x_q}^C & H_{\theta_{x_p} \theta_{y_q}}^C & H_{\theta_{x_p} y_q}^C & H_{\theta_{x_p} \theta_{x_q}}^C & H_{\theta_{x_p} z_q}^C & H_{\theta_{x_p} \theta_{z_q}}^C \\ H_{z_p x_q}^C & H_{z_p \theta_{y_q}}^C & H_{z_p y_q}^C & H_{z_p \theta_{x_q}}^C & H_{z_p z_q}^C & H_{z_p \theta_{z_q}}^C \\ H_{\theta_{z_p} x_q}^C & H_{\theta_{z_p} \theta_{y_q}}^C & H_{\theta_{z_p} y_q}^C & H_{\theta_{z_p} \theta_{x_q}}^C & H_{\theta_{z_p} z_q}^C & H_{\theta_{z_p} \theta_{z_q}}^C \end{bmatrix} \quad (4.8)$$

After calculating all required FRFs of the coupled system, dynamic structural modification matrix $[D_{mm}]$ is calculated and by adding off-diagonal terms of it to $[K_1^*(\omega)]$ will give the identified complex stiffness matrix $[K^*(\omega)]$ representing the joint dynamics in six DOFs.

$$[D_{mm}] = \begin{bmatrix} j \text{ coord.} & -\Delta (6 \times 6) \\ -\Delta (6 \times 6) & k \text{ coord.} \end{bmatrix} \quad (4.9)$$

$$[K_{iden}^*(\omega)] = [K_1^*(\omega)] + [\Delta] \quad (4.10)$$

In Figure 4-17, the comparison of the predicted FRF using initially estimated complex stiffness matrix $[K_1^*(\omega)]$, and the measured FRF using $[K_2^*(\omega)]$ for the assembled substructure at points s and r in y-direction are given.

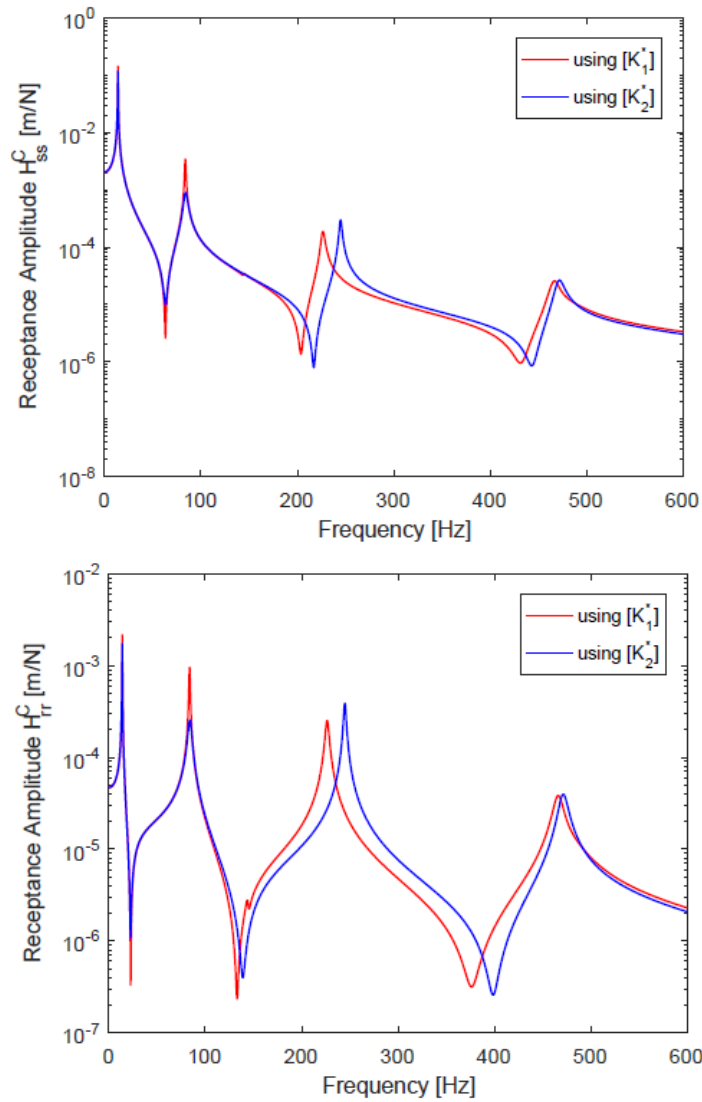


Figure 4-17 Receptances at Points r and s in y-direction

As mentioned in Chapter 3, the sensitivity of FRFs to different joint stiffnesses should be determined before the identification of joint parameters. In Chapter 3, since the joint model is composed of one translational and one rotational stiffness, there are two different sensitive frequency regions for the identification. However, for three-dimensional joint model, all the three translational and three rotational stiffnesses and damping parameters should be identified at their sensitive regions.

The sensitivities of FRFs of the tip point s to joint translational and rotational stiffnesses are shown in Figure 4-18 to Figure 4-23. Sensitivity of the system response to each joint parameter is investigated and tabulated in Table 4-2.

Changing k_{Fx} , $k_{M\theta_y}$ and $k_{M\theta_z}$ affects the receptance amplitude of the coupled system at point s in x-direction as shown in Figure 4-18, Figure 4-22 and Figure 4-23. Likewise, changing k_{Fy} and $k_{M\theta_x}$ affects the receptance amplitude of the coupled system at point s in y-direction as shown in Figure 4-19 and Figure 4-21 and finally changing k_{Fz} and $k_{M\theta_x}$ affects that of in z-direction as shown in Figure 4-20 and Figure 4-21.

It should be noted that if we are interested in vibrations only in one direction, for example the vibration of the coupled beams in transverse direction, we need to do sensitivity analysis only for the parameters k_{Fy} and $k_{M\theta_x}$, since only these two parameters will affect the response of the system in that direction. In this section, the sensitivity analysis was performed for all six stiffnesses values, since the responses in three directions will be examined.

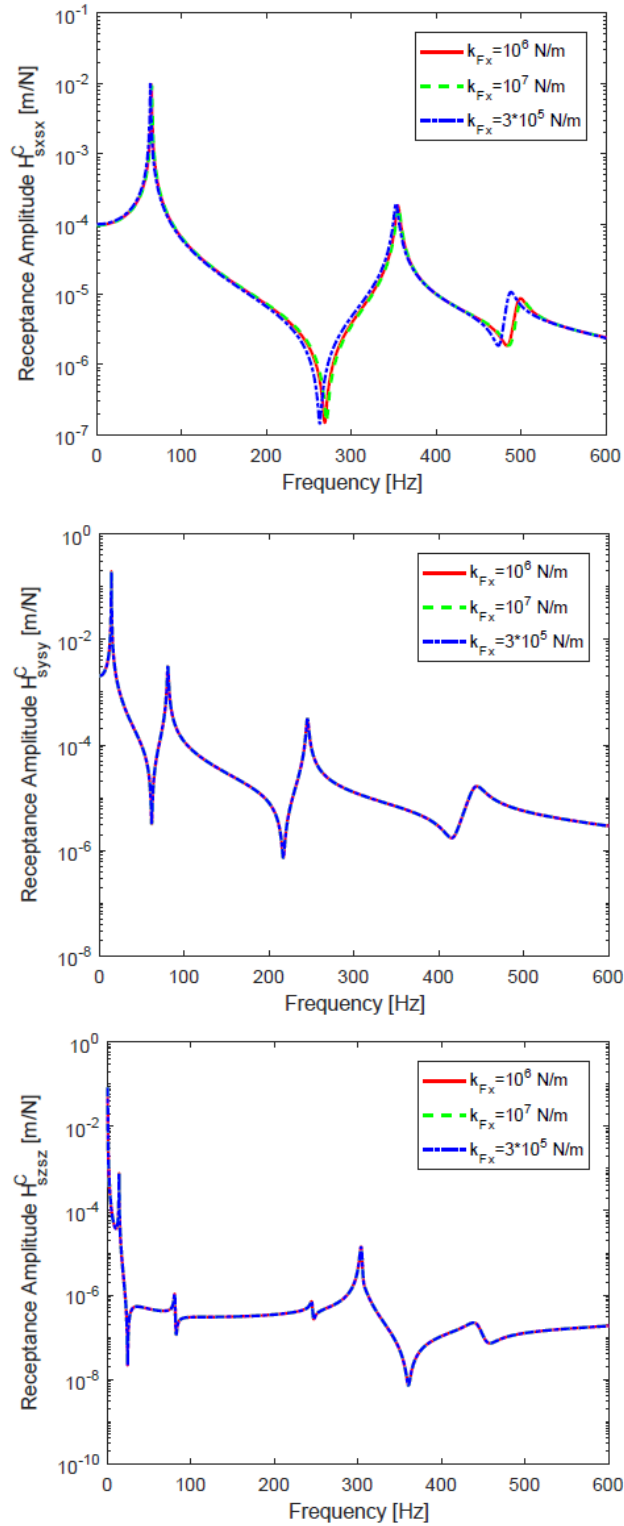


Figure 4-18 Sensitivity of the System Response at Point s to k_{Fx}

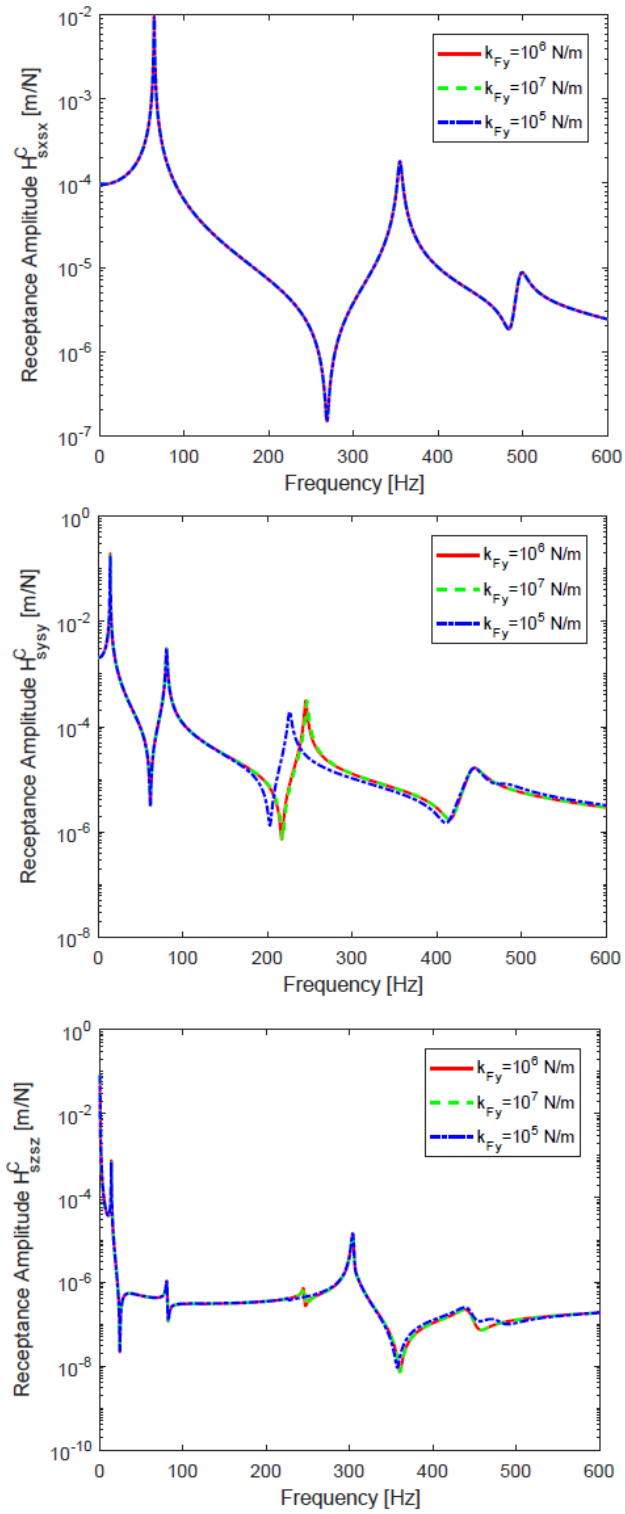


Figure 4-19 Sensitivity of the System Response at Point s to k_{Fy}

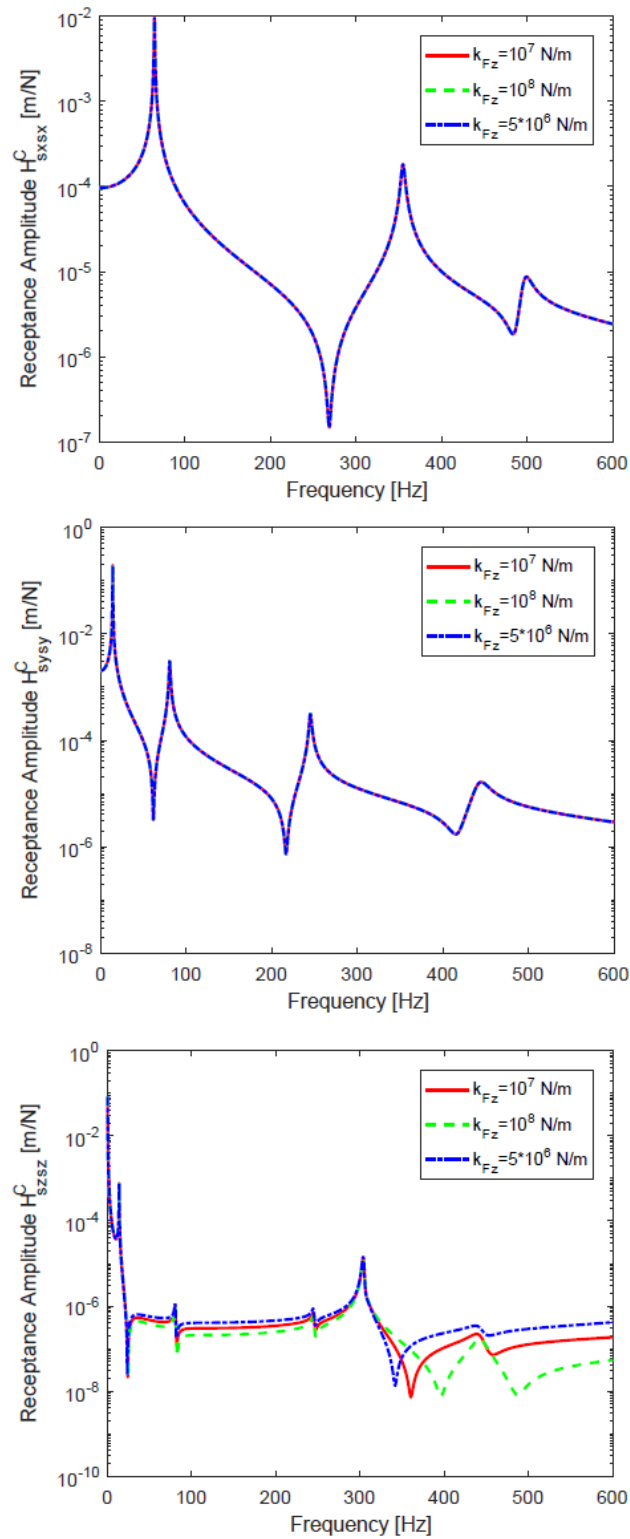


Figure 4-20 Sensitivity of the System Response at Point s to k_{Fz}

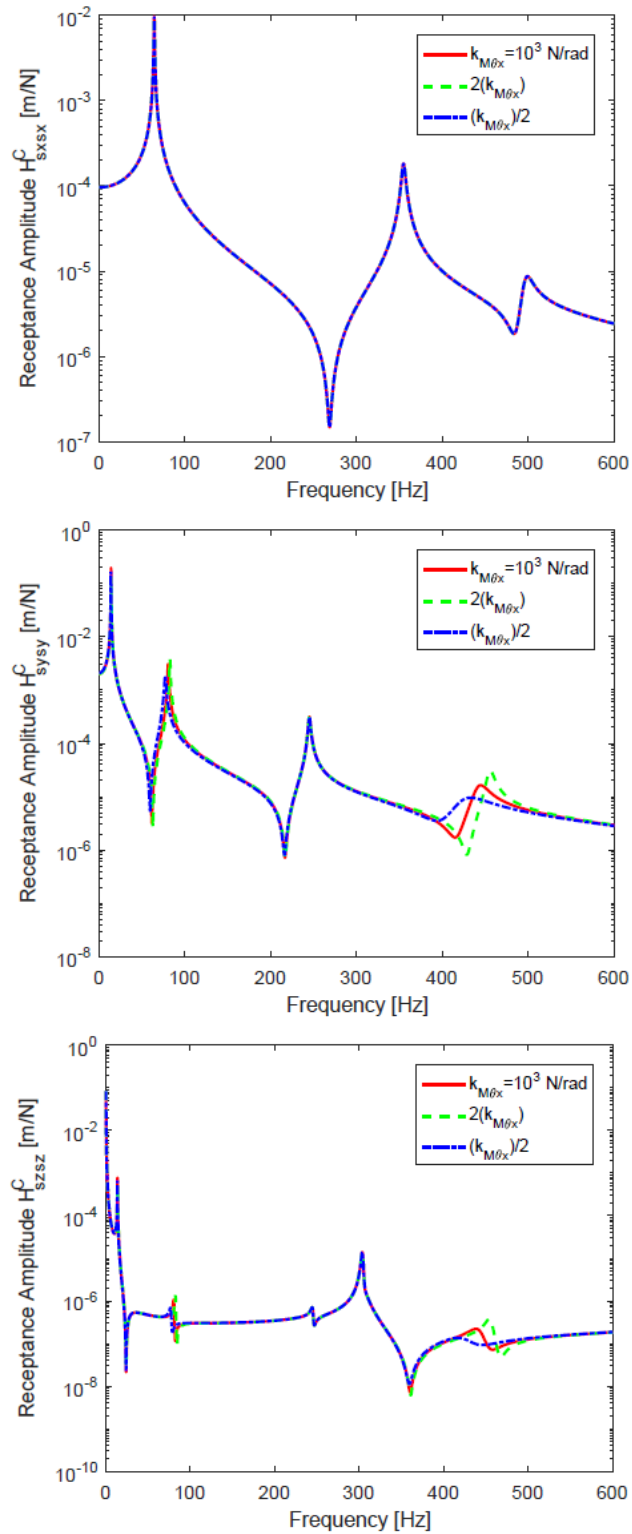


Figure 4-21 Sensitivity of the System Response at Point s to $k_{M\theta_x}$

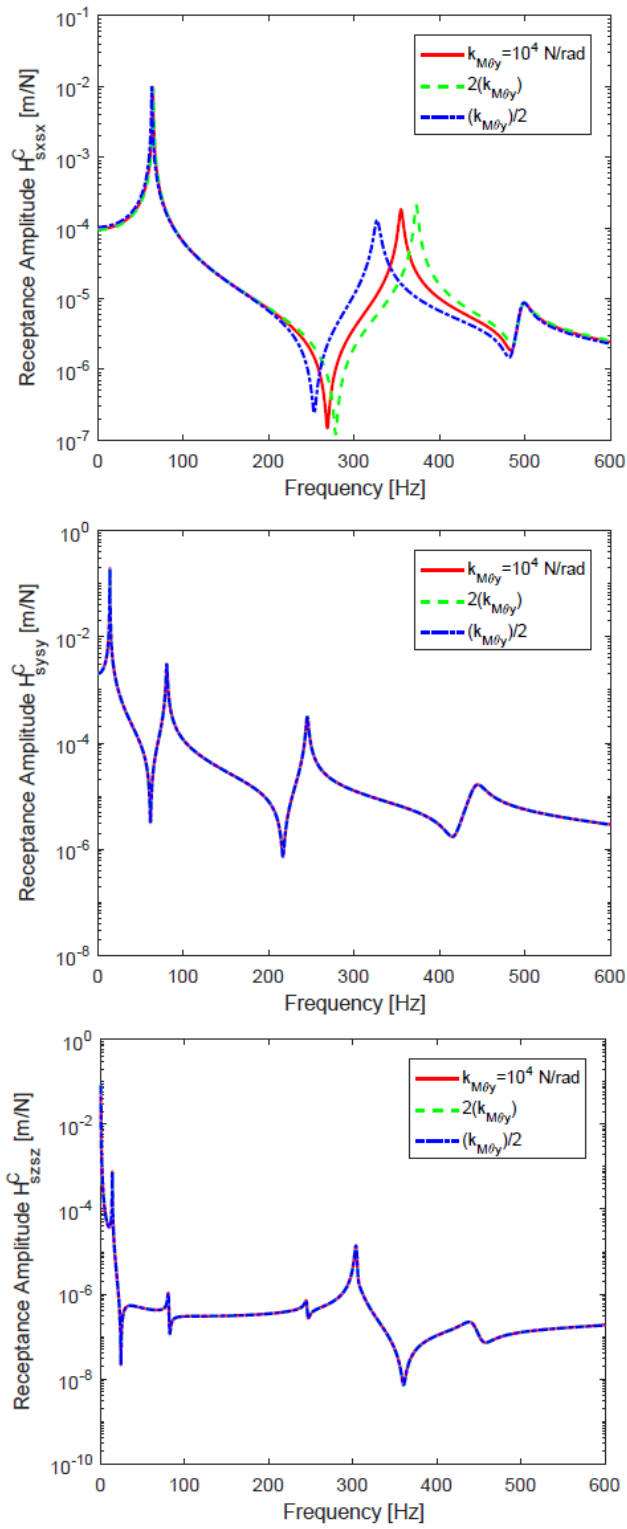


Figure 4-22 Sensitivity of the System Response at Point s to $k_{M\theta_y}$

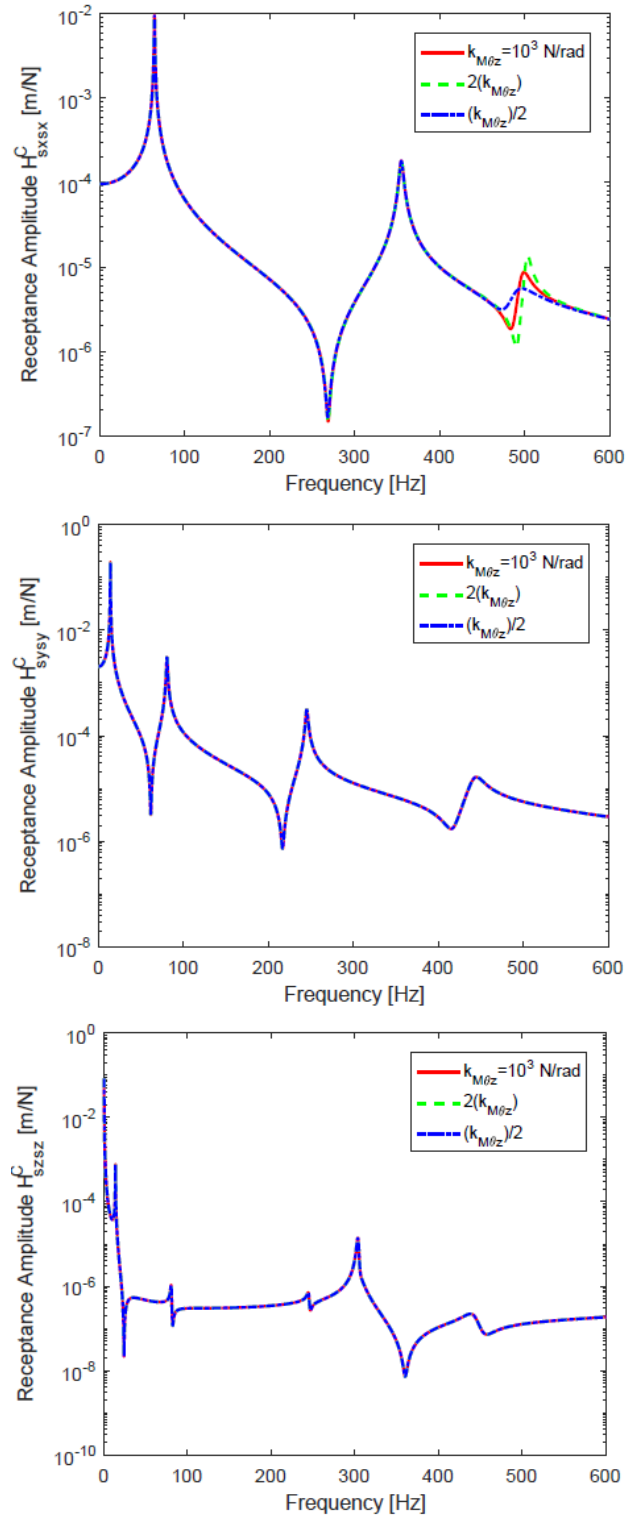


Figure 4-23 Sensitivity of the System Response at Point s to $k_{M\theta_z}$

Table 4-2 Sensitive Regions

	Region 1	Region 2
k_{Fx}	200 Hz - 300 Hz	450 Hz - 520 Hz
k_{Fy}	180 Hz - 300 Hz	-
k_{Fz}	20 Hz - 600 Hz	-
$k_{M\theta_x}$	50 Hz - 120 Hz	350 Hz - 500 Hz
$k_{M\theta_y}$	200 Hz - 500 Hz	-
$k_{M\theta_z}$	475 Hz - 525 Hz	-

Each joint property is identified in the range of frequency where the response is sensitive to that parameter, and the average of the values are taken in that region. The ranges that are used in the identification of the joint properties in this case study are tabulated in Table 4-2.

Now, in order to study the effect of the noise on the identification results, FRFs of the coupled structure, $[{}^E H_{jj}^C]$, $[{}^E H_{kk}^C]$, $[{}^E H_{jk}^C]$ and $[{}^E H_{kj}^C]$, are polluted with 5% random noise, as explained before. The identification results for translational and rotational properties are shown in Figure 4-24 to Figure 4-27, respectively.

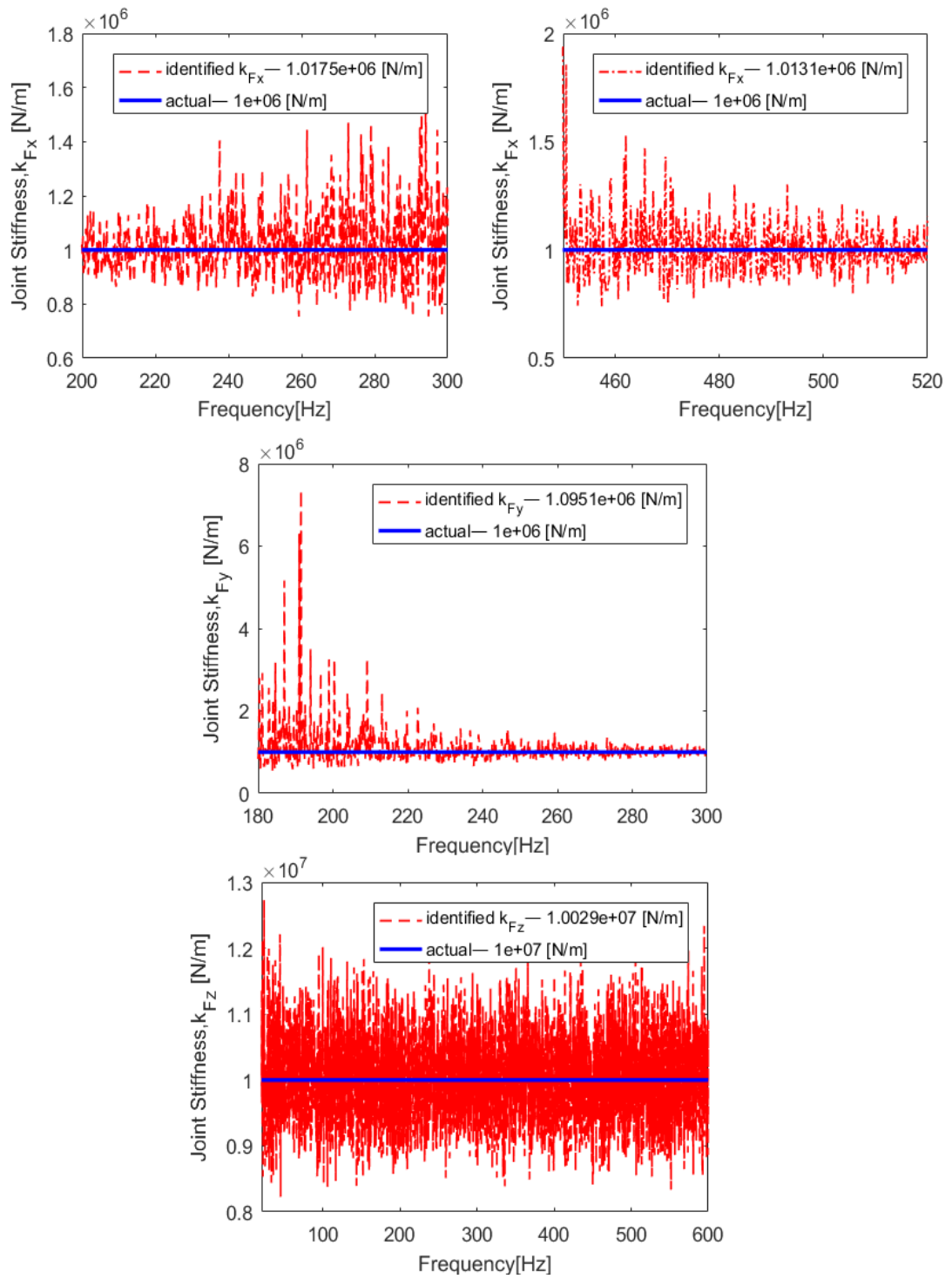


Figure 4-24 Identified Translational Stiffnesses

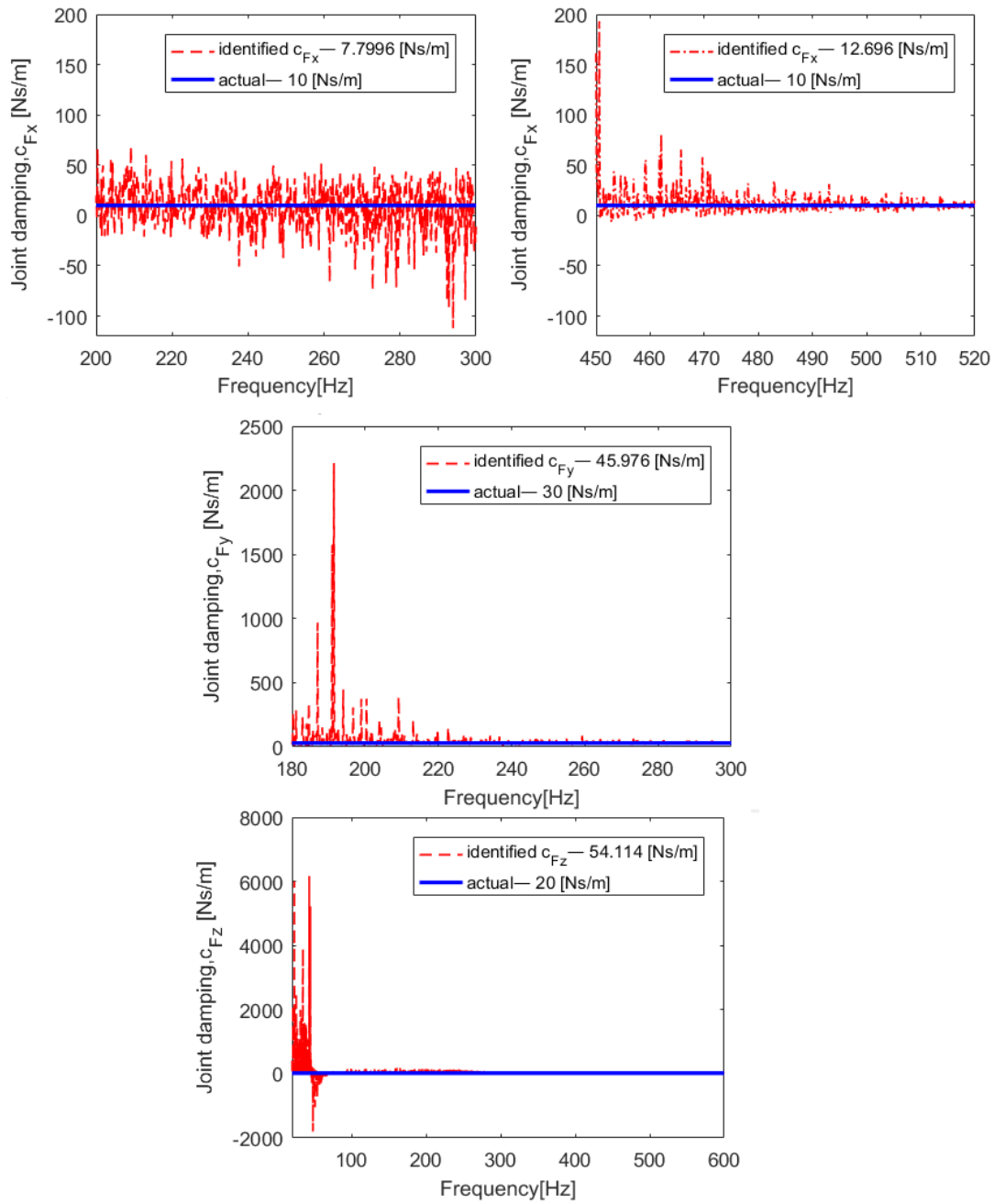


Figure 4-25 Identified Translational Damping

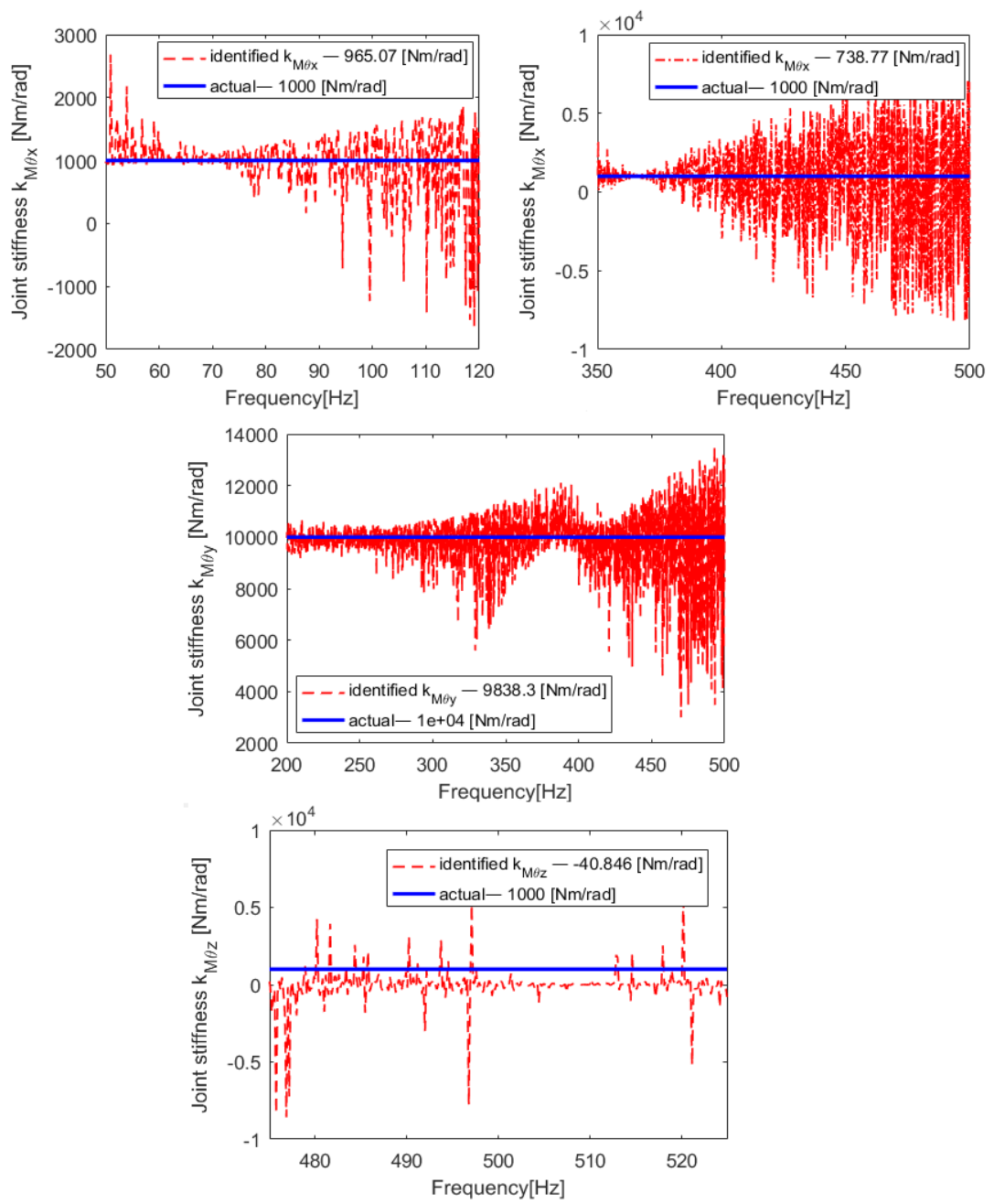


Figure 4-26 Identified Rotational Stiffnesses

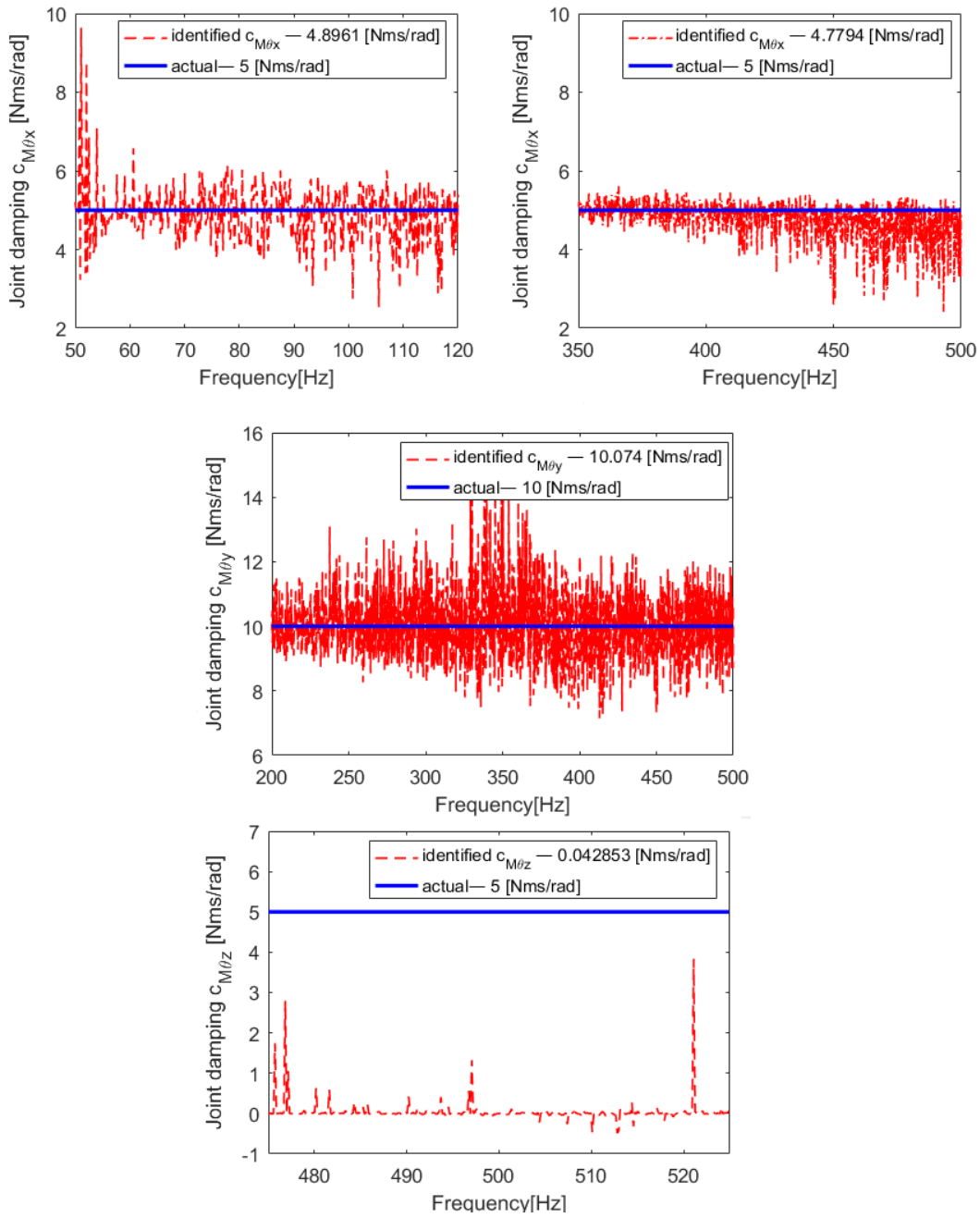


Figure 4-27 Identified Rotational Damping

It is observed that translational joint stiffness identification results are very good compared to translational damping values. Note that, the damping properties are prone to noise much more than the stiffness properties, since their effects on the coupled system dynamics is much less than those of the joint stiffness values. For the damping parameters, the frequency ranges used for the identification of stiffness values are employed. The average values of the identification results in these ranges are given in Table 4-3 and Table 4-4.

Table 4-3 Identified Translational Joint Parameters and Percentage Errors

	Actual Values	Identification Region 1	Identification Region 2
$k_{Fx} [N/m]$	10^6	$1.017 * 10^6$	$1.013 * 10^6$
Error (%)		1.7	1.3
$k_{Fy} [N/m]$	10^6	$1.095 * 10^6$	
Error (%)		9.5	
$k_{Fz} [N/m]$	10^7	$1.003 * 10^7$	
Error (%)		0.3	
$c_{Fx} [N.s/m]$	10	7.799	12.696
Error (%)		-22.01	26.96
$c_{Fy} [N.s/m]$	30	45.976	
Error (%)		53.253	
$c_{Fz} [N.s/m]$	20	54.114	
Error (%)		170.57	

Table 4-4 Identified Rotational Joint Parameters and Percentage Errors

	Actual Values	Identification Region 1	Identification Region 2
$k_{M\theta_x}$ [N.m/rad]	10^3	965.07	738.77
Error (%)		-3.493	-26.123
$k_{M\theta_y}$ [N.m/rad]	10^4	9838.3	
Error (%)		-1.617	
$k_{M\theta_z}$ [N.m/rad]	10^3	-40.846	
Error (%)		-104.08	
$c_{M\theta_x}$ [N.m.s/rad]	5	4.896	4.779
Error (%)		-2.08	-4.42
$c_{M\theta_y}$ [N.m.s/rad]	10	10.074	
Error (%)		0.74	
$c_{M\theta_z}$ [N.m.s/rad]	5	0.042	
Error (%)		-99.16	

4.3.2. Comparison of Two Methods when Applied to 3D Structural Systems

The joint parameters identified by using the proposed method and FRF decoupling method, are shown in Figure 4-28 to Figure 4-31. The joint parameters identified by using two methods and the percentage differences from the actual values are given in Table 4-5 and Table 4-6.

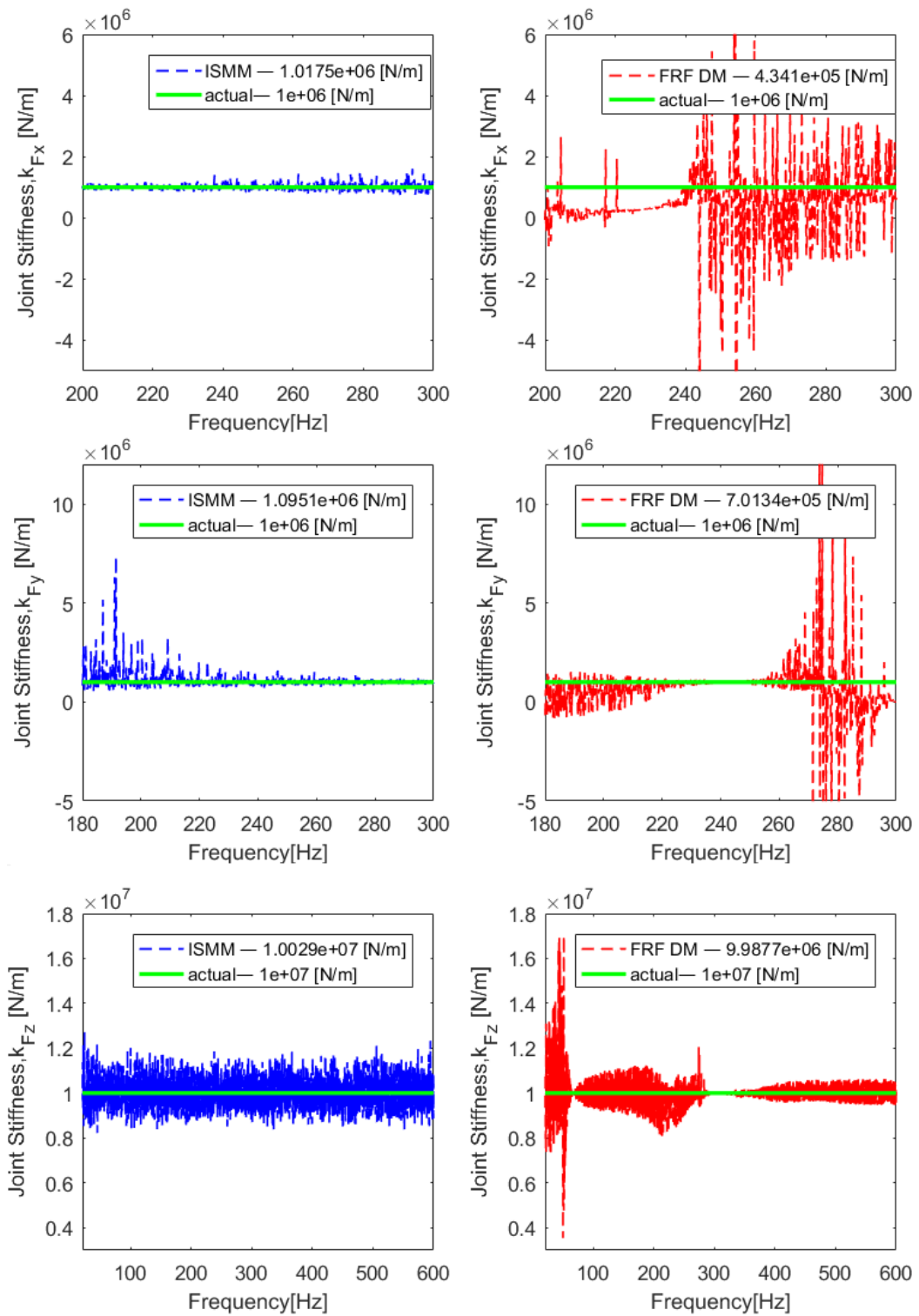


Figure 4-28 Identified Translational Stiffnesses Obtained by Using ISMM and FRF DM

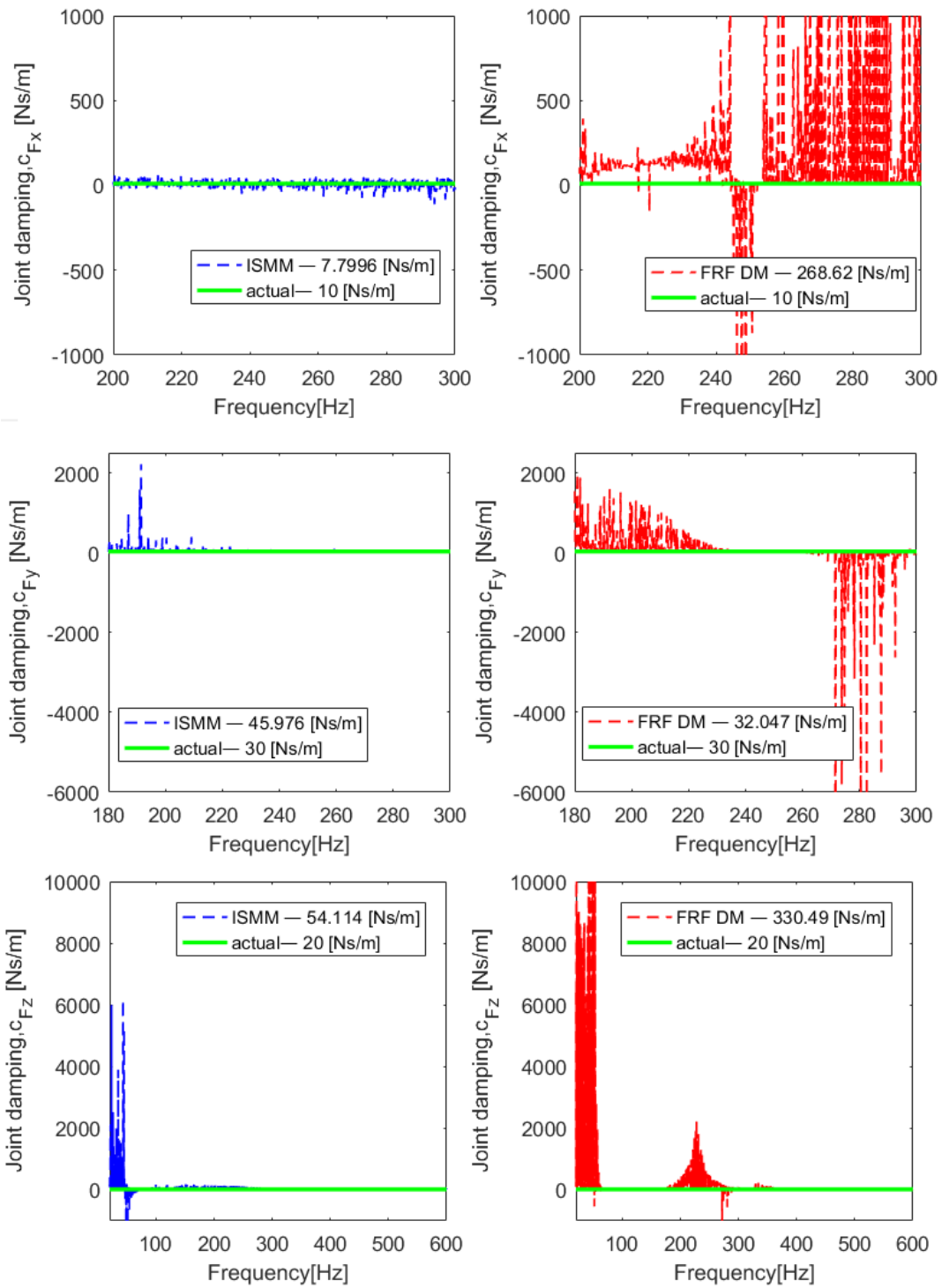


Figure 4-29 Identified Translational Damping Obtained by Using ISMM and FRF DM

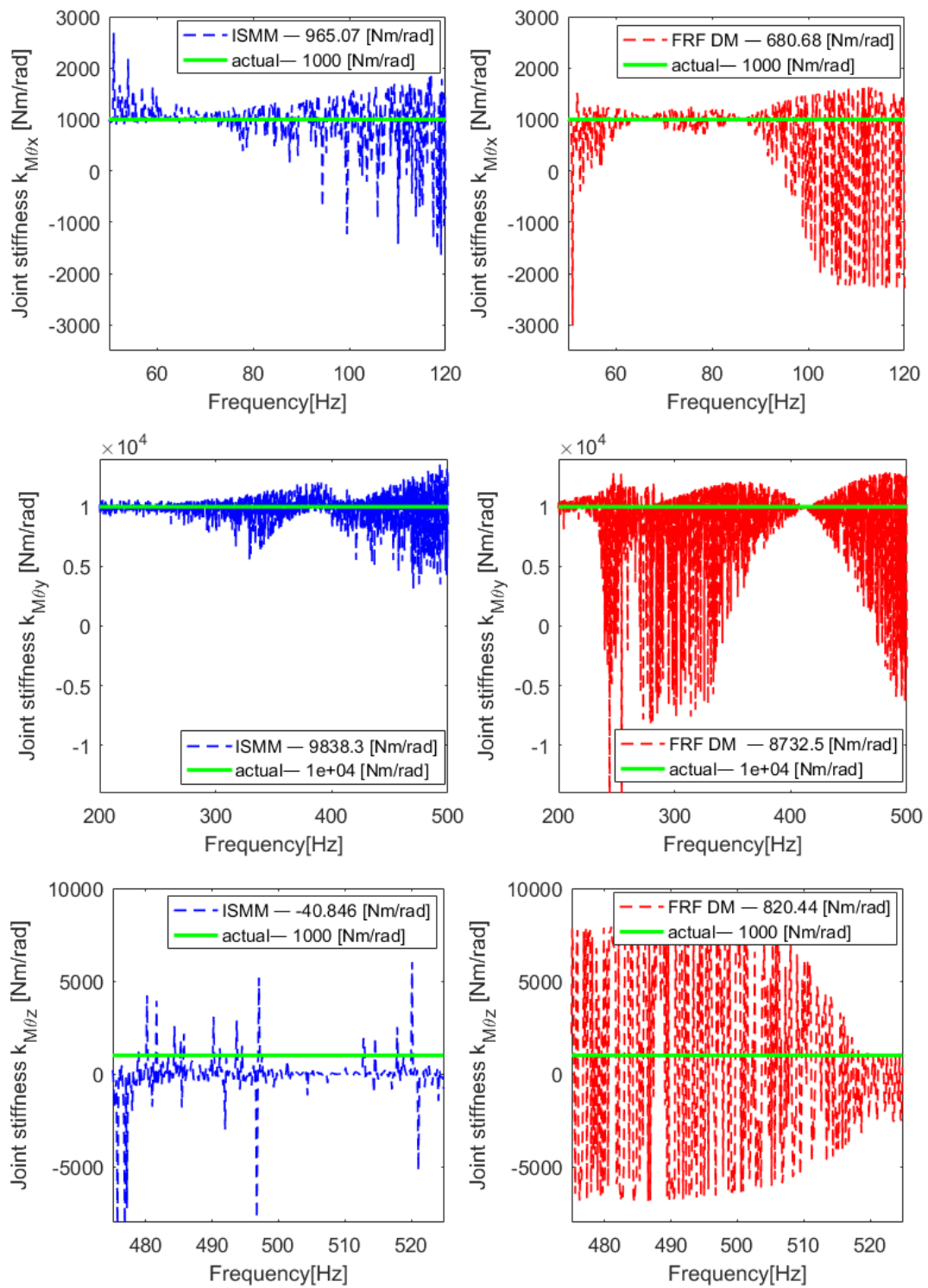


Figure 4-30 Identified Rotational Stiffnesses Obtained by Using ISMM and FRF DM

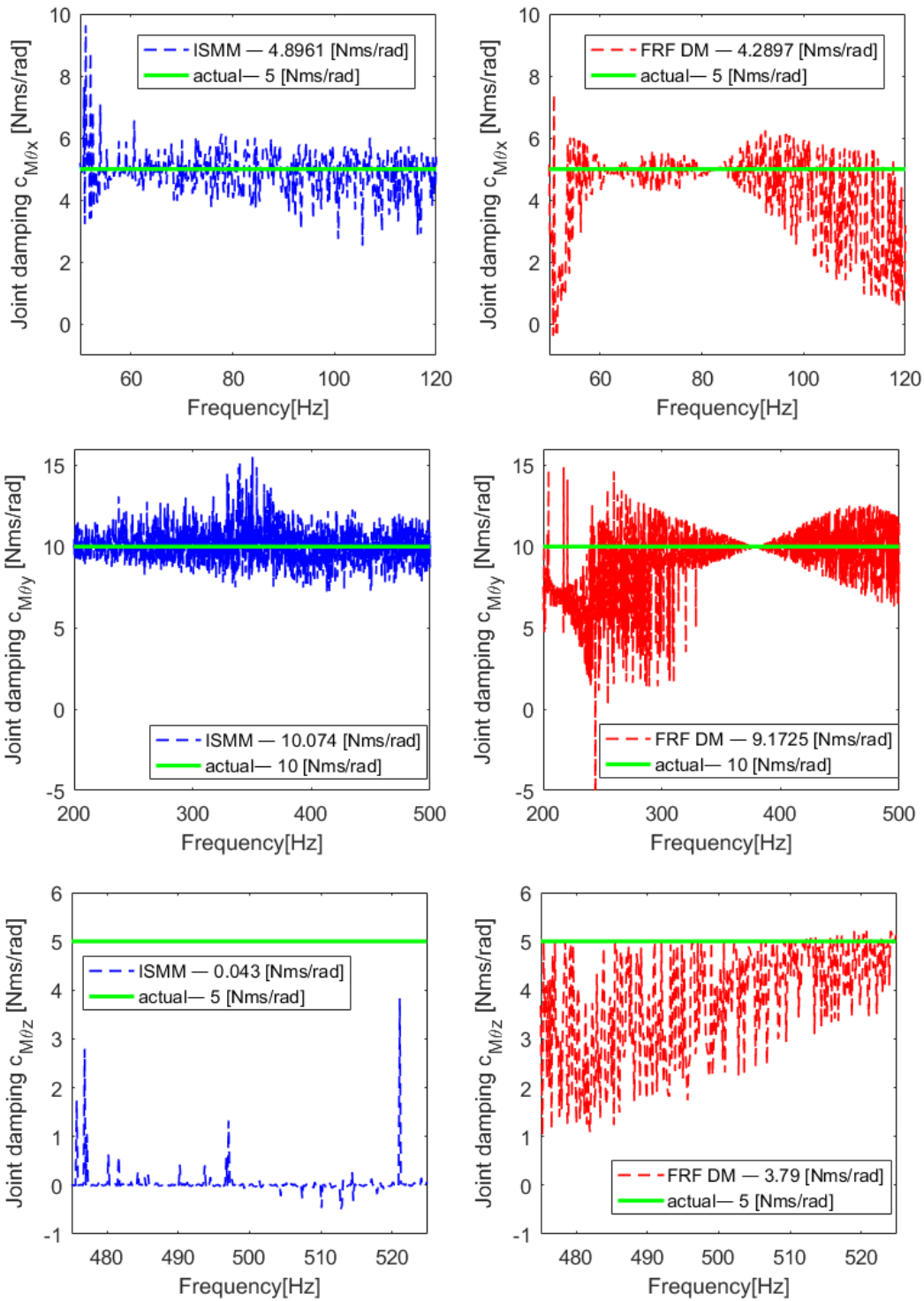


Figure 4-31 Identified Rotational Damping Obtained by Using ISMM and FRF DM

Table 4-5 Comparison of Identified Translational Joint Parameters and Percentage Errors

	Actual Values	ISMM	FRF DM
k_{Fx} [N/m]	10 ⁶	1.017 * 10 ⁶	4.341 * 10 ⁵
Error (%)		1.7	-56.6
k_{Fy} [N/m]	10 ⁶	1.095 * 10 ⁶	7.014 * 10 ⁵
Error (%)		9.5	-29.86
k_{Fz} [N/m]	10 ⁷	1.003 * 10 ⁷	9.987 * 10 ⁶
Error (%)		0.3	-0.13
c_{Fx} [N.s/m]	10	7.799	268.62
Error (%)		-22.01	2586.2
c_{Fy} [N.s/m]	30	45.976	32.047
Error (%)		53.25	6.83
c_{Fz} [N.s/m]	20	54.114	330.49
Error (%)		170.57	1552.45

Table 4-6 Comparison of Identified Rotational Joint Parameters and Percentage Errors

	Actual Values	ISMM	FRF DM
$k_{M\theta_x}$ [N.m/rad]	10 ³	965.07	680.68
Error (%)		-3.493	-31.932
$k_{M\theta_y}$ [N.m/rad]	10 ⁴	9838.3	8732.5
Error (%)		-1.617	-12.675
$k_{M\theta_z}$ [N.m/rad]	10 ³	-40.846	820.44
Error (%)		-104.08	-17.95
$c_{M\theta_x}$ [N.m.s/rad]	5	4.896	4.289
Error (%)		-2.08	-14.22
$c_{M\theta_y}$ [N.m.s/rad]	10	10.074	9.172
Error (%)		0.74	-8.28
$c_{M\theta_z}$ [N.m.s/rad]	5	0.042	3.79
Error (%)		-99.16	-24.2

Knowing natural frequencies and mode shapes of the coupled system may help to understand the reason of the deviation from the actual FRFs, better. As shown in Figure 4-32; the first, third, fourth and sixth modes are basically in y direction. On the other hand, it can be seen that from Figure 4-33 that the second, fifth and seventh modes are basically in x direction.

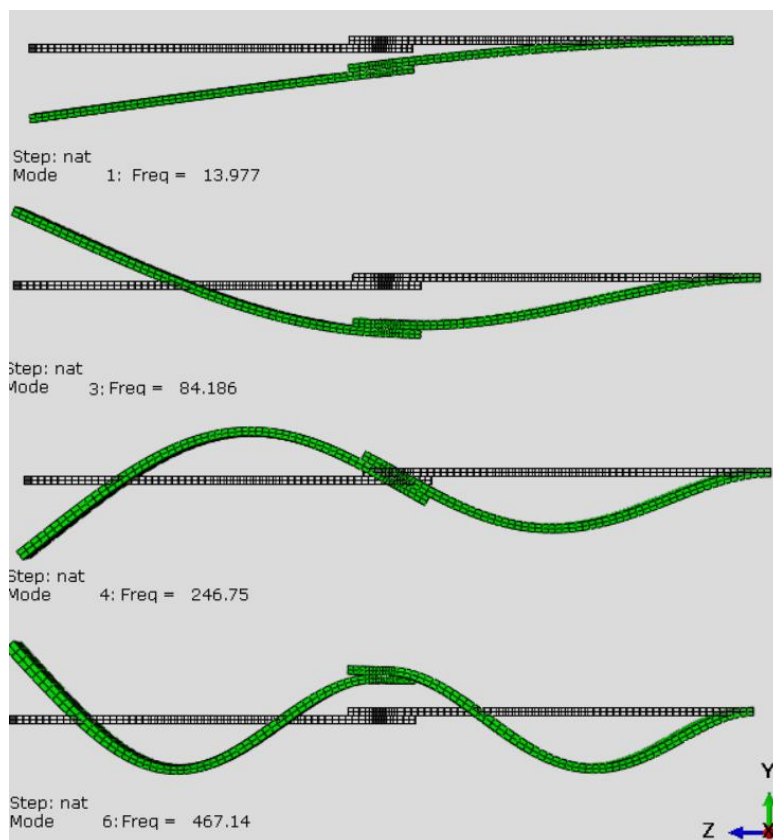


Figure 4-32 Natural Frequencies and Mode Shapes of the Coupled System

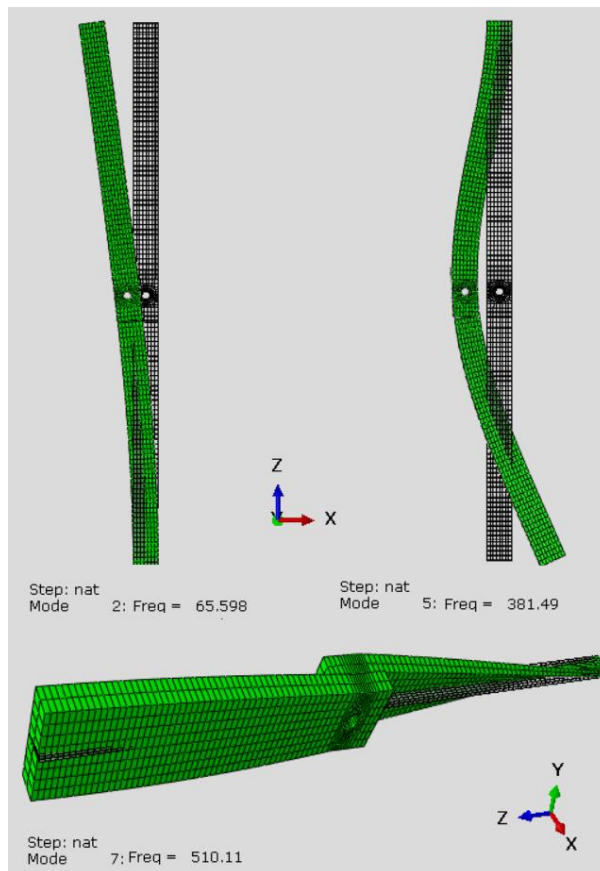


Figure 4-33 Natural Frequencies and Mode Shapes of the Coupled System

The FRFs of the assembled system are regenerated by using the joint parameters identified using ISMM and FRF DM, at the tip point, and they are compared with each other, as well as with the actual FRF in Figure 4-34 to Figure 4-38.

As it can be seen from Figure 4-34, the FRFs regenerated by using the joint parameters obtained from ISMM have some deviations from the actual FRFs in x direction in the third mode which corresponds to the torsional mode of the system (Figure 4-33). From the sensitivity of the related FRF to $k_{M\theta_z}$ (Figure 4-23), it can be seen that it has the maximum effect on the FRFs in that frequency regions. This explains why the accuracy of the regenerated FRF is not so good in this region, as can also be seen from Table 4-6, since $k_{M\theta_z}$ could not be identified accurately.

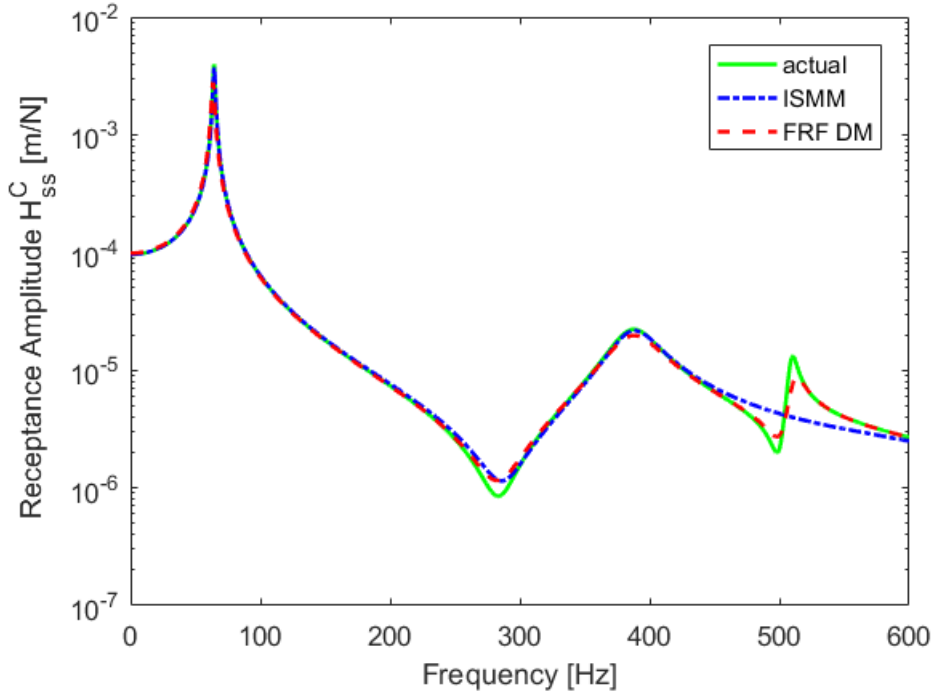


Figure 4-34 Comparison of the FRFs of the Tip Point Calculated Using Joint Parameters Identified by Using ISMM and FRF DM in x Direction

In order to quantify errors for the comparison of FRFs calculated using joint parameters identified by employing ISMM and FRF DM, two different error criteria defined in [36] are used.

The first one is “Amplitude Error” which is the difference between the maximum receptance amplitudes obtained by using joint parameters identified and the exact maximum receptance amplitude in the frequency range of interest, and it is defined as

$$Amplitude\ Error = \left| \frac{x_{max}^{exc} - x_{max}^{obt}}{x_{max}^{exc}} \right| \times 100 \quad (4.11)$$

The second one is “Frequency Error” which is the difference between the resonance frequency values corresponding to the maximum receptance amplitude obtained and the exact value. It is expressed as follows

$$Frequency\ Error = \left| \frac{\omega_{max}^{exc} - \omega_{max}^{obt}}{\omega_{max}^{exc}} \right| \times 100 \quad (4.12)$$

The errors related with FRFs calculated in x direction in two specific frequency ranges (Figure 4-35) are given in Table 4-7.

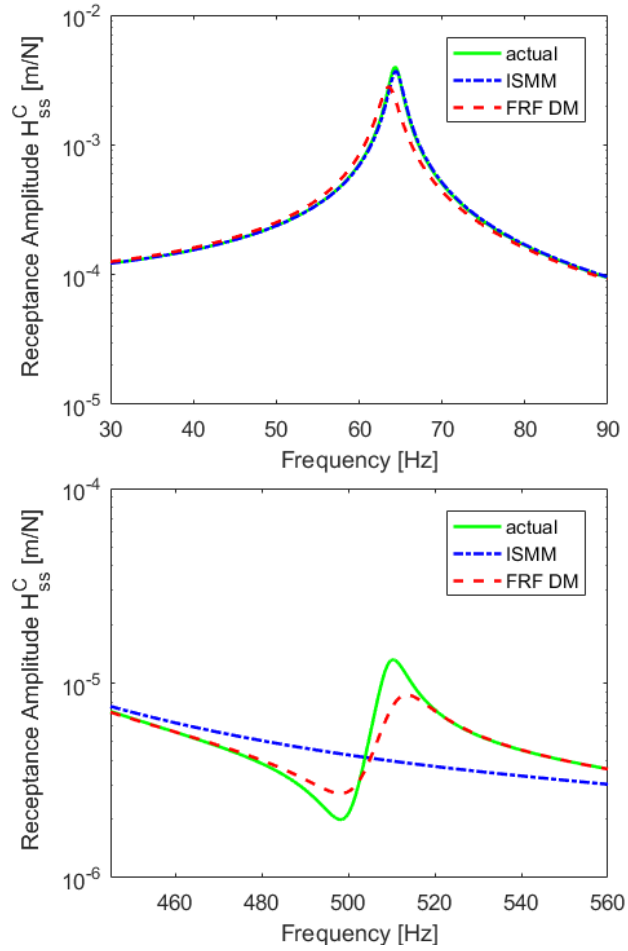


Figure 4-35 Comparison of the FRFs of the Tip Point in Frequency Ranges
30 Hz - 90 Hz and 445 Hz - 560 Hz

Table 4-7 Amplitude and Frequency Errors for the Receptance H_{ss}^C in x – Direction

		Amplitude Error (%)	Frequency Error (%)
30 Hz – 90 Hz	ISMM	6.66	0.25
	FRF DM	29.70	1.24
445 Hz – 560 Hz	ISMM	--	--
	FRF DM	34.16	0.62

From Figure 4-36, it can be seen that the FRFs regenerated by using the joint parameters obtained from ISMM perfectly match with the actual FRF in y direction (transverse direction) but the FRFs regenerated by using the joint parameters obtained from FRF DM have some slight deviations from the actual FRF. It is observed that while the differences between the identified values using ISMM and FRF DM and the actual ones are not very small, their effect on the system dynamics is not so significant.

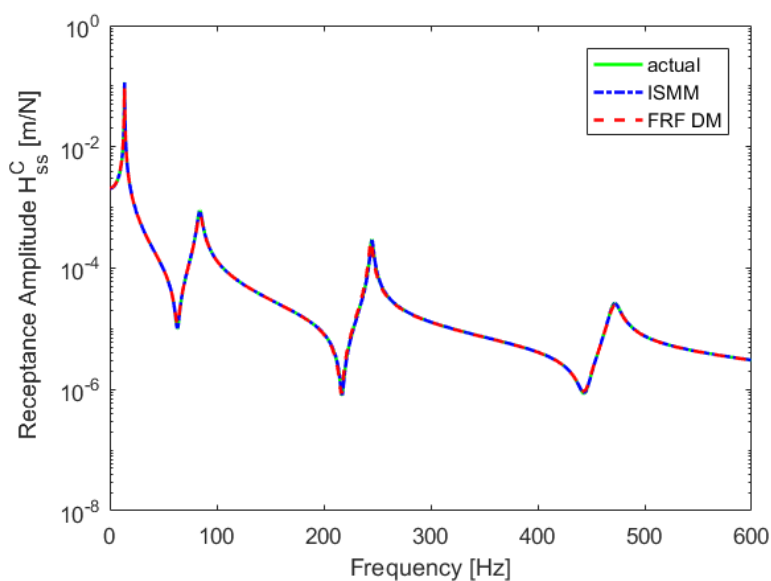


Figure 4-36 Comparison of the FRFs of the Tip Point Calculated Using Joint Parameters Identified by Using ISMM and FRF DM in y Direction

Again, in order to quantify errors, amplitude error and frequency error are calculated for the FRFs calculated in y direction by using identified parameters (Figure 4-37) are given in Table 4-8.

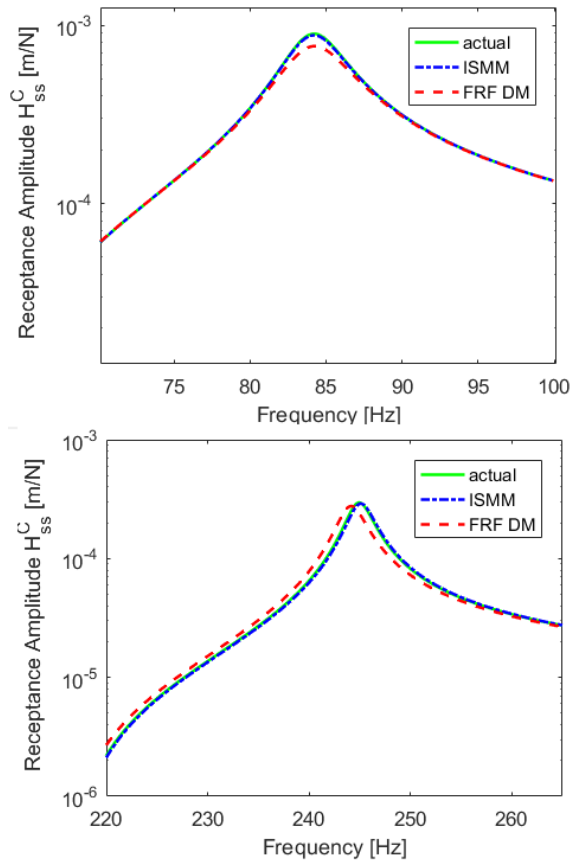


Figure 4-37 Comparison of the FRFs of the Tip Point Calculated Using Joint Parameters Identified by Using ISMM and FRF DM

Table 4-8 Amplitude and Frequency Errors for the Receptance H_{ss}^C in y – Direction

		Amplitude Error (%)	Frequency Error (%)
70 Hz – 100 Hz	ISMM	1.89	0
	FRF DM	14.76	0
220 Hz – 265 Hz	ISMM	1.97	0.06
	FRF DM	6.65	0.32

Finally, it can be seen from Figure 4-38 that the FRFs regenerated by using the joint parameters obtained from ISMM and FRF DM perfectly match with the actual FRF in z direction.

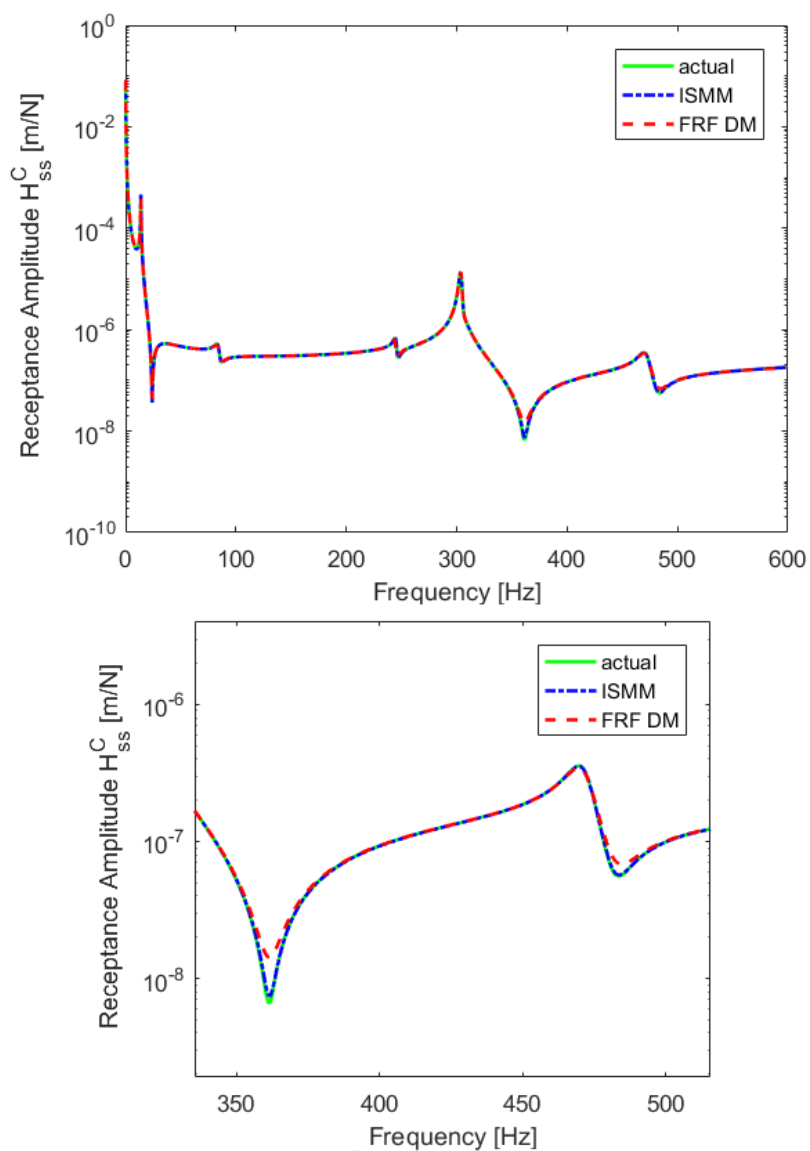


Figure 4-38 Comparison of the FRFs of the Tip Point Calculated Using Joint Parameters Identified by Using ISMM and FRF DM in z Direction

4.3.3. Case Study 2

FRFs involving rotational information are of the type, rotation/force, translation/moment and rotation/moment and they may represent 75% of the whole FRF matrix which cannot be ignored. The primary reason for the problems in obtaining rotational data are mainly due to the fact that there are no angular transducers available or practical means of implementing momentary excitations. In acquiring a complete view of the system dynamics, data regarding rotational degrees of freedom plays a major role. In this case study, obtaining RDOF related FRFs from translational FRFs in identifying joint parameters for all six DOFs is studied. As explained before, in this case, the bolt is modeled using three-dimensional brick elements. Therefore, it is not possible to obtain RDOFs related FRFs from the finite element simulation. Furthermore, in real applications we will need experimentally measured values.

In order to estimate the RDOF related FRFs of the assembled system at the joint coordinates, j and k , finite difference method is used as explained in Chapter 2. In this study, since identification are done for all six DOFs, one set of measurement is not enough to obtain all the information.

As a reminder of the method, Figure 2-5 given in Chapter 2 can be revisited. Three points on the structure can be defined: point 2 is the reference point at which RDOF FRFs are required, and points 1 and 3 are measurement points. The close-accelerometers method has been performed with three accelerometers placed in constant distance close to one another, as shown in Figure 4-39. By using Eqns. (2.49) and (2.50), the predicted receptance matrix that includes rotational FRFs for point 2 can be obtained.

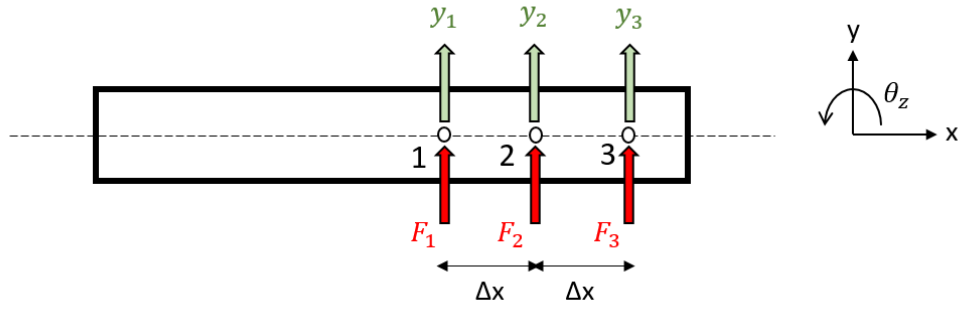


Figure 4-39 Finite Difference Method

In this case study, in order to obtain $[y_{mm}]$ which is the measured receptance matrix corresponding to joint coordinates, we need at least 4 sets of measurements. The goal is to obtain as many of the elements of this matrix ${}^E H_{pq}^C$; but it is not possible due to the geometry of the substructures, which will be explained in section 4.3.3.1.

$${}^E H_{jj}^C = \begin{bmatrix} H_{x_j x_j}^C & H_{x_j \theta_{y_j}}^C & H_{x_j y_j}^C & H_{x_j \theta_{x_j}}^C & H_{x_j z_j}^C & H_{x_j \theta_{z_j}}^C \\ H_{\theta_{y_j} x_j}^C & H_{\theta_{y_j} \theta_{y_j}}^C & H_{\theta_{y_j} y_j}^C & H_{\theta_{y_j} \theta_{x_j}}^C & H_{\theta_{y_j} z_j}^C & H_{\theta_{y_j} \theta_{z_j}}^C \\ H_{y_j x_j}^C & H_{y_j \theta_{y_j}}^C & H_{y_j y_j}^C & H_{y_j \theta_{x_j}}^C & H_{y_j z_j}^C & H_{y_j \theta_{z_j}}^C \\ H_{\theta_{x_j} x_j}^C & H_{\theta_{x_j} \theta_{y_j}}^C & H_{\theta_{x_j} y_j}^C & H_{\theta_{x_j} \theta_{x_j}}^C & H_{\theta_{x_j} z_j}^C & H_{\theta_{x_j} \theta_{z_j}}^C \\ H_{z_j x_j}^C & H_{z_j \theta_{y_j}}^C & H_{z_j y_j}^C & H_{z_j \theta_{x_j}}^C & H_{z_j z_j}^C & H_{z_j \theta_{z_j}}^C \\ H_{\theta_{z_j} x_j}^C & H_{\theta_{z_j} \theta_{y_j}}^C & H_{\theta_{z_j} y_j}^C & H_{\theta_{z_j} \theta_{x_j}}^C & H_{\theta_{z_j} z_j}^C & H_{\theta_{z_j} \theta_{z_j}}^C \end{bmatrix} \quad (4.13)$$

The point corresponding to the joint coordinate “j” is shown as J11 (which is the same point with rp1) in Figure 4-40 and Figure 4-41.

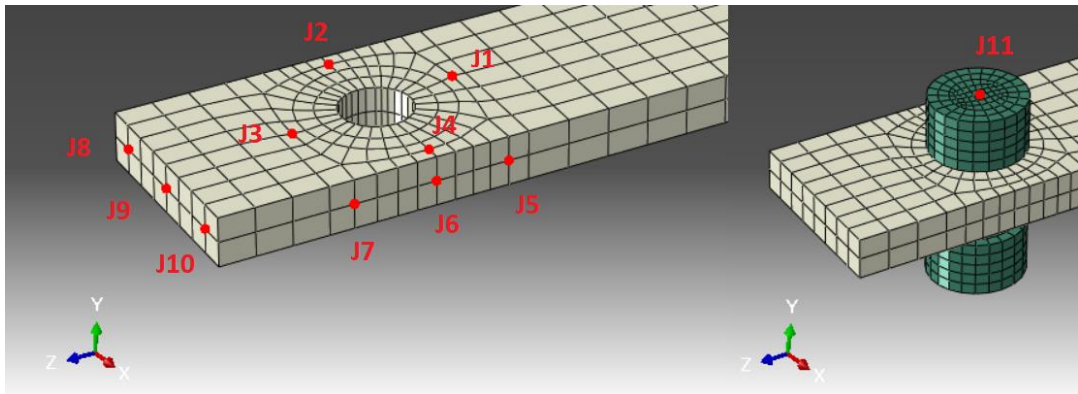


Figure 4-40 Measurement Points for j coordinate

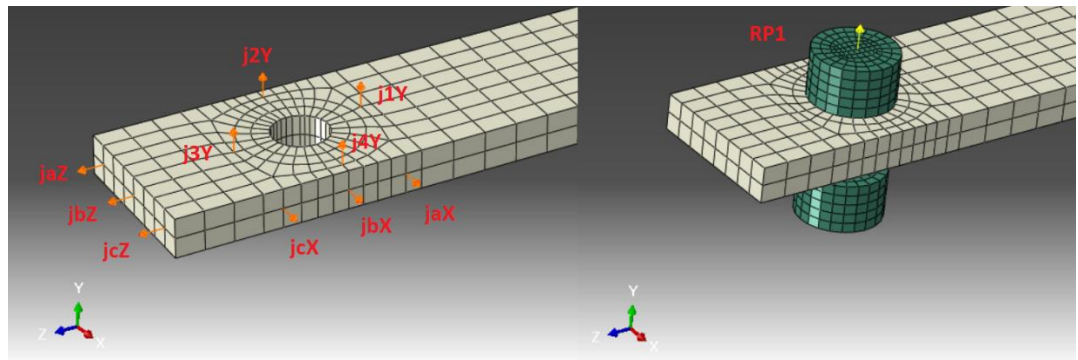


Figure 4-41 Force Points for j coordinate

The point corresponding to the joint coordinate “k” is shown as K11 (which is the same point with rp2) in Figure 4-42 and Figure 4-43.

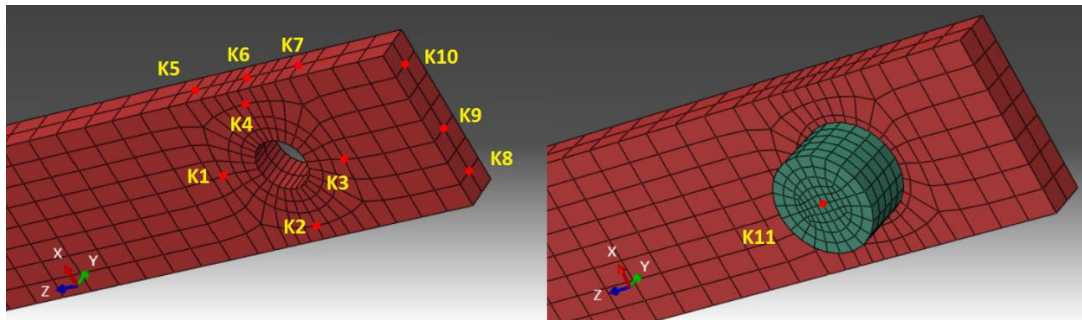


Figure 4-42 Measurement Points for k coordinate

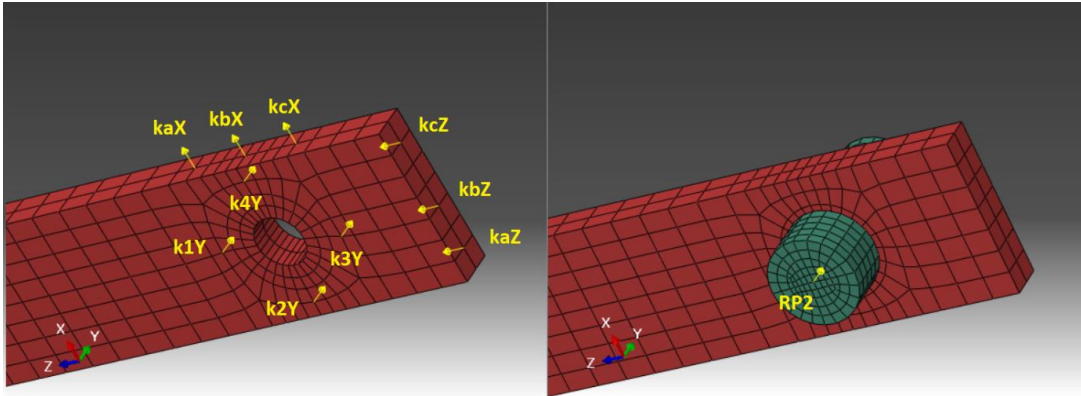


Figure 4-43 Force Points for k coordinate

As can be seen from Figure 4-40 to Figure 4-43, there are three measurement and three excitation points at each axis. In order to explain the procedure better, an example calculation for estimated H_{jj}^C and H_{kj}^C is shown below.

Measurement 1

As shown in Figure 4-44, jcX , jbX and jaX are the force excitation points and J3, RP1 and J1 are the measurement points where the accelerometers are placed at. sz is the constant spacing between points on z axis.

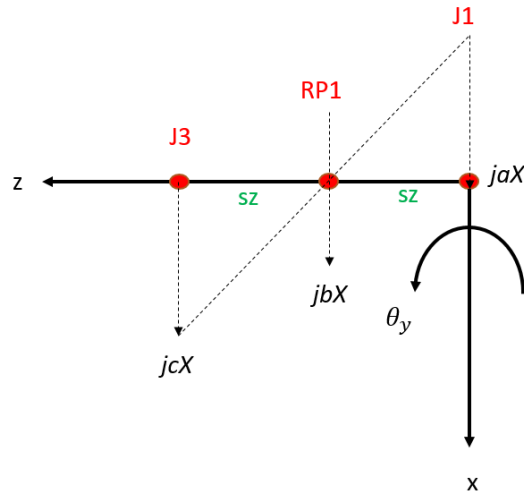


Figure 4-44 Measurement 1 Points

Transformation matrix is obtained using constant spacing as follows

$$[T_{zc}] = \frac{1}{2s_z} \begin{bmatrix} 0 & 2s_z & 0 \\ -1 & 0 & 1 \end{bmatrix} \quad (4.14)$$

Then, rotational FRF at points RP1 and RP2 are calculated by using the second-order central transformation matrix as follows:

$$[H_{est1}] = \begin{bmatrix} H_{xx} & H_{x\theta_y} \\ H_{\theta_y x} & H_{\theta_y \theta_y} \end{bmatrix} = [T_{zc}] \cdot [H_{meas1}] \cdot [T_{zc}]^T \quad (4.15)$$

where $[H_{est1}]$ represents the estimated FRFs in x and θ_y at points RP1 and RP2, and $[H_{meas1}]$ denotes the measured translational FRFs at points $j1, rp1$ and $j3$ for the calculation of ${}^E H_{jj}^C$ and $k1, rp2$ and $k3$ for the calculation of ${}^E H_{kj}^C$ which are shown in Eqns. (4.16) and (4.17), respectively.

$$[H_{meas1}] = \begin{bmatrix} H_{j1jaX} & H_{j1jbX} & H_{j1jcX} \\ H_{rp1jaX} & H_{rp1jbX} & H_{rp1jcX} \\ H_{j3jaX} & H_{j3jbX} & H_{j3jcX} \end{bmatrix} \text{ for } {}^E H_{jj}^C \quad (4.16)$$

$$[H_{meas1}] = \begin{bmatrix} H_{k1jaX} & H_{k1jbX} & H_{k1jcX} \\ H_{rp2jaX} & H_{rp2jbX} & H_{rp2jcX} \\ H_{k3jaX} & H_{k3jbX} & H_{k3jcX} \end{bmatrix} \text{ for } {}^E H_{kj}^C \quad (4.17)$$

Excitation and measurement points are shown in Figure 4-45 and Figure 4-46 for ${}^E H_{jj}^C$ and ${}^E H_{kj}^C$, respectively.

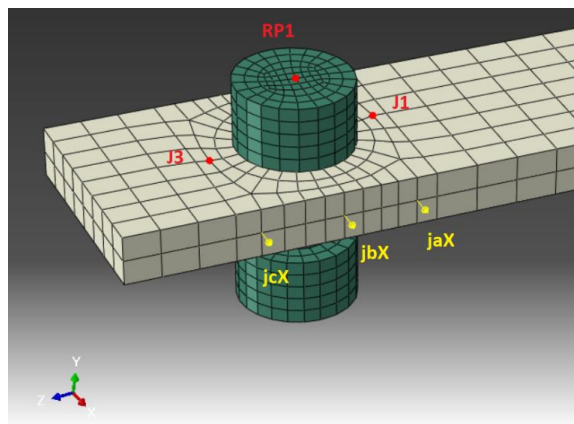


Figure 4-45 Measurement 1 Points for the Calculation of ${}^E H_{jj}^C$

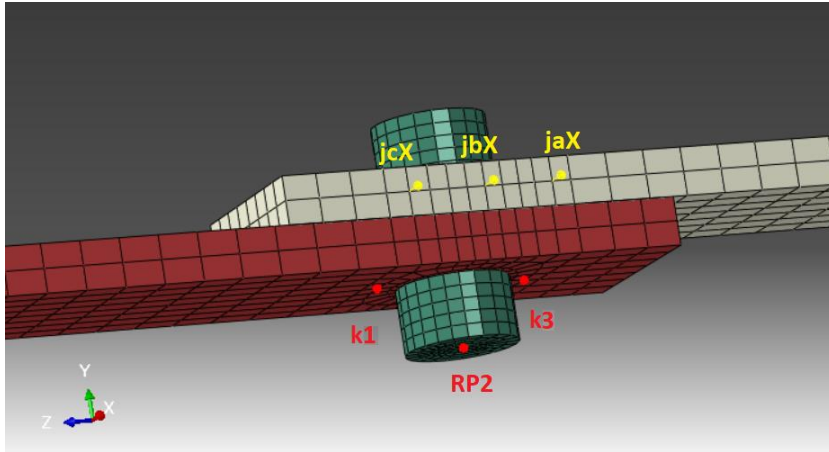


Figure 4-46 Measurement 1 Points for the Calculation of ${}^E H_{kj}^C$

Measurement 2

As shown in Figure 4-47, jcZ , jbZ and jaZ are the force excitation points and J2, RP1 and J4 are the measurement points where the accelerometers are placed at. s_x is the constant spacing between points at x axis.

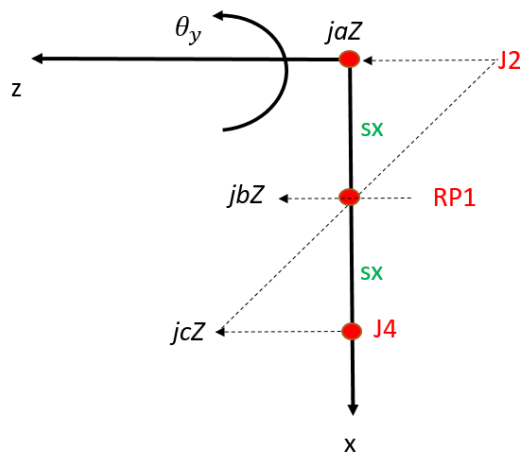


Figure 4-47 Measurement 2 Points

Transformation matrix is obtained using constant spacing as follows

$$[T_{xc}] = \frac{1}{2s_x} \begin{bmatrix} 0 & 2s_x & 0 \\ -1 & 0 & 1 \end{bmatrix} \quad (4.18)$$

Then, rotational FRF at points RP1 and RP2 are calculated by using the second-order-central transformation matrix as follows:

$$[H_{est2}] = \begin{bmatrix} H_{zz} & H_{z\theta_y} \\ H_{\theta_y z} & H_{\theta_y \theta_y} \end{bmatrix} = [T_{xc}] \cdot [H_{meas2}] \cdot [T_{xc}]^T \quad (4.19)$$

where $[H_{est2}]$ represents the estimated FRFs in z and θ_y at points RP1 and RP2, and $[H_{meas2}]$ denotes the measured translational FRFs at points $j2, rp1$ and $j4$ for the calculation of ${}_E H_{jj}^C$ and $k2, rp2$ and $k4$ for the calculation of ${}_E H_{kj}^C$ which are shown in Eqns. (4.20) and (4.21), respectively.

$$[H_{meas2}] = \begin{bmatrix} H_{j2jaZ} & H_{j2jbZ} & H_{j2jcZ} \\ H_{rp1jaZ} & H_{rp1jbZ} & H_{rp1jcZ} \\ H_{j4jaZ} & H_{j4jbZ} & H_{j4jcZ} \end{bmatrix} \text{ for } {}_E H_{jj}^C \quad (4.20)$$

$$[H_{meas2}] = \begin{bmatrix} H_{k2jaZ} & H_{k2jbZ} & H_{k2jcZ} \\ H_{rp2jaZ} & H_{rp2jbZ} & H_{rp2jcZ} \\ H_{k4jaZ} & H_{k4jbZ} & H_{k4jcZ} \end{bmatrix} \text{ for } {}_E H_{kj}^C \quad (4.21)$$

Excitation and measurement points are shown in Figure 4-48 and Figure 4-46 4-49 for ${}_E H_{jj}^C$ and ${}_E H_{kj}^C$, respectively.

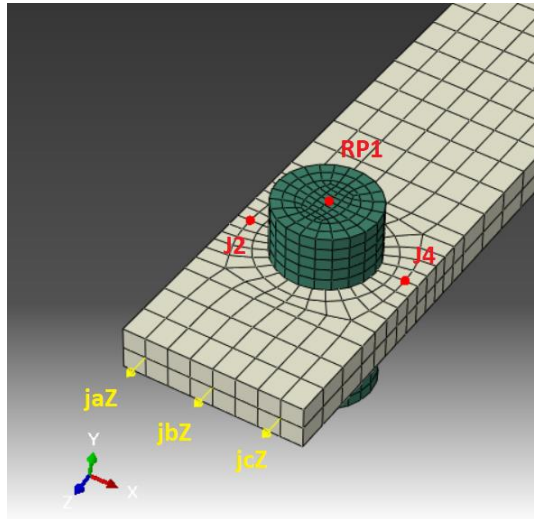


Figure 4-48 Measurement 2 Points for the Calculation of ${}_E H_{jj}^C$

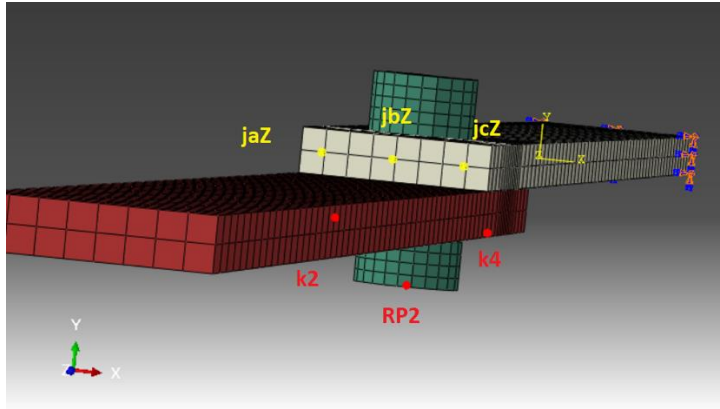


Figure 4-49 Measurement 2 Points for the Calculation of ${}_E H_{kj}^C$

Measurement 3

As stated in Figure 4-50, j2Y, RP1Y and j4Y are the force excitation points and J2, RP1 and J4 are the measurement points that accelerometers are placed. s_x is the constant spacing between points at x axis.

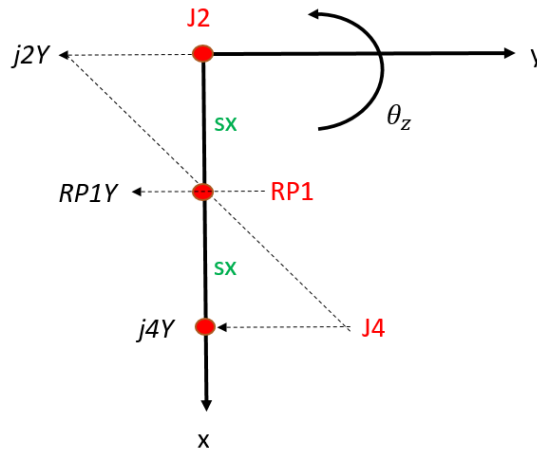


Figure 4-50 Measurement 3 Points

Rotational FRF at points RP1 and RP2 are calculated by using the transformation matrix in Eqn. (4.16) as follows:

$$[H_{est3}] = \begin{bmatrix} H_{yy} & H_{y\theta_z} \\ H_{\theta_z y} & H_{\theta_z \theta_z} \end{bmatrix} = [T_{xc}] \cdot [H_{meas3}] \cdot [T_{xc}]^T \quad (4.22)$$

where $[H_{est3}]$ represents the estimated FRFs in y and θ_z at points RP1 and RP2, and $[H_{meas3}]$ denotes the measured translational FRFs at points $j2, rp1$ and $j4$ for the calculation of ${}_E H_{jj}^C$ and $k2, rp2$ and $k4$ for the calculation of ${}_E H_{kj}^C$ which are shown in Eqns. (4.23) and (4.24), respectively.

$$[H_{meas3}] = \begin{bmatrix} H_{j2j2Y} & H_{j2RP1Y} & H_{j2j4Y} \\ H_{rp1j2Y} & H_{rp1RP1Y} & H_{rp1j4Y} \\ H_{j4j2Y} & H_{j4RP1Y} & H_{j4j4Y} \end{bmatrix} \text{ for } {}_E H_{jj}^C \quad (4.23)$$

$$[H_{meas3}] = \begin{bmatrix} H_{k2j2Y} & H_{k2RP1Y} & H_{k2j4Y} \\ H_{rp2j2Y} & H_{rp2RP1Y} & H_{rp2j4Y} \\ H_{k4j2Y} & H_{k4RP1Y} & H_{k4j4Y} \end{bmatrix} \text{ for } {}_E H_{kj}^C \quad (4.24)$$

Excitation and measurement points are shown in Figure 4-51 and Figure 4-52 for ${}_E H_{jj}^C$ and ${}_E H_{kj}^C$, respectively.

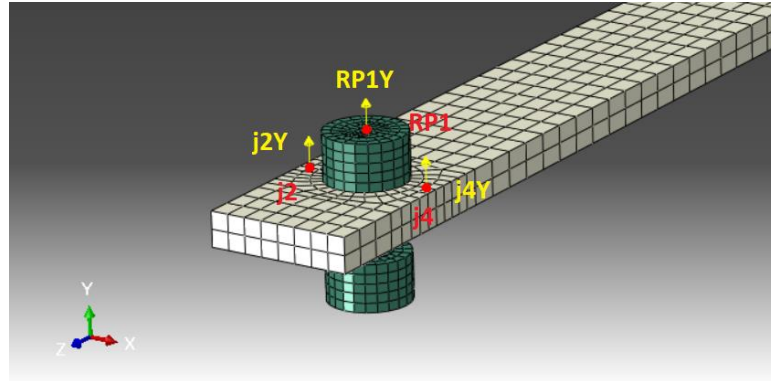


Figure 4-51 Measurement 3 Points for the Calculation of ${}_E H_{jj}^C$

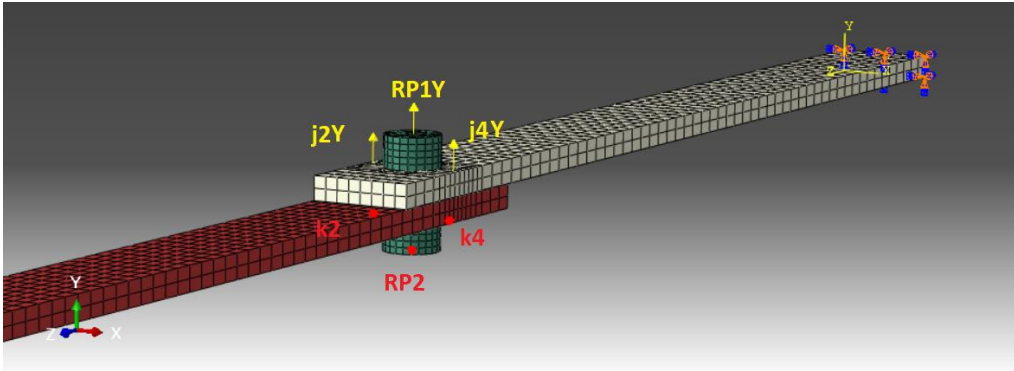


Figure 4-52 Measurement 3 Points for the Calculation of ${}_E H_{kj}^C$

Measurement 4

As stated in Figure 4-53, $j1Y$, $RP1Y$ and $j3Y$ are the force excitation points and $J1$, $RP1$ and $J3$ are the measurement points that accelerometers are placed. sz is the constant spacing between points at z axis.

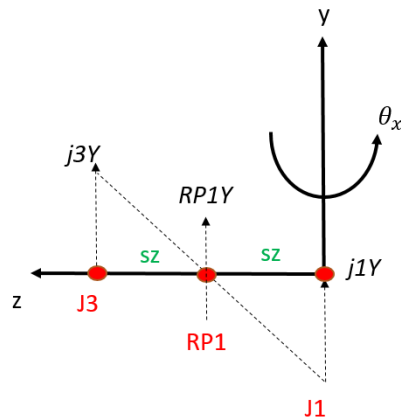


Figure 4-53 Measurement 4 Points

Rotational FRF at points $RP1$ and $RP2$ are calculated by using the transformation matrix in Eqn. (4.12) as follows:

$$[H_{est4}] = \begin{bmatrix} H_{yy} & H_{y\theta_x} \\ H_{\theta_x y} & H_{\theta_x \theta_x} \end{bmatrix} = [T_{zc}] \cdot [H_{meas4}] \cdot [T_{zc}]^T \quad (4.25)$$

where $[H_{est4}]$ represents the estimated FRFs in y and θ_x at points RP1 and RP2, and $[H_{meas4}]$ denotes the measured translational FRFs at points $j1, rp1$ and $j3$ for the calculation of ${}_E H_{jj}^C$ and $k1, rp2$ and $k3$ for the calculation of ${}_E H_{jj}^C$ which are shown in Eqns. (4.26) and (4.27), respectively.

$$[H_{meas4}] = \begin{bmatrix} H_{j1j1Y} & H_{j1RP1Y} & H_{j1j3Y} \\ H_{rp1j1Y} & H_{rp1RP1Y} & H_{rp1j3Y} \\ H_{j3j1Y} & H_{j3RP1Y} & H_{j3j3Y} \end{bmatrix} \text{ for } {}_E H_{jj}^C \quad (4.26)$$

$$[H_{meas4}] = \begin{bmatrix} H_{k1j1Y} & H_{k1RP1Y} & H_{k1j3Y} \\ H_{rp2j1Y} & H_{rp2RP1Y} & H_{rp2j3Y} \\ H_{k3j1Y} & H_{k3RP1Y} & H_{k3j3Y} \end{bmatrix} \text{ for } {}_E H_{kj}^C \quad (4.27)$$

Excitation and measurement points are shown in Figure 4-54 and Figure 4-46 4-55 for ${}_E H_{jj}^C$ and ${}_E H_{kj}^C$, respectively.

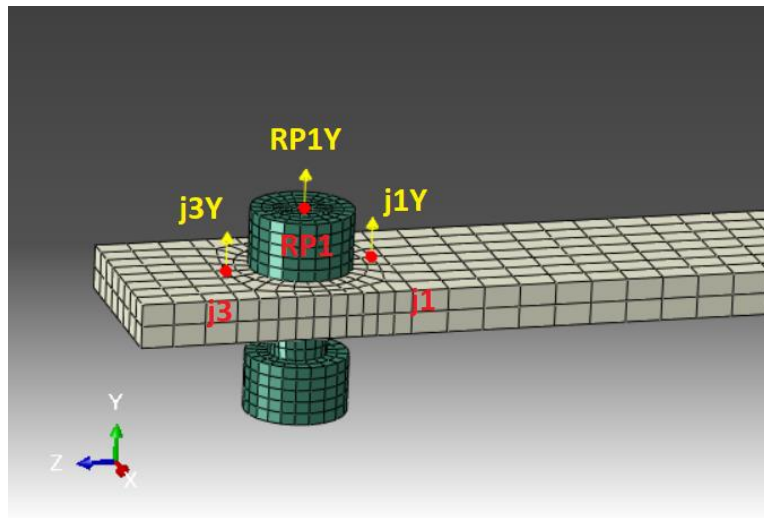


Figure 4-54 Measurement 4 Points for the Calculation of ${}_E H_{jj}^C$

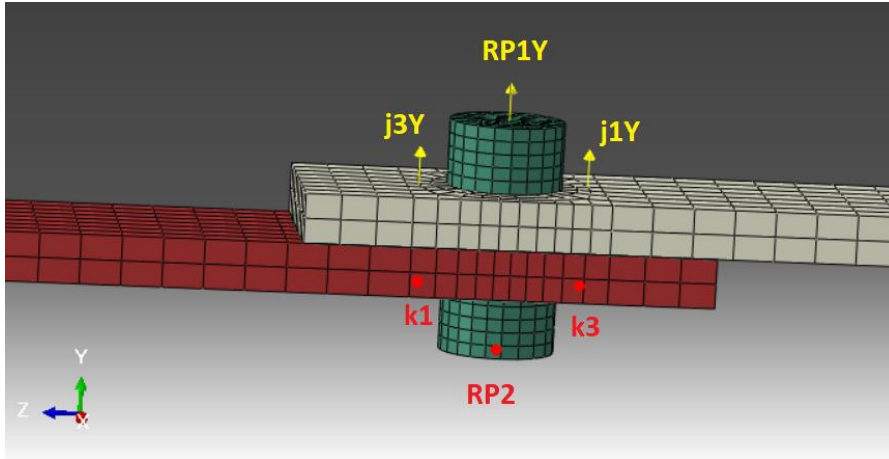


Figure 4-55 Measurement 4 Points for the Calculation of ${}^E H_{kj}^C$

After four set of measurements, 8 elements of ${}^E H_{pq}^C$ can be found as shown below:

$${}^E H_{jj}^C = \begin{bmatrix} H_{x_j x_j}^C & H_{x_j \theta_{y_j}}^C & 0 & 0 & 0 & 0 \\ H_{\theta_{y_j} x_j}^C & H_{\theta_{y_j} \theta_{y_j}}^C & 0 & 0 & 0 & 0 \\ 0 & 0 & H_{y_j y_j}^C & H_{y_j \theta_{x_j}}^C & 0 & H_{y_j \theta_{z_j}}^C \\ 0 & 0 & H_{\theta_{x_j} y_j}^C & H_{\theta_{x_j} \theta_{x_j}}^C & 0 & 0 \\ 0 & 0 & 0 & 0 & H_{z_j z_j}^C & 0 \\ 0 & 0 & H_{\theta_{z_j} y_j}^C & 0 & 0 & H_{\theta_{z_j} \theta_{z_j}}^C \end{bmatrix} \quad (4.28)$$

The components of the matrix which are shown in red are obtained from Measurement 1. The components which are shown in blue, green and orange color are obtained from Measurement 2, 3 and 4 respectively.

The FRF of the assembled system is regenerated by using the identified parameters of the bolted joint, and it is compared with the actual FRF in Figure 4-56. As it can be seen from the regenerated FRFs of the coupled structure in y direction a pretty good match is obtained. However, the same agreement between the regenerated and the actual FRFs for the coupled structure in x direction cannot be obtained, as shown in Figure 4-57. Further investigation showed that the main reason for this difference is not using all the elements of the receptance matrices shown in Eqn. (4.26), in the identification. This point will be explained in detail in section 4.3.3.1.

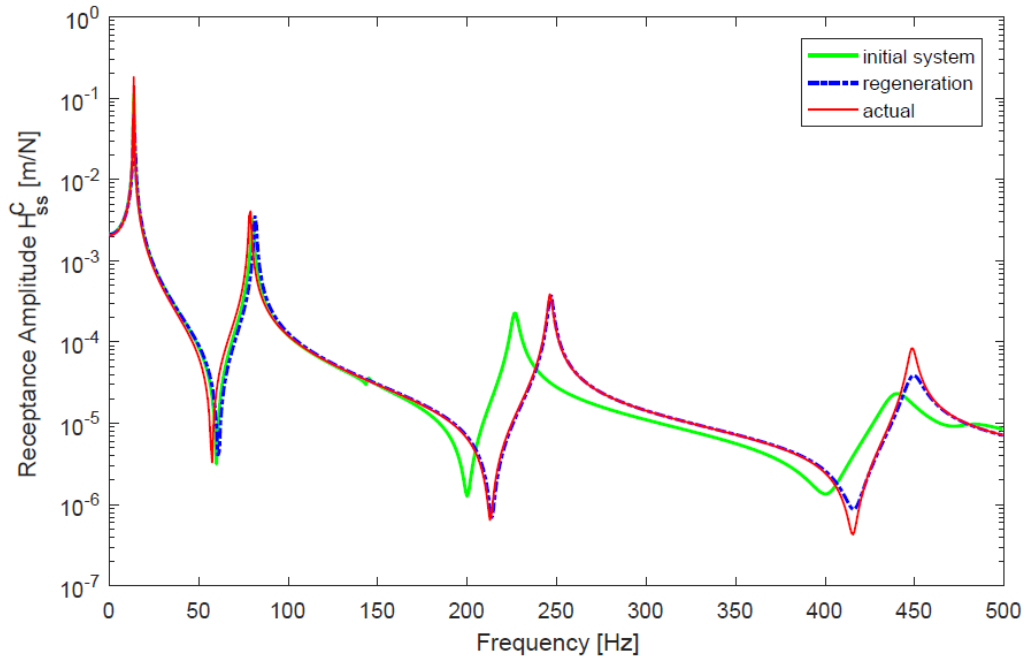


Figure 4-56 Regenerated FRF of the Coupled Structure Using Identified Joint Properties in y Direction

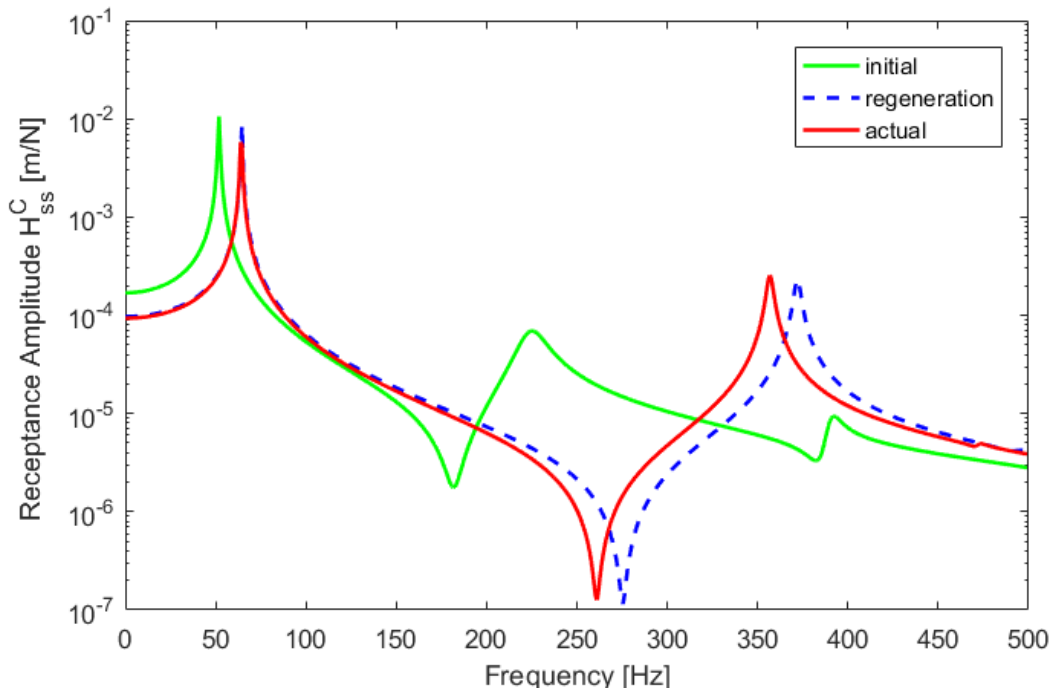


Figure 4-57 Regenerated FRF of the Coupled Structure Using Identified Joint Properties in x Direction

In order to study the transferability of the joint properties identified, the identified joint parameters are used to calculate the receptances of the cantilever beam coupled to a shorter beam (that is, the substructure B is changed). The predicted FRFs are compared with the actual ones (simulated experimental values obtained from the FE analysis of the assembly where 3D elements are used for the bolt). In this case study, the length of substructure B is selected as 0.2 m and the length of substructure A is kept the same (0.3 m). As can be seen from Figure 4-56 and Figure 4-58, except a slight deviation around the first anti-resonance in the response in y-direction, the regenerated FRFs match quite in agreement with the actual FRFs. However, the same observation cannot be made for the response in x direction, as can be seen from Figure 4-59, which is an expected observation, as we could not obtain very good results even with the original substructure B (see Figure 4-57).

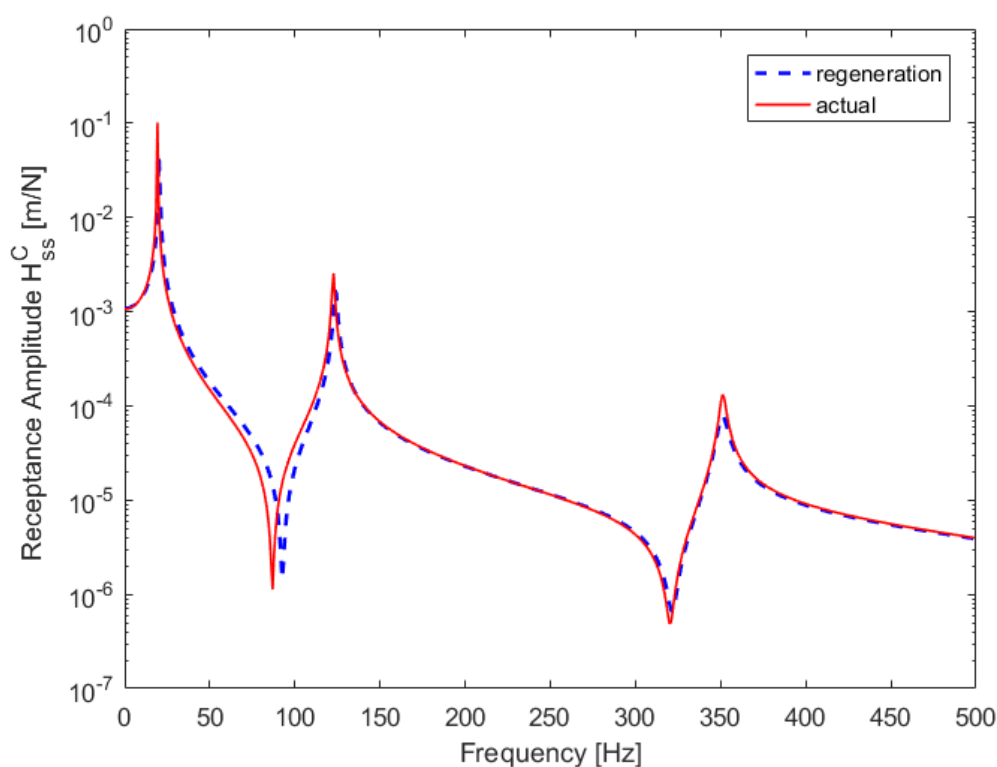


Figure 4-58 Regenerated FRF of the Coupled Structure (using shorter beam for substructure B) Using Identified Joint Properties in y Direction

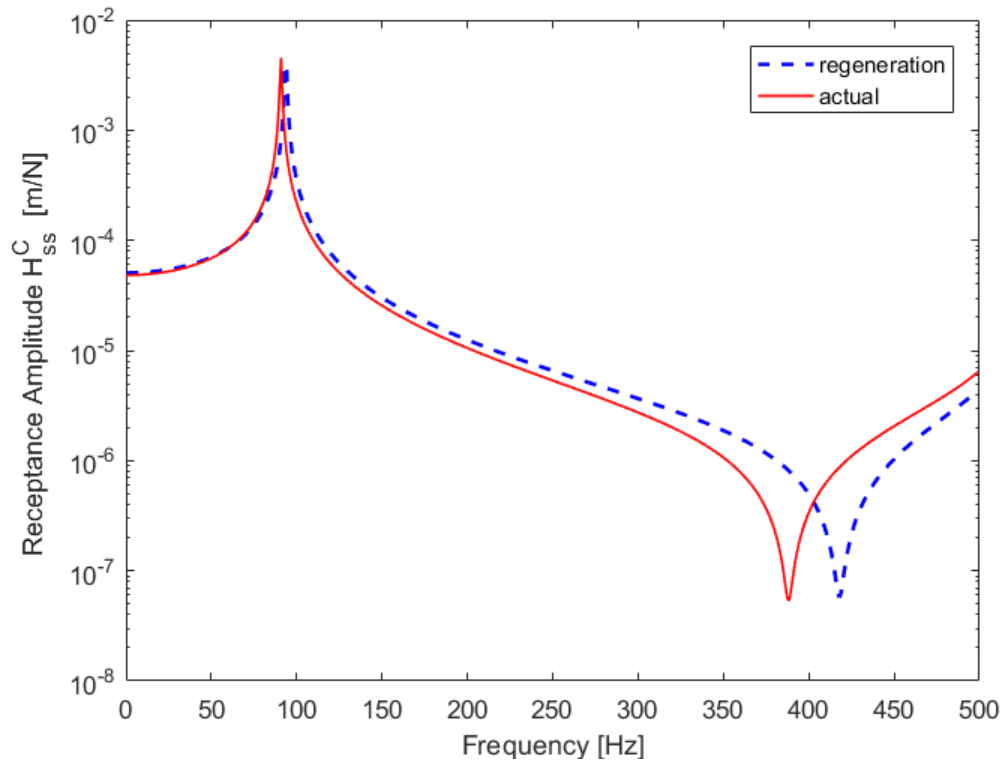


Figure 4-59 Regenerated FRF of the Coupled Structure (using shorter beam for substructure B) Using Identified Joint Properties in x Direction

4.3.3.1. Error Analysis

In case study 2, application and validation of the proposed method is shown by using the simulated experiment data. Since the simulated experiments are expected to reflect the real experimental conditions, the excitation and measurement points are selected by considering the real size of an accelerometer. As mentioned in the section 4.1, the height of the beam cross-sections is 0.006 m. Therefore, we cannot take measurement from the points shown in Figure 4-60.

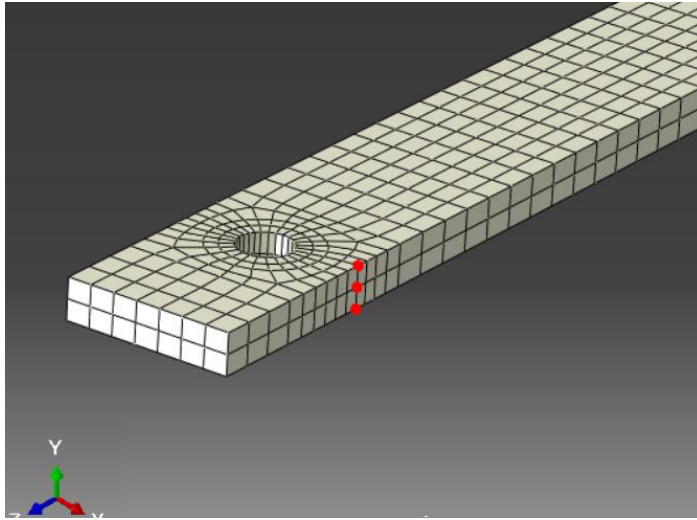


Figure 4-60 Unmeasurable Points

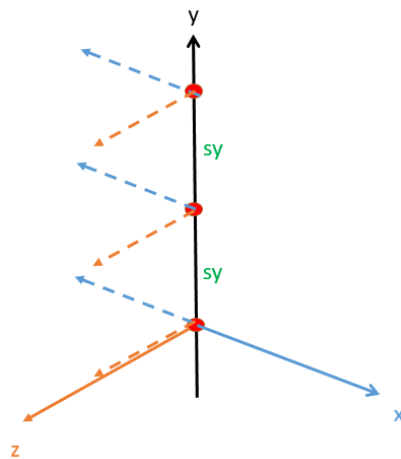


Figure 4-61 Measurement Scheme

There are some consequences of not being able to take measurement from these points. When Figure 4-61 is examined, it can be seen that excitation and displacement measurement in x direction will give the estimated FRFs in x and θ_z directions as follows

$$[H_{est_x}] = \begin{bmatrix} H_{xx} & H_{x\theta_z} \\ H_{\theta_z x} & H_{\theta_z \theta_z} \end{bmatrix} \quad (4.29)$$

In the same way, excitation and displacement measurement in z direction will give the estimated FRFs in z and θ_x directions as shown below

$$[H_{est_z}] = \begin{bmatrix} H_{ZZ} & H_{Z\theta_x} \\ H_{\theta_x Z} & H_{\theta_x\theta_x} \end{bmatrix} \quad (4.30)$$

Since we cannot excite and take the displacement measurements from these points, in the identification of the joint parameters, experimentally measured FRFs of the assembled structure at the connection coordinates of the system cannot fully be determined. Since all components of the receptance matrices $[{}^E H_{jj}^C]$, $[{}^E H_{kk}^C]$, $[{}^E H_{jk}^C]$ and $[{}^E H_{kj}^C]$ cannot be obtained, that will bring further errors.

Even if accurate data (without noise) is used in the identification, the effect of not being able to measure the matrix $[H_{est_x}]$ given by Eqn. (4.27) will cause errors in identified parameters as shown in Figure 4-62 and Figure 4-63. Similarly, not being able to measure the matrix given by Eqn. (4.28) will result in errors in identified parameters as shown in Figure 4-64 and Figure 4-65.

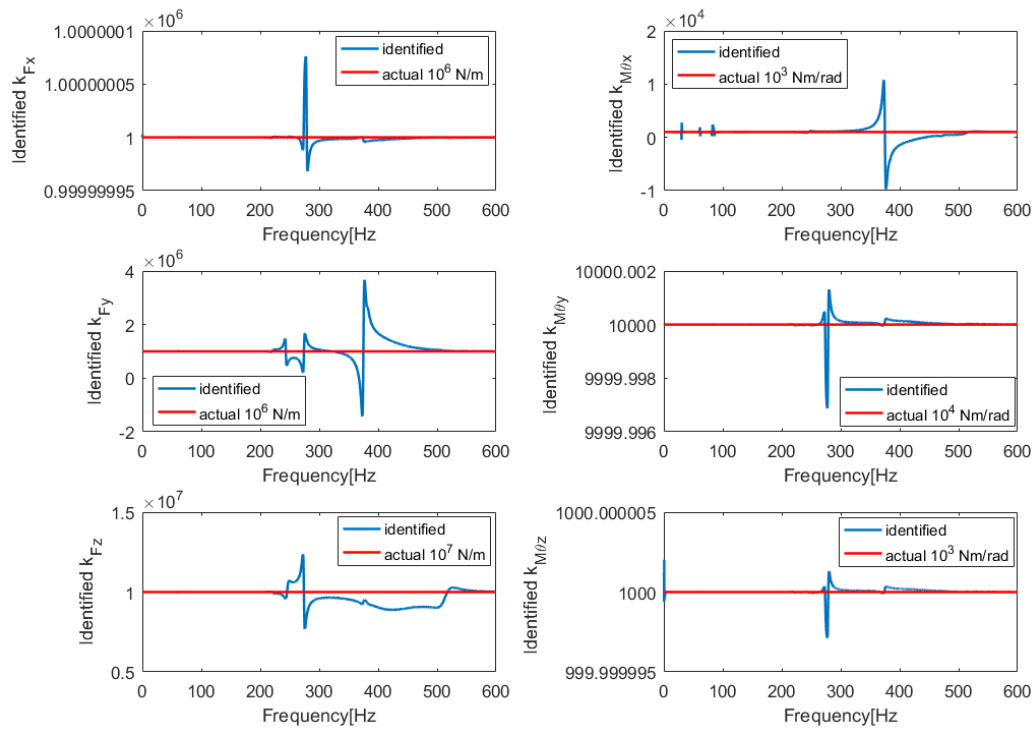


Figure 4-62 The Effect of Unmeasured FRFs on Stiffness Parameters

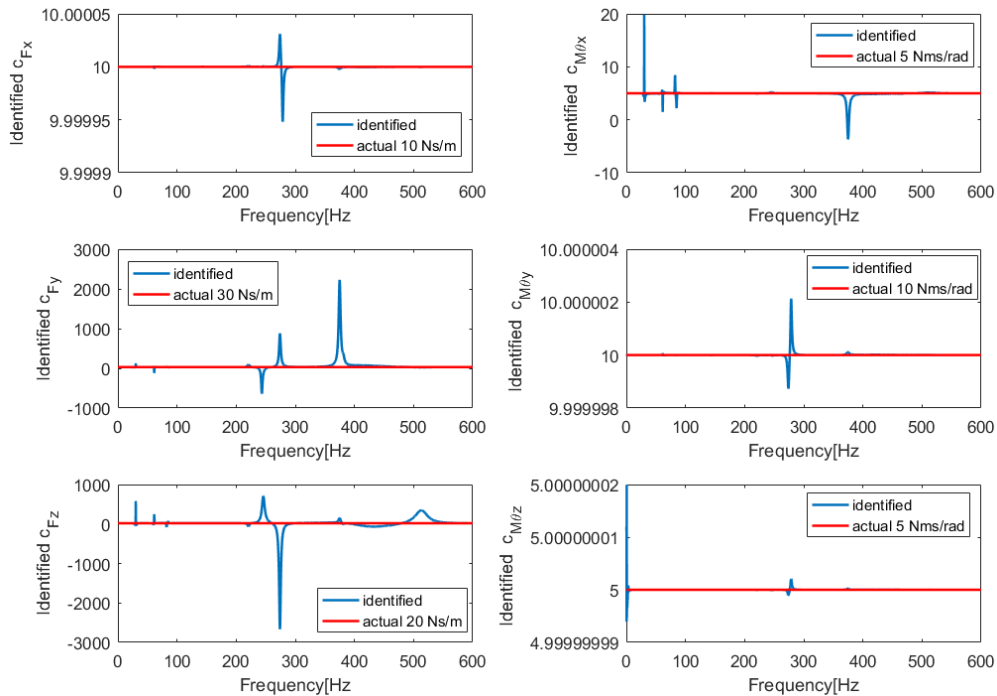


Figure 4-63 The Effect of Unmeasured FRFs on Damping Parameters

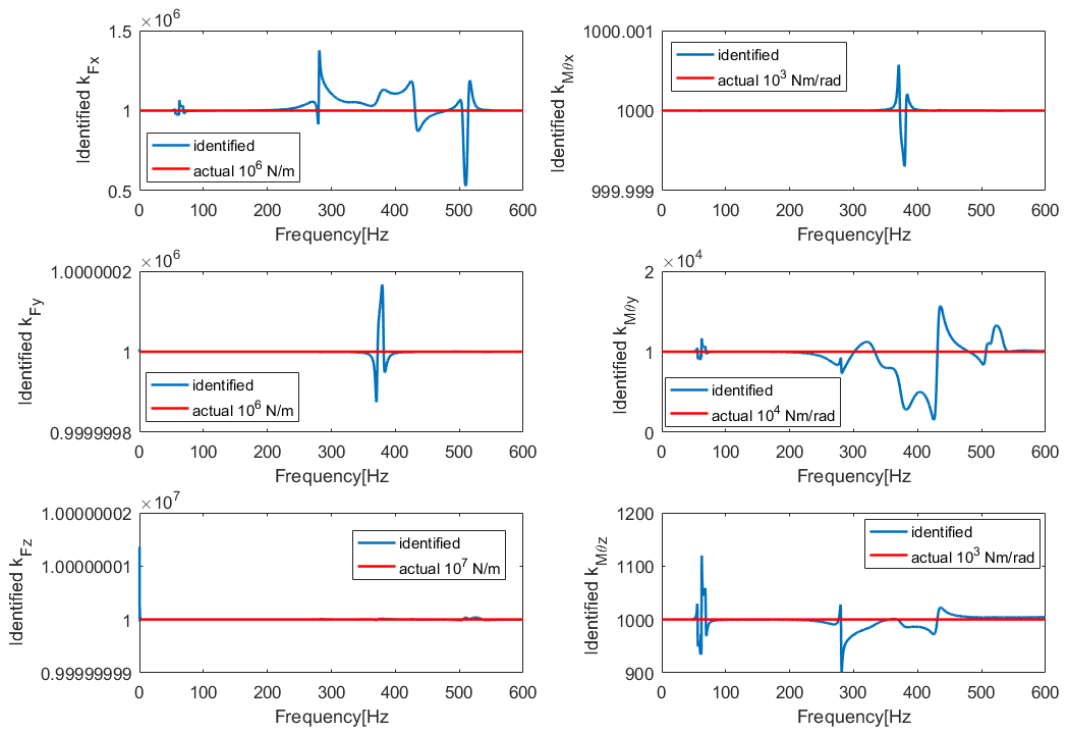


Figure 4-64 The Effect of Unmeasured FRFs on Stiffness Parameters

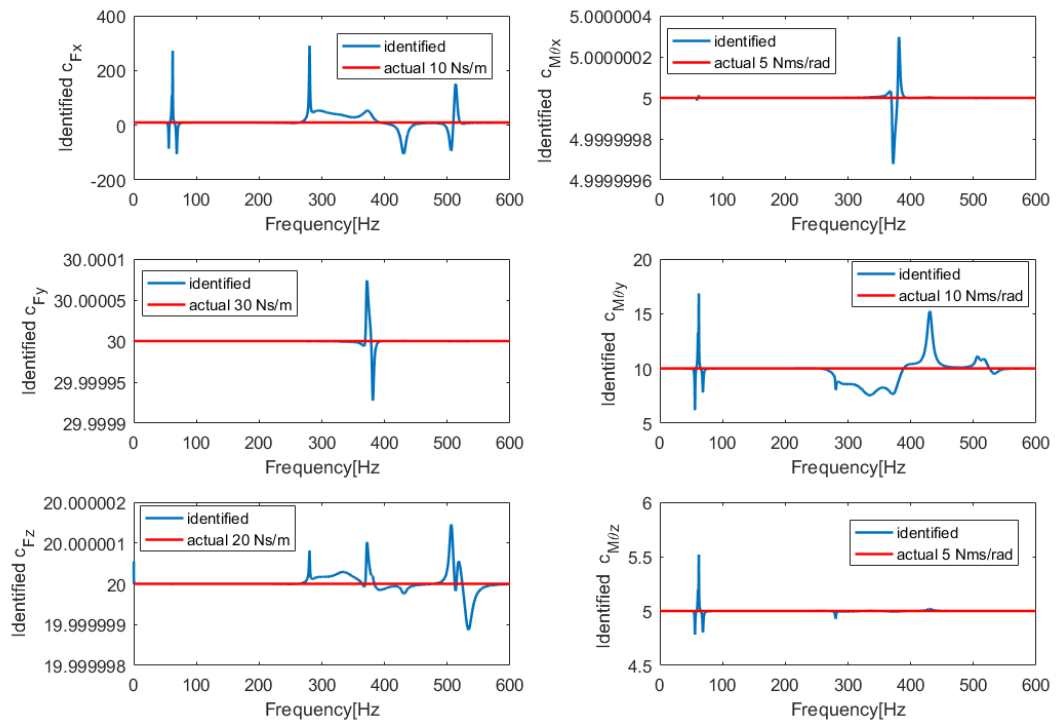


Figure 4-65 The Effect of Unmeasured FRFs on Damping Parameters

CHAPTER 5

CONCLUSION AND FUTURE WORK

5.1. Summary and Conclusions

The main objective of the thesis is to characterize structural joints dynamically. Due to complex dynamic behavior of joints, it is challenging to build a reliable model for joints using only analytical methods, and therefore usually models based on experimental measurements are employed. In this thesis, an FRF based identification method is suggested to obtain dynamic characteristics of bolted joints. The proposed method is based on the structural modification method called Matrix Inversion Method (MIM). The MIM formulation is used in reverse direction. In this approach, the frequency response functions (FRFs) of the coupled structure are experimentally measured and FRFs of the coupled system by using an initially estimated set of joint model parameters are calculated. Then, by using two sets of FRFs of the coupled systems, measured and calculated, the dynamic parameters of the joint consisting of stiffness and damping elements are identified using the so-called Inverse Structural Modification Method (ISMM). The method proposed in this study requires the measurement of only the FRFs of the assembled structure, not individual substructures connected with a bolted joint.

The proposed method is applicable to 2D structures where only two degrees of freedom (DOFs), translation and rotation, are involved, as well as to 3D structures where all DOFs in translation and rotation are involved. Therefore, the validity and the application of the proposed method were investigated on different joint models. The first joint model is used for discrete MDOF systems and it includes only translational joint parameters, the second model is used for beams and it includes rotational parameters as well. This model is used in transverse vibrations of bolted beams. The extended 3D joint model has both translational and rotational stiffness and damping elements; therefore, identification requires measurements in all translational directions.

The validity of the method proposed is demonstrated with various case studies. In these case studies the experimental FRFs of the coupled structure are obtained using simulated experiments, where the measurement errors are simulated by polluting the calculated values.

For the identification of joint parameters in 2D structural systems, in theoretical computations, as well as in obtaining simulated experimental results, 2D beam elements with two DOFs (one transverse displacement and one angular displacement) at each node are used. Both translational and rotational parameters of the joint model are obtained from the information coming from translational displacements only in order to simulate actual measurement in which it is not easy to measure angular displacements directly. In 3D structural systems, however, as the joint model includes translational and rotational parameters in all six DOFs, it is required to make translational displacement measurements in all three directions. The identification is made by using the simulated experiments and by using 3D brick elements with three translational DOFs at each node.

In this study, in addition to presenting a new identification approach for joint dynamics and studying its performance with case studies, several observations were made and some important conclusions were obtained. Some important observations and conclusions are summarized below.

From case studies, it is observed that using only translational parameters for any of the joint models does not simulate the real case accurately, and rotational information is usually important. However, obtaining RDOF related FRFs accurately is not an easy task in three dimensional model. Furthermore, it is observed from the case studies that the errors in the identified rotational joint parameters are higher than those of translational joint parameters. It is also observed that joint damping identification is prone to measurement errors much more than joint stiffnesses identification.

As it was concluded in previous studies, it is also concluded in this study that in both methods it is important first to carry out a sensitivity analysis and then make the

identifications in the frequency regions where the FRFs are sensitive to the related parameters. All joint parameters are identified at their own sensitive regions but it is observed that noise has not less effect in the frequency regions which are sensitive to joint parameters.

It is observed from the case studies that although the errors in identified parameters may have larger values, the FRFs regenerated by using these identified joint parameters and actual FRFs of the coupled structure perfectly match for transverse vibrations for both 2D and 3D bolted beam systems. Moreover, in 3D structural system, the regenerated FRFs again perfectly match with the actual ones for longitudinal vibrations of the beam. However, the model (and/or identified parameters) for the bolted joint for vibrations in the third direction, does not seem to give promising results. Since in actual applications, the joint dynamics in this direction will be basically determined by the friction force, at least for higher force levels, a nonlinear model will be required to represent the joint dynamics accurately in this direction. Therefore, not having accurate results in x direction will not be so significant.

The performance of the proposed method is compared with that of the previously developed joint identification method based on FRF Decoupling [15]. In the previous work [15], the model is developed for 2D systems, and therefore identification in 3D structural systems was not possible. In this thesis, the previously proposed method is also extended to three-dimensional space and the performance of the extended model is studied.

The effect of measurement errors on the identification results is included by polluting the simulated FRFs of the assembled structure with 5% random noise. By using polluted FRFs for simulating measured values, and making use of the FRFs calculated for the coupled system with initially estimated bolt parameters, identification is made. Then the average of the values identified at several frequencies in the frequency

regions sensitive to related joint parameters are calculated and taken as the bolted joint parameters.

In 3D structural systems, the rotational displacement information is obtained from translational displacements by using finite difference formulations. However, due to geometric restrictions, this is not possible in all directions in 3D systems; therefore, the experimentally measured FRFs of the assembled structure at the connection coordinates of the system will not be fully determined and that will bring further errors in the identified parameters of 3D model. It is concluded in this study that in the identification of 2D joint model parameters which are composed of translational and rotational terms (excluding cross coupling terms), the proposed method ISMM gives much better results than FRF Decoupling method. In the identification of 3D joint model parameters, again excluding cross coupling terms, although the differences between the identified values obtained by using ISMM and the actual ones are much lower than the errors in parameters obtained using FRF DM, the effect of this difference on the regenerated FRFs are not much.

However, in order to generalize the above conclusions in confidence, we need to carry out real experiments and identify the bolt parameters by using ISMM and FRF DM with real experimental data.

5.2. Future Work

This research has presented a joint identification technique that is applicable to 2D and 3D structural systems. It focuses on the linear behavior of the joint and any non-linear effect in the joint is ignored. Therefore, the effects of nonlinearities need to be addressed in future studies. Moreover, cross coupling terms can be included into the joint model.

It may also be recommended to study the different techniques to obtain RDOF related FRFs. In this study, finite difference formulations were used but there are methods proposed in recent years, promising much better results than finite difference method.

As a further work, the method proposed here can be used for more complex structures. However, before applying the method to different type of structures, the accuracy of the method need to be validated by using real experimental data.

REFERENCES

- [1] Shuguo,L., Yanhong,M., Dayi, Z.,Jie,H., Studies on Dynamic Characteristics of the Joint in the Aero-Engine Rotor System, *Mechanical Systems and Signal Processing*, 29, pp. 120-136, 2012.
- [2] Chang, I.S., Investigation of Space Launch Vehicle Catastrophic Failures, *Journal of Spacecraft and Rockets*, 33(2), pp.198-205, 1996.
- [3] Grosse, I.R., Nonlinear Axial Stiffness Characteristics of Axisymmetric Bolted Joints. PhD Thesis, Department of Mechanical Engineering, Virginia Polytechnic Institute and State University, 1987.
- [4] Daouk,S., Louf, F., Cluzel, C., Dorival, O., Champany, L., Audebert, S. Study of the dynamic behavior of a bolted joint under heavy loadings. *Journal of Sound and Vibration*, 392, pp. 307-324, 2017.
- [5] Mottershead, J.E., Friswell, M.I., Model Updating in Structural Dynamics: A Survey, *Journal of Sound and Vibration*, 167 (2), pp. 347-375, 1993.
- [6] Nobari, A.S., Robb, D.A., Ewins, D.J., A New Approach to Modal-Based Structural Dynamic Model Updating and Joint Identification, *Mechanical Systems and Signal Processing*, 9 (1), pp. 85-100, 1995.
- [7] Li, W.L., A New Method for Structural Model Updating and Joint Stiffness Identification, *Mechanical Systems and Signal Processing*, 16 (1), pp.155-167, 2002.
- [8] Kim, T.R., Ehmann, K.F., Wu, S.M., Identification of Joint Structural Parameters Between Substructures, *Journal of Manufacturing Science and Engineering*, 113 (4), pp. 419–424, 1991.
- [9] Yuan, J.X., Wu, X.M., Identification of the Joint Structural Parameters of Machine Tool by DDS and FEM, *Journal of Engineering for Industry*, 107 (1), pp. 64-69, 1985.

- [10] Park, S. S., Altintas, Y., Movahhedy, M., Receptance Coupling for End Mills, *International Journal of Machine Tools & Manufacture*, 43, pp. 889–896, 2003.
- [11] Schmitz, T.L., Duncan, G.S., Three-Component Receptance Coupling Substructure Analysis for Tool Point Dynamics Prediction, *Journal of Manufacturing Science and Engineering*, 127, pp. 781-790, 2005.
- [12] Hong, S.W., Lee, C.W., Identification of Linearised Joint Structural Parameters by Combined Use of Measured and Computed Frequency Responses, *Mechanical Systems and Signal Processing*, 5(4), pp. 267-277, 1991.
- [13] Yang, K.T., Park, Y.S., Joint Structural Parameter Identification Using a Subset of Frequency Response Function Measurements, *Mechanical Systems and Signal Processing*, 7(6), pp. 509-530, 1993.
- [14] Lee, D.H, Hwang, W.S., An Identification Method for Joint Structural Parameters Using an FRF Based Substructuring Method and an Optimization Technique, *Journal of Mechanical Science and Technology*, 21, pp. 2011-2022, 2007.
- [15] Tol, Ş., Özgüven, H.N., Dynamic Characterization of Bolted Joints Using FRF Decoupling and Optimization, *Mechanical Systems and Signal Processing*, 54, pp. 124–138, 2015.
- [16] Klaassen, S., Ciğeroğlu, E., Özgüven, H.N., Identifying the Joint Dynamics of a Bolted Beam System by Using FRF Decoupling and the SEMM Expansion Technique, in *Proceedings of Tribomechadynamics*, Houston, Texas, 2019.
- [17] De Klerk, D., Rixen, D., Voormeeren, S.N., Pasteuning, F., Solving the RDOF Problem in Experimental Dynamic Substructuring, in *Proceedings of the International Modal Analysis Conference (IMAC)*, Orlando, 2008.
- [18] Seijs, M.V., Bosch, D.D., Rixen, D.J., Klerk, D., An Improved Methodology for The Virtual Point Transformation of Measured Frequency Response Functions In Dynamic Substructuring, in *Proceedings of the 4th International Conference on*

Computational Methods in Structural Dynamics and Earthquake Engineering, Greece, 12-14 June 2013.

[19] Ewins, D. J., Modal testing: theory and practice, Letchworth, Hertfordshire, England New York: Research Studies Press; Wiley, 1984

[20] Mehrpouya, M., Graham, E., Park, S.S., FRF Based Joint Dynamics Modeling and Identification. Mechanical Systems and Signal Processing, 39, pp. 265-279, 2013.

[21] Özgüven, H. N., Determination of Receptances of Locally Damped Structures, Proceedings of the Second International Conference on Recent Advances in Structural Dynamics, 2, pp. 887-892, 1984.

[22] Özgüven, H. N., Structural Modifications Using Frequency Response Functions, Mechanical Systems and Signal Processing, 4 (1), pp. 53-63, 1990.

[23] Ozşahin, O., Erturk, A., Ozguven, H.N., Budak, E., A Closed-Form Approach for Identification of Dynamical Contact Parameters in Spindle- Holder- Tool Assemblies, International Journal of Machine Tools and Manufacture, 49, pp. 25–35, 2009.

[24] Silva, J.M.M., Maia, N. M. M., Riberio, A. M. R., An Indirect Method for the Estimation of Frequency Response Functions Involving Rotational DOFs, Conference: ISMA 25, Noise and Vibration Engineering, 2000.

[25] Elliott, A.S., Moorhouse, A. T., Pavic, G., Moment Excitation and the Measurement of Moment Mobilities, Journal of Sound and Vibration, 331 (11), pp. 2499- 2519, 2012.

[26] Sattinger, S., Method for Experimentally Determining Rotational Mobilities of Structures, Shock and Vibration Bulletin 50, pp. 17-27, 1980.

[27] Duarte, M. L. M, Ewins, D. J., Rotational Degrees of Freedom for Structural Coupling Analysis Via Finite-Difference Technique with Residual Compensation, Mechanical Systems and Signal Processing, 14 (2), pp. 205-227, 2000.

[28] Gibbons, T.J., Öztürk, E., Sims, N.D., Rotational Degree-Of-Freedom Synthesis: An Optimized Finite Difference Method for Non-Exact Data, *Journal of Sound and Vibration*, 412, pp. 207-221, 2017.

[29] Oldfield M., Ouyang H., Mottershead JE., Simplified Models of Bolted Joints Under Harmonic Loading, *Computers and Structures*, 84, pp. 25–33, 2005.

[30] Hibbit, Karlsson and Sorensen, Inc. ABAQUS Theory Manual, USA, 2001

[31] MIT, Friction Models

Available at:

[https://abaqus-docs.mit.edu/2017/English/SIMACAEGSARefMap/simagsa-c-
cntfriction.htm](https://abaqus-docs.mit.edu/2017/English/SIMACAEGSARefMap/simagsa-c-
cntfriction.htm)

[32] Engineering ToolBox, Friction and Friction Coefficients for various Materials, 2004. [online]

Available at:

https://www.engineeringtoolbox.com/friction-coefficients-d_778.html

[33] Hibbit, Karlsson and Sorensen, Inc. ABAQUS Analysis User's Manual, USA, 2001

[34] Budynas RG., Nisbett JK., Shigley's Mechanical Engineering Design 8th Edition, McGraw Hill

[35] Bowman Distribution –Barnes Group, Fastener Facts, p.90

[36] Ferhatoglu, E., Cigeroglu, E., Özgüven, H.N., A New Modal Superposition Method for Nonlinear Vibration Analysis of Structures Using Hybrid Mode Shapes, *Mechanical Systems and Signal Processing*, 107, pp. 317-342, 2018.

